APPLICATION OF PROCESS ANALYTICAL TECHNOLOGY FOR INVESTIGATION OF FLUID BED GRANULATION AND ACTIVE COATING DURING PROCESS DEVELOPMENT AND SCALE-UP

Dissertation

zur Erlangung des Doktorgrades (Dr. rer. nat.)
der Mathematisch-Naturwissenschaftlichen Fakultät
der Rheinischen Friedrich-Wilhelms Universität Bonn

vorgelegt von
Daniela Steigmiller
aus Ochsenhausen

Juli 2012

Angefertigt mit Genehmigung der Mathematisch-Naturwissenschaftlichen Fakultät der Rheinischen Friedrich-Wilhelms-Universität Bonn

Prüfungskommission

Prof. Dr. K.-J. Steffens (Erstgutachter)

Prof. Dr. A. Lamprecht (Zweitgutachter)

Prof. Dr. H. Schweim (Fachnaher Gutachter)

Prof. Dr. A. Schieber (Fachangrenzender Gutachter)

Tag der Promotion: 23.11.2012

Erscheinungsjahr: 2012

Diese Dissertation ist auf dem Hochschulschriftenserver der ULB Bonn *http://hss.ulb.uni-bonn.de/diss_online* elektronisch publiziert.

Danksagung

Die vorliegende Arbeit entstand in der Zeit von September 2009 bis Juli 2012 in der Abteilung Pharmazeutische Forschung und Entwicklung der Boehringer Ingelheim Pharma GmbH & Co. KG in Biberach. Für die großartige Möglichkeit eine Dissertation in der pharmazeutischen Industrie anzufertigen danke ich Herrn Dr. Schreder und Herrn Dr. Fiebig, die es mir ermöglichten, meine Doktorarbeit im Labor Prozessentwicklung Feste Formen unter optimalen Arbeitsbedingungen anzufertigen.

Meinem Doktorvater Prof. Dr. K.-J. Steffens danke ich für die Übernahme der universitären Betreuung, die Vergabe dieses aktuellen und praxisbezogenen Themas, sowie für seine wissenschaftlichen Anregungen.
Weiterhin bedanke ich mich bei Herrn Prof. Dr. A. Lamprecht für die Anfertigung des Zweitgutachtens, sowie bei Herrn Prof. Dr. H. Schweim und Herrn Prof. Dr. A. Schieber für ihr Mitwirken in der Prüfungskommission.

Darüberhinaus gilt mein Dank Herrn Dr. Michael Braun für die gewährte Unterstützung und die Durchsicht der Arbeit. Die Einbindung in aktuelle Projektarbeit ermöglichte mir wertvolle Einblicke in die Welt der pharmazeutischen Entwicklung und hat mir den Start ins Berufsleben enorm erleichtert.

Allen Kollegen des Labors und der Abteilung möchte ich für Ihre Hilfsbereitschaft und die gute Zusammenarbeit während der letzten Jahre danken. Das angenehme Arbeitsklima innerhalb des Labors hat sehr zum erfolgreichen Abschluss der Arbeit beigetragen.

Außerdem möchte ich mich ganz herzlich bei Frau Dr. Johanna Voegele bedanken, meiner „Doktormama“ und Mentorin, die mir über die gesamte Entstehungszeit dieser Arbeit hinweg immer wieder mit wertvollen Ratschlägen sowie unendlicher Geduld und Sorgfalt beim Korrekturlesen zur Seite stand.

Danke an alle Freunde, die mich während der letzten Jahre unterstützt haben. Ganz besonderer Dank an Carsten, der mir in allen Phasen dieser Doktorarbeit mit unerschütterlicher Zuversicht zur Seite stand und der mich durch seine Liebe und Geduld immer wieder motiviert hat.

Mein größter Dank gilt meiner Familie, meinen Eltern und meinen Geschwistern Benedikt und Sarah, die mich immer darin bestärkt haben, meinen Weg zu gehen. Danke dass ihr immer für mich da seid, danke für eure Unterstützung, euer Vertrauen in mich und euren Beistand.

Vielen Dank an alle, die zum Gelingen dieser Arbeit beigetragen haben!

Meiner Familie

TABLE OF CONTENTS

ACRONYMS AND ABBREVIATIONS

ANOVA	Analysis of Variance
API	Active Pharmaceutical Ingredient
AU	Absorbance Units
AV	Acceptance Value
cGMP	Current Good Manufacturing Practice
cm^{-1}	Inverse centimetre, unit of wavenumbers
CPP	Critical Process Parameter
CQA	Critical Quality Attribute
CU	Content Uniformity
CV	Cross Validation
DoE	Design of Experiments
e.g.	Exempli gratia (Latin), for example
ed.	Edition
Eds.	Editors
EFPIA	European Federation of Pharmaceutical Industries and Associations
EMA	European Medicines Agency
et al.	Et alii (Latin), and others
FCT	Film-coated tablet
FDA	Food and Drug Administration: Agency of the United States Department of Health and Human Services
FT-(NIR) spectrometer	Fourier-Transform (NIR) spectrometer
GC	Glatt Coater
GPCG	Glatt-Powder-Coater-Granulator
h	Hour
HPLC	High-Performance Liquid Chromatography
HR 83	Halogen Dryer, Type HR 83
i.e.	Id est (Latin), that is
ICH	International Conference on Harmonisation of Technical Requirements for Registration of Pharmaceuticals for Human Use
IPP 70-Se	In-line Particle Probe 70-Se

IR	Infrared
kg	Kilogram
LA	Labelled amount of API given in % of the target amount
LOD	Loss on Drying
min	Minute(s)
MIR	Mid-Infrared
MPA	Multi Purpose Analyzer
MSC	Multiplicative Scatter Correction
NCE	New Chemical Entity
NIR	Near Infrared
NIRS	Near Infrared Spectroscopy
no.	Number
PASG	Pharmaceutical Analytical Sciences Group
PAT	Process Analytical Technology
PC	Principal Component
PCA	Principal Component Analysis
PLS	Partial Least Squares
PSD	Particle Size Distribution
pts.	Points
QbD	Quality by Design
R&D	Research and Development
R^2	Coefficient of Determination
RMSECV	Root Mean Square Error of Cross Validation
RMSEP	Root Mean Square Error of Prediction
RW	Relative Width of a Distribution
s rel	Relative standard deviation
SEM	Scanning Electron Microscopy
SEP	Standard Error of Prediction
SFV	Spatial Filtering Velocimetry
SNV	Standard Normal Variate Transformation
SOP	Standard Operating Procedure
UV	Ultraviolet
WSG	Type of a Fluid Bed Granulator

SUMMARY

This thesis discusses the potential applications of process analytical techniques (PAT) and associated benefit of exploiting such in-line and at-line measurement tools during process development of solid dosage forms using case studies of two different development projects. The most critical unit operations of the manufacturing process affecting downstream processability and Critical Quality Attributes of the final drug product to a great extent were fluid bed granulation for the first project (Project A) and active coating of tablets for the second project (Project B).

In Project A, fluid bed granulation processes were investigated by in-line particle size measurements using spatial filtering velocimetry and in-line moisture determination by near infrared spectroscopy (NIRS). Implementation of these in-line tools significantly enhanced process understanding during development.

In-line particle sizing provided insight into the dynamics of particle growth during the different phases of fluid bed granulation process: wetting and nucleation, agglomeration and finally a steady-state phase, when agglomeration and attrition are at par. The resulting particle size distributions obtained with the in-line measurement probe were confirmed by off-line sieve analysis of collected granulate samples during and at the end of granulation. The impact of different filter-shaking modes during granulation, synchronous and asynchronous mode, on the resulting granulate morphology was additionally assessed using an image analysing system and scanning electron microscopy. It was found that the filter-dedusting mode during fluid bed granulation has no impact on the morphology of the final granules.

The effect of varying process parameters on resulting granulate particle size was systematically investigated by means of a Design of Experiments (DoE) study, performed as several fractional factorial designs. The developed statistical model obtained from this study could accurately predict the median granulate size (D_{50}) in dependence on the process parameters inlet air temperature and product temperature in the investigated ranges. Higher inlet air temperature has a positive correlation with particle size resulting in increased D_{50} values, while lower product temperatures yield larger granules.

Furthermore, a NIRS calibration model applying a fibre optic probe and diffuse reflection measuring mode was developed for in-line moisture monitoring during the granulation process, as compaction properties of this granulate are significantly influenced by its

residual moisture. The calibration is built upon Partial Least Squares regression of NIR spectra and reference values generated by loss on drying on a halogen dryer. It is possible to predict the water content in the calibrated range with a precision comparable to the one of the reference method. Although the NIR calibration model was modified repeatedly in the course of the process development phase, its performance particularly increased when the batches manufactured in the framework of the fluid bed granulation DoE had been included. This is reflected in the small Root Mean Square Error of Cross Validation for testing samples of new batches. The end-point of subsequent fluid bed drying step as potential rework process can be determined by in-line NIR measurements. Finally, in-line moisture monitoring by NIRS turned out to effectively support the scale-up activities to commercial scale.

The added value of application of PAT during process development in this project did not save development time, but increased the required understanding of the (inter-) relationships between process parameters and attributes of the produced granulates. Based on this knowledge, reasonable specifications for routine manufacturing can be selected and process windows or design spaces for single unit operations can be implemented.

Project B involves an active coating process of tablet cores in a drum coater, where tablets are layered by a film-coating liquid containing the Active Pharmaceutical Ingredient (API). Critical process parameters affecting content uniformity of the API on the final drug product were assessed by means of a DoE study. It was found that the spray rate has the maximum influence on content uniformity of the drug product. Content uniformity can be improved by reducing the spray rate, reducing the solid content of the coating suspension by adding water or by increasing the rotation speed of the drum coater.

One of the objectives of this study was to perform a feasibility assessment regarding the development of a NIRS method for end-point determination of the coating process in real-time. Currently, the end-point is estimated by indirect measurements. An appropriate at-line measurement procedure and a NIR calibration model were established for determination of the actual API content. The calibration is based on time-consuming HPLC reference values, which is the current standard release test. Two distinct models were developed: one focusing on measurements of individual tablets and one using a rotating sample cup as a measuring device, which allows the simultaneous measurement of a larger surface area of several tablets. Principal Component Analysis proves the specificity of both final models for the API. A complete validation approach including

further validation parameters i.e. linearity, precision, accuracy as well as robustness was exemplarily realised for the NIR method considering individual tablets. In conclusion, near infrared spectroscopy is found to be an appropriate tool for end-point determination of the active coating process, but further optimisation of the manufacturing process itself might be necessary for reducing variability in content uniformity of the film-coated tablets.
The benefit of applying NIRS as a PAT tool in active coating processes compared to conventional HPLC analysis is mainly related to saving of time because the bulk product can directly be processed further without delay between completion of a unit operation and sampling, analysis and release.

In the last section, important regulatory requirements concerning the submission of PAT data and specifics for NIR data are summarised.

ZUSAMMENFASSUNG

Im Rahmen dieser Arbeit werden potentielle Einsatzmöglichkeiten von prozessanalytischen Technologien und die damit verbundenen Vorteile durch die Nutzung von in-line und at-line Messsystemen während der Prozessentwicklung für feste Darreichungsformen anhand zweier unterschiedlicher Entwicklungsprojekte untersucht. Kritische Prozessschritte, welche die weitere Verarbeitbarkeit und die Kritischen Qualitätsattribute des Arzneimittels maßgeblich bestimmen, sind zum einen die Wirbelschichtgranulierung (Projekt A) und das Wirkstoffcoating von Tabletten (Projekt B).

In Projekt A wurden Feuchtgranulierprozesse in der Wirbelschicht von in-line Partikelgrößenmessungen mittels Ortsfiltermethode (Spatial Filtering Velocimetry) und in-line Feuchtebestimmungen mittels Nahinfrarotspektroskopie (NIRS) beleuchtet. Dank der eingesetzten Technologien konnte das Prozessverständnis während der Entwicklungsphase maßgeblich gesteigert werden.

Die in-line Partikelgrößenmessungen ermöglichten Einblicke in die Dynamik des Partikelwachstums während der verschiedenen Phasen der Wirbelschichtgranulierung: Benetzung und Keimbildung, Agglomeration sowie schließlich das Erreichen eines Gleichgewichts zwischen Granulatwachstum und –abrieb. Die in-line gemessenen Partikelgrößenverteilungen wurden durch off-line durchgeführte Siebanalysen bestätigt, für welche Proben während und direkt nach der Granulatherstellung entnommen wurden. Die Auswirkung von verschiedenen Verfahren der Filterentstaubung, synchronem und asynchronem Rütteln während der Granulierung, auf die Granulatmorphologie wurde zusätzlich mit Bildanalyseverfahren und durch Rasterelektronenmikroskop-Aufnahmen untersucht. Die Ergebnisse zeigten, dass die unterschiedlichen Rüttelmechanismen keinen Einfluss auf die Morphologie der finalen Granulate haben.

Der Effekt unterschiedlicher Prozessparameter wurde systematisch untersucht, indem mit Hilfe Statistischer Versuchsplanung mehrere fraktionell faktorielle Versuchspläne erstellt und ausgewertet wurden. In Abhängigkeit von den Prozessparametern Zulufttemperatur und Produkttemperatur war eine präzise Vorhersage der resultierenden mittleren Korngröße (D_{50}) mit Hilfe des entwickelten statistischen Modells innerhalb der untersuchten Bereiche möglich. Höhere Zulufttemperaturen wirken sich positiv auf die mittlere Partikelgröße aus und führen zu höheren D_{50}-Werten, während niedrigere Produkttemperaturen in gröbere Granulatstrukturen resultieren.

Da die Tablettiereigenschaften des untersuchten Granulats hauptsächlich von dessen Restfeuchte bestimmt werden, wurde ein NIR-Kalibriermodell unter Anwendung einer faseroptischen Sonde und diffuser Reflexionmessung entwickelt, um während des Granulierprozesses die Feuchtigkeit im Granulat überwachen zu können. Die Kalibrierung basiert auf Partial Least Squares Regression von NIR-Spektren und den jeweiligen Referenzwerten, die als Trocknungsverlust auf einem Halogentrockner bestimmt wurden. Der Wassergehalt kann im kalibrierten Bereich mit einer Genauigkeit vorhergesagt werden, die in der Größenordnung des Fehlers der Referenzmethode liegt. Obwohl das Kalibriermodell im Laufe der gesamten Prozessentwicklung wiederholt angepasst wurde, konnte die Vorhersagekraft für neue Chargen durch Integrieren der DoE-Chargen besonders deutlich gesteigert werden. Dies spiegelt sich in einem niedrigen Root Mean Square Error of Cross Validation beim Testen der Proben neuer Chargen wider. Desweiteren gelang es, den Trocknungsendpunkt eines Trocknungsschrittes innerhalb eines potentiellen Rework-Prozesses mittels in-line NIR-Messungen zu bestimmen. Schließlich stellte sich die NIR-Spektroskopie zur in-line-Kontrolle des Wassergehaltes als effektive Technologie heraus, um Scale-up-Aktivitäten in den kommerziellen Maßstab zu unterstützen.
Der Zusatznutzen, den die Anwendung von PAT während der Entwicklung dieses Projektes brachte, ist nicht mit Zeitersparnis verknüpft, sondern besteht in einer Vertiefung des geforderten Verständnisses der (Wechsel-)Beziehungen zwischen Prozessparametern und Attributen des Endproduktes. Durch dieses Wissen können zutreffende Spezifikationen für die Routineherstellung gesetzt werden, sowie Prozessfenster oder Design Spaces für einzelne Herstellschritte etabliert werden.

Projekt B beinhaltet als grundlegenden Prozessschritt das Wirkstoffcoating von Tabletten in einem Trommel-Coater, wobei Tabletten mit einer filmbildenden Suspension, die unter anderem den Wirkstoff enthält, überzogen werden. Kritische Prozessparameter, die die Gleichförmigkeit des Wirkstoffgehalts der finalen Filmtabletten beeinflussen, wurden mit Hilfe statistischer Versuchsplanung bewertet und die Sprührate als wichtigster Faktor identifiziert. Durch die Verringerung der Sprührate, das Herabsetzen des Feststoffanteils der Coating-Suspension sowie die Erhöhung der Umdrehungsgeschwindigkeit der Coating-trommel kann eine gleichförmigere Verteilung des Wirkstoffes auf den Tabletten erreicht werden.

Die Untersuchung der Machbarkeit, eine NIR-Methode zur Endpunktbestimmung des Wirkstoffcoatings in Echtzeit zu entwickeln, war ein weiteres Thema dieser Arbeit, da die Echtzeitbestimmung mit der derzeitigen Standardtestmethode HPLC nicht möglich ist. Zu diesem Zweck wurden zwei unterschiedliche at-line Messverfahren eingeführt: NIR-Messungen der einzelnen Tabletten sowie NIR-Messungen mehrerer Tabletten in einem rotierenden Probenbecher, welche die gleichzeitige Messung einer größeren Oberfläche aus mehreren Tabletten ermöglicht. Zu beiden Messverfahren wurden entsprechende NIR-Kalbriermodelle entwickelt, welche auf HPLC-Daten als Referenzwerte für den jeweiligen Wirkstoffgehalt basieren. Die Spezifität der beiden finalen Modelle wurde jeweils mittels Hauptkomponentenanalyse bestätigt. Ein umfänglicher Validierungsansatz, der Linearität, Genauigkeit, Richtigkeit sowie Robustheit des Modells als weitere Validierungsparameter umfasst, wurde beispielhaft für die Methode für Einzeltabletten durchgeführt. Schlussfolgernd kann Nahinfrarotspektroskopie als geeignete Technologie zur Endpunktbestimmung für das Wirkstoffcoating angesehen werden; jedoch sollte der Herstellprozess im Hinblick auf Gleichförmigkeit des Gehalts der Filmtabletten zunächst weiter optimiert werden.
Der Vorteil, NIR-Spektroskopie als prozessanalytische Technologie für Wirkstoffcoating von Tabletten einzusetzen, ist in der Zeitersparnis gegenüber konventioneller HPLC-Analytik zu sehen: Das Bulkprodukt kann direkt ohne die zeitliche Verzögerung zwischen dem Ende des Herstellschrittes und Musternahme, Analyse und Freigabe weiterprozessiert werden.

Im Abschlusskapitel werden wichtige regulatorische Anforderungen, welche die Einreichung von PAT-Daten sowie Spezifika für NIR-Daten betreffen, zusammenfassend diskutiert.

1. INTRODUCTION

The aim of the pharmaceutical industry is to develop drug products with consistent quality which translates into reliable efficacy and safety. Currently, the importance of the quality of drug products is strongly emphasised by regulatory agencies which launched several broadly based initiatives in the past years. Although there is no common definition of the term quality, most definitions imply meeting or exceeding customers´ need [1]. In its strategic priorities for the years 2011 – 2015 [2], the importance of safety of medication is strongly emphasised.

1.1 QUALITY BY DESIGN

An often cited article of the Wall Street Journal, published in 2003, observed that application of science and engineering in product development for pharmaceutical products even lagged behind the manufacturing of potato chips and laundry soaps.

The necessity for implementing changes in pharmaceutical manufacturing setting towards higher operational excellence is also driven by financial reasons: late-stage failures of new products, safety withdrawals and patent expiry have intensified the pressure for pharmaceutical industry [3]. The productivity of Research and Development (R&D) has fallen: the number of approved new chemical entities (NCE) has decreased from 40 per year in 1990 to less than 30 per year in 2000, while the R&D expenditure has doubled during the same time [4].

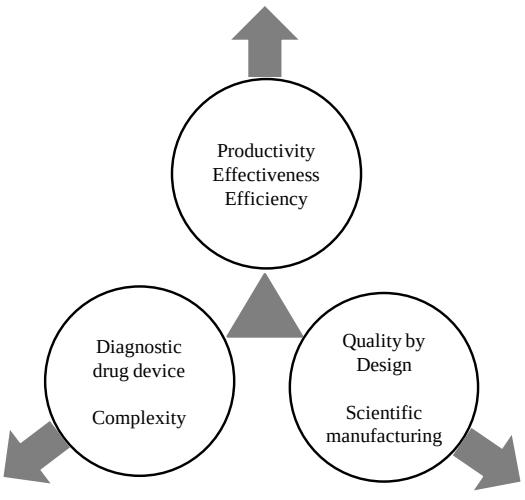

Figure 1 Pharmaceutical development between the poles of product-related, regulatory and efficiency requirements [3]

One of the main driving forces for a change in pharmaceutical development and manufacturing was the announcement of "Pharmaceutical cGMPs for the 21st Century: A Risk-Based Approach" [5]. The American Food and Drug Administration (FDA) announced this paradigm shift in 2002 in order to modernise the current regulatory approach and to define the agency´s vision of a risk-based assessment of drug manufacture and product quality [6]. Among others, one goal of this campaign was to encourage the early adoption of new technological advances by the pharmaceutical industry as part of the current Good Manufacturing Practice (cGMP).

This brought about what has been called "perhaps the most exciting period of change in pharmaceutical manufacturing of the past three decades" [6]. The attempt to reach the performance of other industries, e.g. semiconductor field with regards to failure rate, evoked the introduction of the Quality by Design approach. It was noted that pharmaceutical manufacturers test quality into the product by performing extensive release testings for the final product rather than manufacture a product in which quality is built-in by design. Pharmaceutical Quality by Design pursues a systematic, risk-based, holistic and proactive approach which begins with predefined objectives and stresses product and process understanding and process control [7]. The effort is the translation of quality, which is important for the patient, into attributes of the drug product. These attributes are called Critical Quality Attributes (CQA) [8]. They are affected by variability of attributes of the raw materials or intermediates involved in the manufacture of a drug product, referred to as Critical Material Attributes (CMA), and different parameters during manufacture, referred to as Critical Process Parameters (CPP). The common understanding is that if all sources of variability were defined and their relationships with the CQAs understood, their effects would be assessed and controlled more easily. Finally, this approach would lead to the desired product in which quality is built-in by design.

1.2 PAT INITIATIVE

Even more attention was paid on the preceding initiative, which was launched in 2003 by the FDA. Its intention is to encourage the pharmaceutical industry to enhance the use of process analytical technology (PAT). PAT aims at strengthening process understanding of manufacturing processes, can support the shift from empirical to science-based manufacturing and was intended to be a part of the larger cGMP initiative [9].

The FDA defines PAT as "a system for designing, analyzing, and controlling manufacturing through timely measurements (i.e., during processing) of critical quality and performance attributes of raw and in-process materials and processes, with the goal of ensuring final product quality" [10]. Timely measurements according to this guidance include in-line, on-line and at-line measurements, which are defined as follows:

- In-line: Measurement where the sample is not removed from the process stream and can be invasive or non-invasive.
- On-line: Measurement where the sample is diverted from the manufacturing process, and may be returned to the process stream.
- At-line: Measurement where the sample is removed, isolated from, and analyzed in close proximity to the process stream.

The PAT-measurements presented and discussed in this thesis are carried out in-line (Project A) and at-line (Project B).

1.2.1 Benefits of implementation of PAT and reasons for rejection

The implementation of PAT in pharmaceutical manufacturing brings about several advantages, which can be classified into three categories: scientific benefits, regulatory and business profits.

Business-related advantages involves reducing risks and reducing costs [11]; risks can be related to safety and reducing costs arise out of improvements in process control which lead to shortened transition and batch cycle times. This can be realised by the ability to react quickly to process disturbances and reducing product variability. Moreover, the yield could be increased by decreasing off-specification production, thus minimising consumption of expensive ingredients.

One of the highest costs, when bringing a new drug to market, are the development costs, which can add up to 30 – 35 % of the total costs [12]. Thus the implementation of PAT during product development can be of enormous value, if time-to market is influenced.

Further benefits of implementing PAT result not only in reduced cycle times and facilitating continuous processing, but also in omission of laborious end-product testings in favour of release based on in-process documentation [13]. This is a step into the real-time release testing paradigm, which is also strongly encouraged by regulatory agencies. Quality Assurance or Quality Control units usually account for 20 – 30 % of manufacturing costs. Estimations assume that adoption of PAT could reduce this number to < 5 % [14].

PAT is considered to be both strategic and tactical, because it supports establishment of plans to achieve company goals and defines projects aligned with these plans; key performance indicators of operational performance could be improved and product time-to-market could be shortened [14].

The gain in process understanding and hence improved control of manufacturing processes are the main benefits in scientific field: predictive models have to be put in place in order to respond to process deviations and therefore obtain consistent product quality. In contrast to conventional In-Process Controls (IPC), in-line PAT measurements allow monitoring of the entire manufacturing process in real-time instead of collecting single point data at different time intervals. Hence, process trajectories of successfully manufactured batches can be better established using PAT.

Although more batches not meeting the predefined release criteria may be inadvertently identified by PAT measurements, statistical simulations suggest that considering larger sample sizes would lead to fewer batch rejects in routine production. Additionally, traditional sampling complicates continuous improvement, because the required number of samples is at least hundreds to detect changes in process capability [6]. Even more important, PAT can reduce time-to-market of a product by decreasing failure rates during development and therefore directly influences profitability [15].

However, adoption of process analytical technology in the pharmaceutical industry continues to face a number of barriers, which can be broadly classified into three categories: real and perceived technological barriers, lack of economic incentive and regulatory disincentives [6]. The general confidence in use of advanced multivariate modelling in pharmaceutical manufacturing is still lacking. Concerns also exist regarding extended inspections and triggering additional authority questioning when implementing PAT.

Moreover, PAT is sometimes considered as labour-reductive which may be perceived as a risk by the operating personnel. This is unlikely, but new personal skills and capabilities may be required.

The main argument of the industry to be reluctant to full application of PAT is the concern of being non-compliant to regulatory requirements. But if there is no possibility to adjust processes when variability in raw materials or in the manufacturing processes is detected, PAT does not bring an extensive value, but requires a lot of additional documentation.

A study on return on investment when deploying PAT and Lean Manufacturing, realised by Cogdill et al. [16], revealed that many pharmaceutical companies could benefit by improving the manufacturing performance. Due to the FDA definition of PAT, which focuses on quality management, Lean Management has not been an integral component of PAT applications, but could be used to deploy the maximum benefit [16].

1.2.2 PAT tools

Process analytical technology is considered as a toolbox of different techniques and includes:

- Multivariate tools for design, data acquisition and analysis e.g. Design of Experiments
- Process analysers: in-line and on-line measurement techniques including advanced spectroscopic tools as well as temperature or pressure monitoring during manufacture
- Process control tools
- Continuous improvement and knowledge management tools [17].

Meanwhile, a number of advanced measuring techniques are available which are capable to meet the requirements of PAT. The best-known is probably NIR-spectroscopy, which is a very versatile tool and is applied for raw material identification [18], during granulation [19] and blending processes [20], analyses of tablet hardness [21] and dissolution of matrix tablets [22] as well as investigation of drug products even after packaging [23].

Another common spectroscopic technique is in-line Raman spectroscopy, which can be applied to monitor processes correlated to API manufacturing, but also to control different manufacturing processes of drug products [24].

Currently, Terahertz literature is more extensively used for in-line and at-line determination of film-coat thickness [25] – [30].

Moisture-monitoring during fluid bed processes can either be realised by NIRS [31] or microwave resonance technique [32], [33].

For in-line or on-line particle sizing in fluid beds, particle probes as the Parsum probe [34], [35] or the Lasentec probe, of which the measuring principle is Focused Beam Reflectance Measurement [36], [37] are used.

This thesis focuses on two measuring tools: the Parsum probe for particle size measurements and near infrared spectroscopy for quantitative determination of moisture and API content. Both techniques are considered as appropriate to enhance process understanding during process development and scale-up of a NCE in the sense of the PAT initiative and therefore support the accomplishment of a FDA demand, which involves "Meeting the needs of tomorrow"[5].

2. OBJECTIVES

The multiple applications of process analytical technologies and the obtained benefits during process development and scale-up of solid dosage forms are analysed based on two different projects. The discussed development projects are in the stage of process development, both dealing with fix-dose combinations of two active pharmaceutical ingredients (API).

The objective is to enhance the understanding of the most critical manufacturing step in the process chain by means of several PAT techniques. These techniques include different PAT tools as well as advanced statistical methods. Their combination is intended to support effectively process development of solid dosage forms by assessing effects of varied process parameters during manufacturing. Sometimes, standard and compendial IPC data show no difference but in-line measurements allow a deeper insight into the process by generating much more data points and delivering results in real time. Moreover, sampling during manufacture is not necessary when measuring in-line. Sampling itself may disturb the process or lead to inadvertent process-interruptions. Therefore, the application of PAT tools and the resulting knowledge gain is to be investigated during process development and scale-up activities to production site.

The unit operation of Project A which is most critical and extremely affects downstream processability is a fluid bed granulation. At first, the comparability of the Parsum probe, a new tool for in-line particle size measurements, to conventional sizing methods is to be proven. Then, its benefit for process optimisation with regard to the effect of filter-dedusting and the effects of process parameters on median particle size is investigated.

Additionally, a method based on near infrared spectroscopy is developed for in-line moisture determination during the granulation process. The use of PAT tools to support process development, to enable development of predictive process models and to facilitate scale-up of manufacturing processes is discussed.

Project B is based on an active coating process, where a film-coating suspension containing API is sprayed onto tablet cores. The first goal here is to systematically screen critical process parameters by means affecting the uniformity of API content of film-coated tablets by means of a Design of Experiments and thus support gain of process knowledge.

Moreover, an estimation of the feasibility of near infrared spectroscopy for determination of the coating end-point is to be given and the effort for validation of the developed method is to be demonstrated. This feasibility study is considered as exploration of the potential of a NIR quantification model for low dosed APIs. In this case, the challenge is to prove the general feasibility of the substitution of a time-consuming and destructive method by an at-line spectroscopic method.

Although there are undoubted benefits of the application of PAT principles during development, plenty of concerns still exist with regard to submission of PAT data. Therefore, regulatory requirements for submission of PAT data are compiled to allow an overview of existing guidances.

3. INSTRUMENTS AND METHODS

3.1 NEAR INFRARED SPECTROSCOPY

3.1.1 Historical development

For a long time, NIR spectroscopy (NIRS) was considered as a "sleeper" compared to other spectroscopic techniques, because the chemometrics behind were unknown, illogical or presumed to be illegitimate [38]. The associated wavelength region was discovered and described by Sir William Herschel as early as in 1800 [39], when he diffracted sunlight with the aid of a prism. But for a long time, nearly no use was made of this discovery.
It was in the 1960s, when Karl Norris published his work using near infrared spectroscopy for analysing agricultural products, reprinted in 1996 [40].
The exploit of NIR spectroscopy began with the progress of the computational power in the 1980s. Computers are of great importance for NIR data acquisition and evaluation. Nowadays, NIR spectra are recorded and evaluated extremely fast and sophisticated software allows the interpretation of complex spectra even without profound expertise. As a result, NIRS is now used in plenty of different industries. Beside the agricultural and food industry, the technique is also applied in most manufacturing industries as in semiconductor industry [41] and in refining industries for classification of motor oils [42]. Moreover, this tool is applied in medicine e.g. for non-invasive blood glucose tests [43].
Today, its use is so widespread, that T. Davies announced that the "giant" among spectroscopic techniques had been woken up [44].

3.1.2 Physico-chemical fundamentals

3.1.2.1 Spectral region of near infrared radiation

The near infrared (NIR) spectral region is defined as the region between the visible and the mid-infrared (MIR) wavelength range. The spectral region extends from 780 nm to 2500 nm according to the European Pharmacopoeia [45]. As it is more common to refer to the wavenumbers as in the mid-infrared region, this means about 12500 cm^{-1} to about 4000 cm^{-1}. The location of the NIR radiation in the electromagnetic spectrum is depicted in Figure 2.

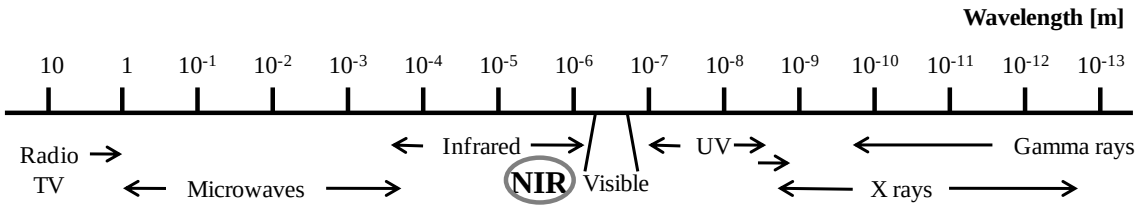

Figure 2 Electromagnetic spectrum

The wavenumber $\tilde{\nu}$ is the reciprocal of the wavelength λ and is typically in spectroscopy expressed in the unit cm^{-1}.

$$\tilde{\nu} = \frac{1}{\lambda} \qquad \text{Eq. 1}$$

Hence, the wavenumber is directly proportional to the frequency of the absorbed radiation and also to its energy.

3.1.2.2 Vibrations

NIR and MIR spectroscopy are both vibrational spectroscopic techniques which detect absorption of radiation due to vibrations of atomic bonds. The uptake of specific energy quanta induces stretching and deformation vibrations of atomic bonds and a change in the respective dipole moment. In contrast, changes in the dipole moment due to molecule rotations are induced and detected in far infrared spectroscopy.

3.1.2.2.1 Stretching vibrations

The change of the inter-atomic distance along the bond-axis is called stretching vibration. Stretching vibrations of several atomic bonds can be either symmetric or asymmetric. A schematical illustration of these two stretching vibrations is presented in Figure 3.

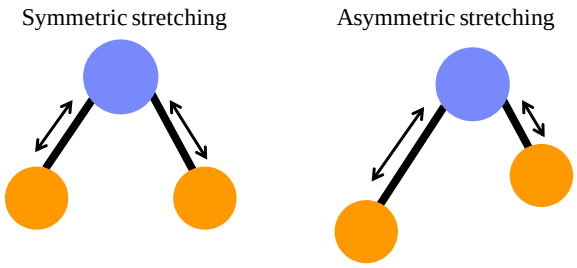

Figure 3 Symmetric and asymmetric stretching vibrations

3.1.2.2.2 Bending vibrations

Bending or deformation vibrations change the angle between two atomic bonds. These changes occur as in-plane or out-of plane vibrations. The differences are illustrated in Figure 4.

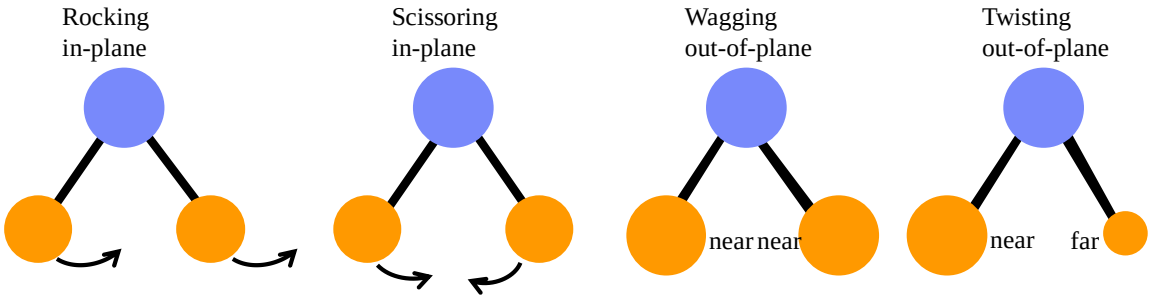

Figure 4 Types of bending vibrations

3.1.2.2.3 Fundamental, overtone and combination vibrations

At room temperature, molecules are in their ground state of energy. By irradiation of material with infrared light, specific energy quanta can be absorbed and higher levels of energy can be attained.

The vibrational frequency v is described in the following equation, when considering a diatomic oscillator and is dependent on the force constant of the bonding strength between the atoms (f) and the reduced mass (μ).

$$v = \frac{1}{2\pi}\sqrt{\frac{f}{\mu}} \qquad \text{Eq. 2}$$

The reduced mass of two atoms with the masses m and M is defined as:

$$\mu = \frac{m*M}{m+M} \qquad \text{Eq. 3}$$

Figure 5 illustrates schematically the potential energy and the related energy levels according to the harmonic and anharmonic oscillator model. Contrary to the harmonic oscillator model, which is symmetric and parabolic in shape, the anharmonic oscillator model is characterised by a dissociation level, which means that the interatomic distance cannot be infinite but approaches a dissociation level. Moreover, experiments showed that deviating from the harmonic oscillator model, the distances between succeeding vibrational energy levels (v) are not equal.

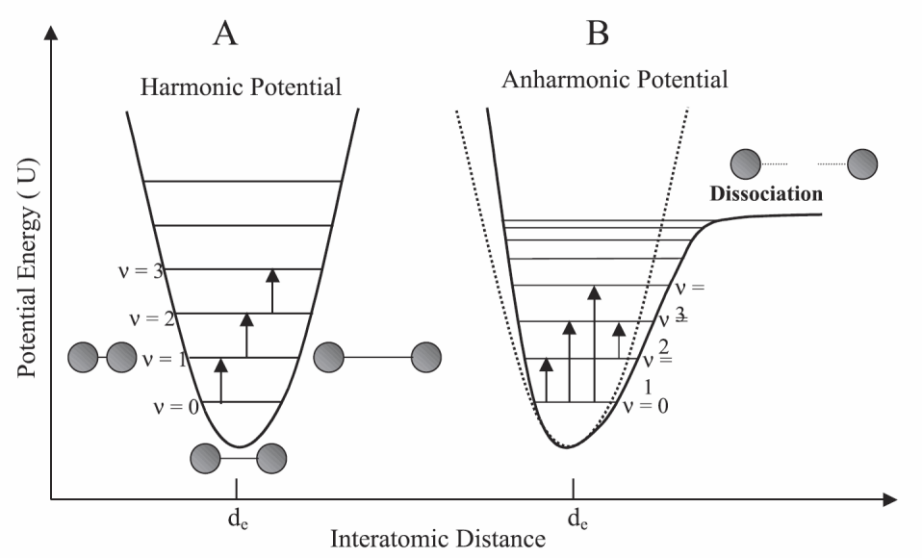

Figure 5 Harmonic (A) and anharmonic (B) oscillator model [46]

The transition from the ground state (v = 0) to the first excited energy level (v = 1) is called fundamental transition of which the occurrence is most probable and the required excitation energy is lowest. The resulting absorption peaks, which can be found in the mid-infrared wavelength range, are of high intensity.

Selection rules according to classical quantum mechanics allow transitions to the next energy level, whereas transitions over multiple energy levels are “forbidden transitions”. These so-called overtone vibrations are mainly detected in the NIR range.

The first overtone vibration is thus the transition from the ground stage of energy v = 0 to the level v = 2, second overtone vibrations overcome the energy difference from v = 0 to v = 3. The probability for the transitions of 1^{st} and 2^{nd} overtone vibrations is low, thus the intensity of their absorption peak decreases compared to IR spectroscopy which focuses on fundamental oscillations. NIR radiation is applicable to excite these oscillations since its energy is higher than of mid-infrared light.

Beside of overtone vibrations, combination vibrations are also induced by NIR radiation. The frequency of combination vibrations corresponds approximately to the sum of frequencies of multiple fundamental vibrations.

Moreover, the relatively low probability of overtone and combination vibrations corresponds to the low absorptivity in NIR spectroscopy. This fact is appreciated by the users since there is no necessity of time-consuming sample preparation like diluting or manufacturing of a pellet compressed of a mixture of the sample and potassium bromide, as it is necessary for the mid-infrared spectroscopy.

Due to the fact that overtone vibrations require a high degree of mechanical anharmonicity of the vibrating atoms in the molecule which means a profound difference in the mass of the vibrating atoms, mainly C-H, N-H, S-H and O-H bonds are NIR-active.

Detection of overtone and combination vibrations results in an absorption spectrum in which the peaks are in a high degree overlapping and not as distinct as in an IR spectrum. Hence, chemometric techniques are required to interpret the complex NIR spectra. An overview over the chemometric techniques which have been carried out in context with this work is given in chapter 3.1.5.

3.1.3 Near infrared spectrometer

Near infrared spectrometers consist of a light source, a filter, grating or interferometer system with a wavelength range in the NIR region and an appropriate detector typically of lead sulphide or indium gallium arsenide to collect and measure the light transmitted or reflected by the sample [47].
Several types of NIR spectrometers are widespread used: interference-filter spectrometers, grating based dispersive, acousto-optic tuneable filter units or multichannel Fourier-transform- (FT-) spectrometers [48]. The difference between dispersive and FT-spectrometers is illustrated below.

3.1.3.1 Dispersive spectrometer

The wavelengths are observed sequentially in a dispersive spectrometer, when the diffracting element e.g. a prism or a moving grating is scanned. The dispersive element separates individual frequencies from the radiation emitted by the light source. The radiation passes through the sample and is measured by a detector. This method is time-consuming, since only one wavelength is measured at the same time.

3.1.3.2 Fourier-transform spectrometer (Michelson interferometer)

FT-spectrometers collect all wavelengths simultaneously (Multiplex or Felgett Advantage). FT-NIR-spectrophotometers equipped with interferometers recover the intensities of individual wavelengths in the NIR region. This technique is advantageous concerning the achieved wavelength precision and accuracy as well as the resulting high signal-to-noise ratio and scan speed.
FT-spectrometers are usually based on the Michelson interferometer (see Figure 6). This interferometer consists of a beam splitter (e.g. a semi-transparent mirror) and two mirrors, a fixed one and a precisely movable one. Light from the source is divided into two beams by the beam splitter. One beam is transmitted through the splitter to the stationary mirror; the other beam is reflected to the movable mirror. The radiation is reflected back from the respective mirror to the beam splitter. There the beams are superimposed, but again separated into two beams: one illuminating the sample and reaching the detector, the other one being reflected back to the source.

For measurements, the distance of the movable reflection mirror to the beam splitter is varied and the intensity of interference is measured at the detector. This intensity of interference is called interferogram [49].

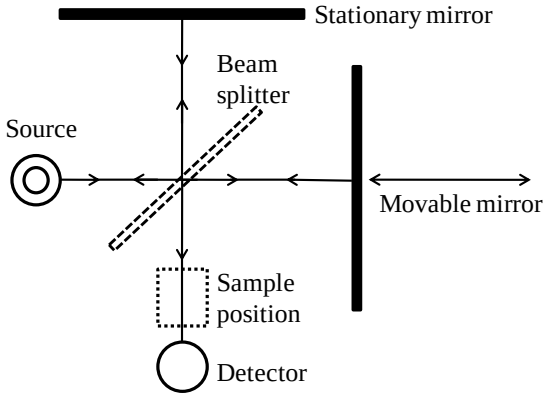

Figure 6 Michelson interferometer

The collected interferogram is transformed to a frequency-domain single-beam spectrum. For calculating the reflectance spectrum, a reference spectrum is subtracted from the single-beam spectrum. Usually, reflectance spectra are converted into pseudo-absorbance spectra which are calculated as the negative logarithm of the reflectance [50].

FT-spectrometers offer several advantages compared to dispersive spectrometers [49]:

- Jacquinot´s advantage or the advantage of optical throughput:
  A large number of photons is guided into the optical system and can be effectively collected because no slits are needed in the spectrometer.
- Fellgett´s advantage or the advantage of multiplexing:
  All wavelengths are detected simultaneously by a single photodetector in contrast to dispersive spectrometers, which detect only one wavelength at a certain time point.
- Connes´advantage:
  Spectra with high wavenumber precision can be obtained because a laser beam of short wavelength is used to measure precisely the position of the movable mirror.

3.1.3.3 Multi purpose analyzer

The NIR spectrophotometer used for this work is the Multi Purpose Analyzer (MPA, Bruker Optics, Ettlingen, Germany), presented in Figure 7. This is a FT-NIR spectrometer equipped with a fibre optic probe for measurements in diffuse reflection mode, an integrating sphere for reflection measurements as well as an external transmission unit. Using the transmission mode, either tablets or liquids can be measured. Diffuse reflection mode is mainly applied for in-line measurements with the probe inserted directly into the manufacturing equipment, e.g. during fluid bed granulation processes. The corresponding software is OPUS version 6.5 (Bruker Optics, Ettlingen, Germany), which was used for measuring and development of the NIR methods discussed in this work.

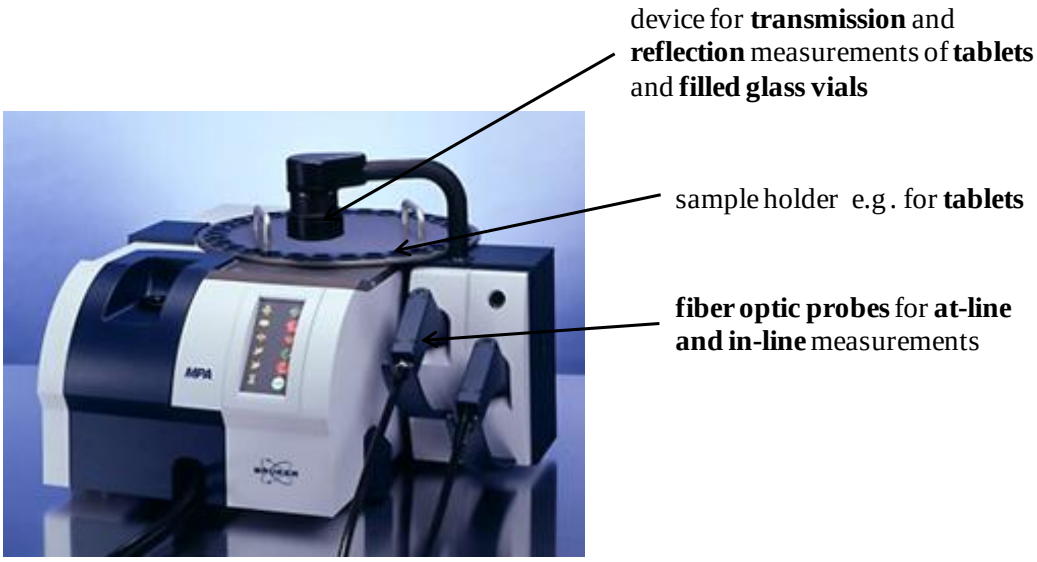

Figure 7 Multi Purpose Analyser and measuring equipment from Bruker Optics [51]

NIR measurements in the framework of Project A were realised by using the probe in diffuse reflection mode in an in-line set-up. The fibre optic probe consists of 14 fibres, the radius of its light spot is approximately 3 mm and the effective wavelength range reaches from 500 nm – 2500 nm.

NIR spectra for Project B were recorded using the probe for at-line measurements of tablets in a homemade set-up. The second approach for tablets refers to the diffuse reflection measurements by means of an integrated sphere. This set-up is usually applied to measure solids or liquids in a glass vial by minimises disturbing influences of straylight with a cap. The illuminated diameter using the integrating sphere for reflection mode is approximately 15 mm.

3.1.4 Acquisition of spectral data

In general, NIR spectra are collected using one of the following three measuring modes: transmission, diffuse reflection or transflection.

3.1.4.1 Transmission

Measurements in transmission mode detect the radiation which has passed through the sample. This mode of data acquisition is typically known from UV-VIS spectroscopy of liquid samples.

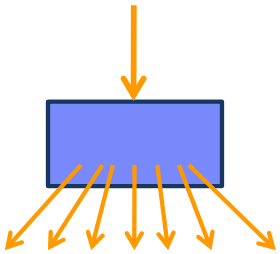

Figure 8 Transmission

Transmission is defined as the fraction of incident radiation I at defined wavelengths which can be detected after radiation with the intensity I_0 has been passed through a sample [45].

$$T = \frac{I}{I_0} \qquad \text{Eq. 4}$$

For measurements in transmittance mode, the sample is placed between the optical light source and the detector. The result can be either expressed in transmission or absorbance values [45].

$$A = -log_{10}\, T = log_{10} \left(\frac{1}{T}\right) \qquad \text{Eq. 5}$$

The transmission mode is often applied when tablets or liquids are to be analysed. The relatively high penetration depth in the sample is advantageous, while at the same time, the sample thickness which can be measured is limited.

3.1.4.2 Diffuse Reflection

The cumulative effect of the phenomena absorption, refraction and reflection on solid surfaces is defined as diffuse reflection.

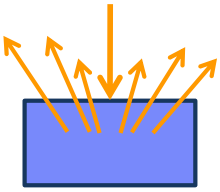

Figure 9 Diffuse reflection on solid samples

The ratio of the intensity of light reflected by the sample to the one reflected by a reference surface is measured in reflectance spectroscopy. Most frequently applied reference surfaces are gold and ceramic standards. Considerations should be given to physical attributes of the sample such as packing density, sample depth and variations in measuring e.g. probe pressure, sample cell variation and coverage of detector window [47].
The relation between scattering coefficient (S) and absorption coefficient (K) in diffuse reflection is described in the Kubelka-Munk-Equation, explained e.g. by W. Kessler [52] and P. R. Griffiths and J.M. Olinger [53]. R'_∞ is defined as the reflectance of a sample of infinitely small thickness and low absorptivity.

$$f(R'_\infty) = \frac{(1-R'_\infty)^2}{2R'_\infty} = \frac{K}{S} = \frac{2.302 * \varepsilon * c}{S} \qquad \text{Eq. 6}$$

It can be derived from this equation that the reflectance of a sample is only dependent on the ratio of the two constants K and S, and not of the absolute values of absorption and scatter. Moreover, it can be used for quantitation, since it is related to the concentration c of an analyte with the absorptivity ε.

3.1.4.3 Transflection

Transflection measuring mode is a hybrid of transmission and reflection [48].
A reflection plate behind the sample reflects the transmitted radiation back through the sample to the detector which is located in front of the sample and thus on the same side as the light source. Using this technique, the incident radiation passes twice the sample.

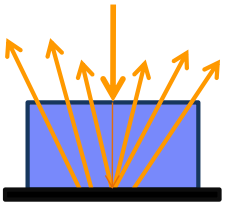

Figure 10 Transflection

3.1.5 Data mining - Chemometrics

Chemometrics implies the application of mathematical and statistical methods in order to plan, develop or evaluate experiments and results. Furthermore, a maximum of chemical information can be assessed by using these multivariate data analysing techniques.
The term “chemometrics” was first applied by Svante Wold in 1972.
Chemometrics is applied in order to build up either a descriptive model for the relationships and structure of a system or to use it for quantitative prediction of the properties of the system. Multivariate data analysis constitutes an important part of the chemometrics and is needed for quantitative evaluation of NIR spectra.
Mathematical tools which are often applied in this field are Multilinear Regression, Principal Component Analysis (PCA), Partial Least Squares (PLS) and cluster analysis.
The multivariate models in this work are computed applying PCA and PLS, thus those two are shortly in section 3.1.5.2 and 3.1.5.3, respectively.

3.1.5.1 Design of Experiments

Design of Experiments (DoE) is the term used for statistical techniques applied to study the effects of multiple variables simultaneously and economically. Sir A. Fisher was the first who used DoE to investigate growing conditions for crops in the early 1920s [54].
Design of Experiments covers the identification of important factors influencing the process, the planning and set-up of experiments, running and evaluating the trials and optimising the process based on the results. Factors or input variables can be either continuous (e.g. temperature) or discrete (e.g. synchronous or asynchronous filter-dedusting). If both the factors and the result are continuous and thus quantifiable, a quantitative model can be generated to describe the effects of factors at random levels.

The dependent variable is the result of the experiment, often termed response, which can be predicted by applying the model equation on any combination of settings of the independent factors inside the design space.

DoE replaces the former approach "Trial-and-Error", which is mainly based on experience. Experiments are carried out changing only one factor at a time, by keeping all other factors constant. This leads to a huge number of trials needed, since every possible combination is to be tested. Despite of the large number of experiments, the interaction of factors can not be assessed and optimisation of parameter setting is difficult to achieve.
The more efficient approach of DoE requires fewer trials, but thorough selection of parameter settings and changing multiple parameters at the same time. Usually, the factor settings are standardised for running the experiments by using the descriptions high (+), low (-) and zero (0).
Design of Experiments implies three principles [55]:

- Randomisation: the experiments are performed in random order to prevent uncontrollable factors or trends over time biasing the results,
- Replication for assessing the inter-batch variation for constant settings, and
- Blocking: the effect of a nuisance factor, which are known and controllable but not of interest, is systematically eliminated.

There are plenty of different experimental designs possible, all of them using extreme combinations of factor settings and the centre point, which is obtained by setting all investigated factors to a medium setting. The design can be either full factorial or fractional factorial. Full factorial means testing all corners of multidimensional design, while fractional factorial designs require only a part of these trials.
For instance, a DoE considering three variables would require $2^3 = 8$ trials (corresponding to the eight corners (blue) of the cube in Figure 11 for a full factorial design plus potential centre point runs (orange) and replicates. A fractional factorial design would rather incorporate only a part of these trials, given as green corners in Figure 11. The resolution of fractional designs is lower than for full factorial ones due to partly aliasing main effects and interactions.

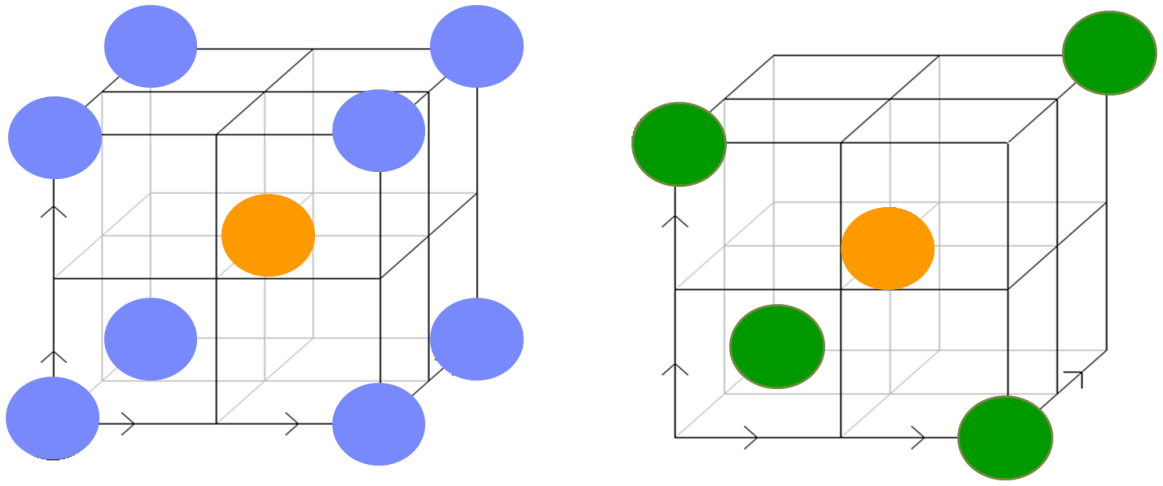

Figure 11 Full factorial and fractional factorial design for three factors including a centre point

Response surface designs are often applied when a statistical model is built based on the results and optimal combinations for factor setting in order to obtain a desired response can be calculated. The effect of investigated parameters is most frequently assessed by evaluating the analysis of variance (ANOVA). This formal statistical method breaks down the total observed variability in the response into separate effects due to the factors and their interactions. Moreover, the statistical significance of each effect is determined [56].

The definition of DoE, expressed in the words of Mark Anderson [57]: “DoE takes some of the art out of experimentation, replaces it with science, and yields better results.”

3.1.5.2 Principal Component Analysis

The procedure of Principal Component Analysis (PCA) was published by Karl Pearson in 1901. PCA aims at reducing plenty of observed variables to a small number of latent variables. The latent variables are called factors or principal components. These factors are linear combinations of the original ones meaning that they are constituted of the linear sum of the weighted original variables [52].

The mathematical procedure uses an orthogonal transformation: the first principal component accounts for most of the variability in the data set and each succeeding one account itself for most of the remaining variability. Moreover, each principal component is supposed to be orthogonal to the previous one.

The loading describes the proportion of the factor with regard to the total variance of the matrix.
Each object of the original data set is transformed using the principal components as factor space. Then scores can be considered as the coordinates in the multidimensional factor space.

3.1.5.3 Partial Least Squares Regression

Partial Least Squares Regression (PLS) is related to PCA. The principal components are not chosen in the way that they account for as much as possible of the variance in the data set, but to explain as much as possible of the observed variables. Thus the structure of the y-data is not only used for the regression, but also for determination of the principal components.
A major limitation of this technique is the probability of chance correlations. Spectral variations which are present in the calibration spectra may be correlated to the targeted analyte without being caused by features of the analyte. Therefore some critics assume PLS to work in a "black-box" manner [58].

3.1.5.4 Validation of regression models

The performance of the computed calibration models is usually assessed by validation procedures. There are two distinct approaches, external and internal validation, which are described in 3.1.5.4.1 Test Set Validation and 3.1.5.4.2 Cross Validation, respectively.

3.1.5.4.1 Test Set Validation

Test Set Validation is an external validation approach. Two separate sample sets are required for calibration and validation. A calibration model is computed based on one sample set which is then used to predict the values of the other sample set.
The Root Mean Square Error of Prediction (RMSEP) is appropriate to evaluate the validity of the calibration model. It is calculated based on the following equation:

$$RMSEP = \sqrt{\frac{\sum_{i=1}^{n}(Y_{REF\,i} - Y_{PRED\,i})^2}{n}} \qquad \text{Eq. 7}$$

Y_{REF} is the reference value e.g. the content of active in a pharmaceutical dosage form. The difference of the reference value and the value predicted by the calibration model, Y_{PRED}, for each of n samples in the test set contributes to the RMSEP.
Some caution is required when performing a Test Set Validation: the test set has to be representative for the collective data set composed of calibration and test data [11]. Hence, Test Set Validation is not suitable for assessment of trends if data is classified by time.
The calculation speed for Test Set Validation is higher than for Cross Validation especially if high numbers of spectra are covered.

3.1.5.4.2 Cross Validation

Cross Validation (CV) is an internal validation approach using the same data set for calibration and validation but mimicking to validate the calibration model on independent test data. But contrary to the external validation, it does not waste data for testing only.
In full CV with n calibration spectra, one repeats the calibration n times, each time treating one spectra of the whole calibration set as prediction object [59].
For each calibration procedure, the calibration model is constructed without the removed sample or a segment of correlated samples from the calibration data set. The predicted values for the left-out samples are used for calculating a calibration error. These single values are condensed in the Root Mean Square Error of Cross Validation (RMSECV).

$$RMSECV = \sqrt{\frac{\sum_{i=1}^{n}(Y_{REF_i} - Y_{PRED_i})^2}{n}} \qquad \text{Eq. 8}$$

Y_{REF} accounts for the reference value, while Y_{PRED} stands for the predicted value of the cross validation cycle and n refers to the number of samples in the training set [60].
The RMSECV is often applied to evaluate the performance of a calibration model.

3.1.6 Data pre-processing

Data pre-processing techniques are mathematical procedures which are applied in order to minimise noisy influences on the NIR spectra. The target is to increase the information level of the desired spectral features, while other spectral influences shall be minimised.
These techniques are no substitute for accurate data collection, but can increase the grade of information in the spectra. Especially for solid samples, undesired variations are primarily caused by light scattering. These undesired variations often constitute the major part of the total variation in the sample set, and can be observed as shifts in baseline and other phenomena called non-linearities [61].
Other reasons for spectral variations can be the interaction of compounds due to intermolecular forces e.g. hydrogen bonds, path length variations and spectral distortions like baseline and wavelength shift or stray light [49].
For some applications, the level of scatter is not regarded as noise, but used to determine physical parameters of the sample. In these cases, pre-processing techniques are applied to intensify the information of scatter e.g. for the determination of particle sizes of granules by NIRS.

Generally, two categories of data pre-processing techniques are distinguishes: derivations and corrections of scatter effects. The most important of these techniques are described below.

3.1.6.1 First derivation

After first derivation of spectra, drifts of the baselines are levelled out and the spectral resolution is increased. Overlapping peaks can be separated by derivation and therefore quantitative evaluation is facilitated.
Calculation of the derivation is usually performed using a smoothing filter according to Savitzky-Golay, where derivations are carried out using a polynomial fit.
First derivatives are often applied when a constant background is to be removed [62].

3.1.6.2 Second derivation

The advantages of second derivation are the same than for the first derivation, but besides equalising baseline effects like first derivation, also linear scatter effects are removed.

3.1.6.3 Multiplicative Scatter Correction

An average spectrum out of all calibration samples is used to estimate the scatter effect on the spectra. Then the other spectra are corrected based on the assumption that they contain the same level of scatter. Each spectrum is fitted to the average spectrum using a Least-Squares approach [62].
This Multiplicative Scatter Correction (MSC) is mainly used for spectra which have been recorded in diffuse reflection mode, when the samples have inhomogeneously distributed centres of scatter. Since scatter effects are dependent on the wavelength and the refractive index, they differ over the whole spectrum; scatter effects are more intense in the range of small wavelengths.

3.1.6.4 Standard Normal Variate transformation

The procedure was described in detail by Barnes in 1989 [63]. Standard Normal Variate (SNV) transfomation removes slope variation of spectra. This technique is based on the calculation of an average spectrum, which is constituted of the average absorption values of the chosen spectra for each wavelength. This average spectrum is then subtracted from the original spectrum. This centres the spectrum near the baseline. Additionally, the standard deviation of the spectra is calculated and each absorption value of the respective wavelength is then corrected according to the equation below:

$$x_{i,SNV} = \frac{(x_i - \bar{x})}{\sqrt{\frac{\sum_{i=1}^{p}(x_i - \bar{x})^2}{p-1}}} \qquad \text{Eq. 9}$$

$\bar{x}$ is the average value for all absorption values of the whole spectrum. The denominator is the standard deviation over all spectra.
The results of SNV are very similar to the ones of MSC.

3.1.7 Performance parameters of calibration models

The following chapters explain some of the most important performance parameters of calibration models, by means of which the quality of calibration methods can be assessed.

3.1.7.1 Bias

Systematic differences from the reference values are referred to as bias. Its value should be close to zero; otherwise the calibration model seems to be erroneous.

3.1.7.2 Coefficient of determination

The coefficient of determination (R^2) is the proportion of variability which is accounted for by the calibration model and is appropriate to assess the predictive ability of the model. It gives information about the goodness of fit of the model.
The more its value approximates 100%, the better is the model.

3.1.7.3 Prediction error

The prediction error of a calibration model consists of two parts: one can be seen as remaining interference error due to unmodelled interferences in the data set and the other one is called estimation error due to random noise. Prediction error can often be reduced by using more or better data, by improving the model or by simplifying the calibration data set.
Martens and Næs [59] illustrate the prediction error as a function of the complexity of the model. Underfitting considers a too small number of principal components, overfitting in contrast too many. Although overfitted models are characterised by high coefficient of determinations, they yield in bad prediction results for unknown samples. Both over- and underfitting result in insufficient modelling and therefore low prediction performance.

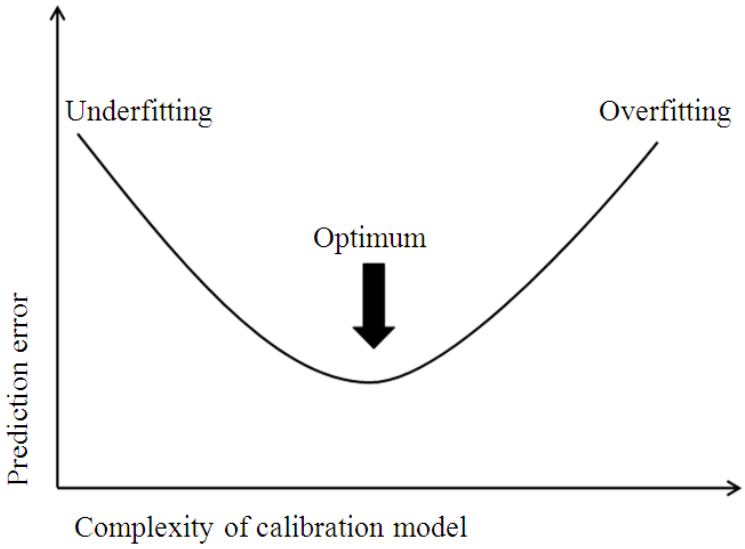

Figure 12 Prediction error as a function of the complexity of the model based on [59]

The performance of the calibration model can be assessed by comparing the Standard Error of Prediction (SEP) to the standard deviation of the reference method.

$$SEP = \sqrt{\frac{\sum_{i=1}^{n}(Y_{REF\,i} - Y_{PRED\,i})^2}{n-1}} \qquad \text{Eq. 10}$$

3.1.7.4 Precision and Accuracy

Precision of a measuring system includes repeatability and reproducibility of the test results. The former one is variation in measurements of a sample which are carried-out by the same operator on the same equipment under the same conditions; the latter is considered as the conformance between measurement results of the same sample under different conditions. Different conditions can be either understood as different instruments or changing operators.

The residual standard deviation measures the deviation of the experimental values from the regression line, thus representing an indicator of the precision of the regression. The relative residual error can be comparable to the relative standard deviation obtained in precision studies [64].

Figure 13 elucidates the difference between precision and accuracy: Precision describes the width of a probability distribution for obtaining a certain value for the same sample.

Opposed to this, accuracy characterises the deviation between predicted values and reference values, of which the latters are considered as ‘true’.

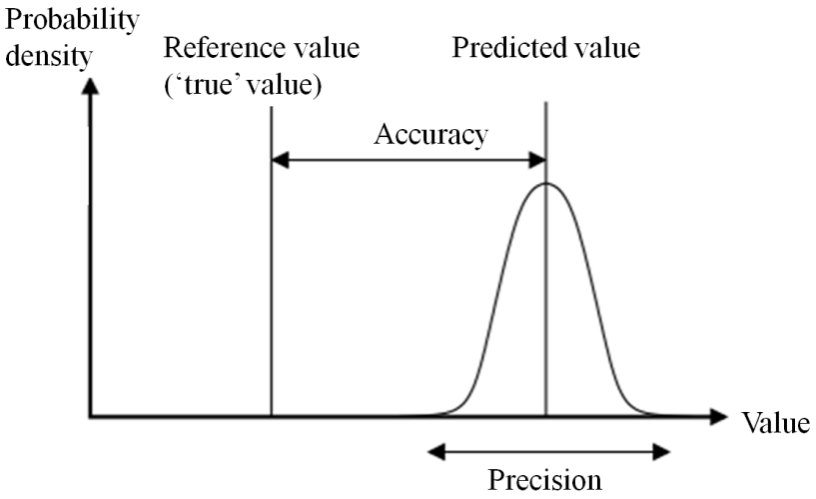

Figure 13 Distinction of precision from accuracy

3.1.8 Advantages of near infrared spectroscopy

Near infrared spectroscopy is a highly advantageous technique compared to other techniques like MIR spectroscopy.

Due to different possible measuring modes, almost all kind of samples can be measured. It can be widely applied since both qualitative (e.g. identity tests) and quantitative evaluations are possible.

For most applications, time-consuming sample pre-treatment is not necessary; the sample can be directly measured because of low absorptivity of NIR radiation. This allows the use of NIRS during the manufacturing process. The penetration depth is higher than in IR spectroscopy, but the analysis is rapid and non-destructive. Thus it is appropriate to be applied in-line during manufacturing processes, for instance of pharmaceutical drug products and can support real time release testings.

Moreover, physical and chemical properties can be analysed simultaneously by a single measurement since the diffusely reflected light contains information on both attributes [61].

Besides, substitution of conventional destructive analyses by NIR spectroscopy decrease analysis time and cost. Furthermore, worker´s safety is improved by reducing handling of

and exposure of analysts to hazardous chemicals. More importantly, implementation of this approach can lead to an improved quality control [65].
Therefore, NIRS is considered to be one of the most flexible and efficient techniques in spectroscopy.

3.1.9 Disadvantages of near infrared spectroscopy

The development of a NIR calibration model for quantitation is challenging and time-consuming. Plenty of samples have to be manufactured especially for calibration purpose, which is particularly difficult in a manufacturing environment. Hence, calibration samples are usually manufactured on laboratory equipment using respective material and processes. Nevertheless, even deviations such as using another press type for compression into tablets can lead to calibration models which are not applicable for real manufacturing processes. An example for a biased calibration model based on synthetic calibration samples was described by Sarraguça et al. [66].
Furthermore, NIR models for quantitation rely on reference methods, which themselves contain a certain degree of variation. This test method can be the major source of variation in NIR prediction results of calibration models [67].
Moreover, it is necessary to correct or update existing NIR calibration methods when a drift whether slope or bias error is obvious. This can be due to process or measurement equipment age, environmental conditions change or the application of new lots of raw materials [68].
The effective sample size in near infrared analysis is often significantly smaller than for conventional methods because the illuminated area of the sample is usually relatively small due to the area of the beam. Therefore, heterogeneity on a ‘micro’ scale can be detected by NIRS, but may not be consistent with results of reference methods [47].

3.2 SPATIAL FILTERING VELOCIMETRY

Spatial Filtering Velocimetry (SFV) – or Spatial Filter Velocimetry as it is termed by other authors) – is applied for the determination of particle size distributions.
This technique aroused more and more attention in the pharmaceutical industry during the last five years. The velocity of moving particles is measured and these data are then translated into particle size information.

The measuring principle of the probe applied in this work, the Parsum probe IPP 70-Se (Parsum, Gesellschaft für Partikel-, Strömungs- und Umweltmesstechnik mbH; Chemnitz), and applications of this tool in pharmaceutical manufacturing are described in the following chapters.

3.2.1 Measuring principle of the Parsum probe

The Parsum probe is based on a modified spatial filtering technique and contains a fibre-optical array and a single fibre for spot scanning. The measuring principle was explained in detail by Petrak [69]. The spatial filter converts light obscuration signals into particle size information, more precisely, into chord length information of the measured particles. The measured chord length is the distance between two points on the outline of the analysed particle in its direction of moving [34]. Hence, the measured particle size depends on the particle form; but chord length and particle size are equal for spherical particles.

Two signals are necessary for determination of the particle size: first, an obscuration frequency of a fibre-optical array and secondly, the duration of an impulse of a single optical fibre. A scheme of this set-up is depicted in Figure 14.

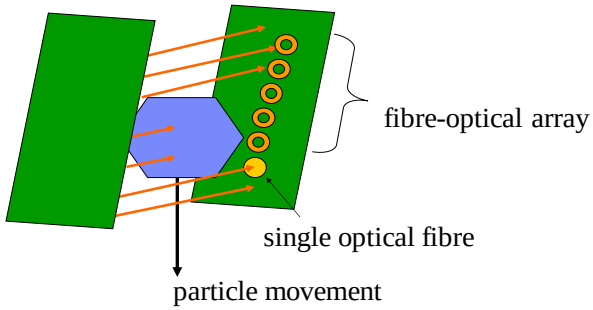

Figure 14 Schematic set-up of the measuring volume of the Parsum probe

A linear array of optical fibres, composed of multiple photodetectors, is illuminated by a laser beam. Each particle passing the measuring volume results in light obscuration on the fibre-optical array. The obscuration of a photodetector leads to an impulse with the same duration than the time of shadowing. The duration of the impulse depends on the particle size (meaning here the chord length in direction of the particle movement) and the velocity of the particle. Several photodetectors produce these obscuration impulses successively which are condensed to a shadow frequency for each particle. Its velocity v is derived from the described shadow frequency which has been described above.

The second signal, the duration t of an obscuration impulse of the single optical fibre is also necessary to calculate the particle size x. The relation between duration t and particle size x is described in the following equation, which takes into account the diameter of the optical fibre d [35]:

$$x = t * v - d \qquad \text{Eq. 11}$$

The generation of the impulse triggered by a moving particle in front of the single optical fibre and its dependence on the particle size are explained in Figure 15.

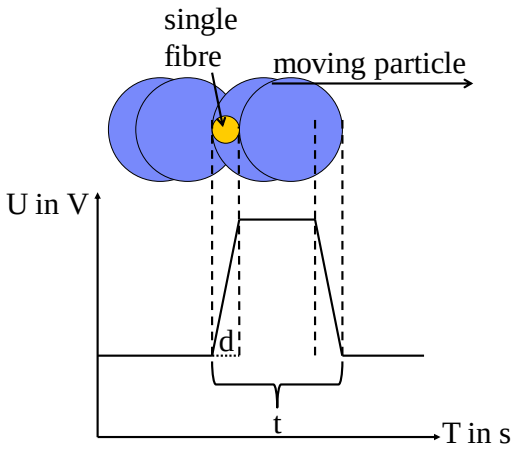

Figure 15 Relation between the duration of the impulse by the single optical fibre and the particle size

The particles are classified into several groups according to the measured chord lengths. Two types of chord length distributions are calculated: a quantity-based distribution and a volume-based distribution. These kinds of particle size distributions are explained in chapter 3.3.5.2.

The measurements are realised by means of the dedicated software (Inline particle probe, version 7.13 (Parsum, Gesellschaft für Partikel-, Strömungs- und Umweltmesstechnik mbH; Chemnitz)).
For in-line measurements during a granulation process, the distribution is calculated out of the total number of values in the circular buffer. A circular buffer stores constantly a defined number of values, replacing the oldest value by a new one. The size of the circular buffer was selected to amount to 10000 particles.
The Parsum probe is able to measure up to 6000 particles per second during the investigated granulation processes and the content of the circular buffer and thus the actual particle size distribution are logged every 20 s. This enables the operator to gain a real-time insight into the manufacturing process, since changes in particle sizes appear instantly on the connected monitor.

3.2.2 Applications of Spatial Filtering Velocimetry in pharmaceutical manufacturing

The measurement range of the Parsum probe extends from 50 µm to 6 mm, thus typical pharmaceutical granules can be analysed.
Parsum measurements can be carried out either in-line or at-line. For in-line applications, the probe is inserted directly into the product vessel e.g. the product container of a fluid bed granulator. At-line measurements are performed by means of a vibrating plate, which is required to bring the particles in motion and to make them pass the measuring volume.

Petrak [70] assumes that the advantages of the Parsum probe e.g. low hardware requirements, the ability of real-time measurement, robust design and reasonable costs are the reason for being applied to more and more different pharmaceutical unit operations such as fluid bed processes, mixing and coating, high shear granulation, spray drying, sieving, grinding and dosing as well as transportation and filling.
Different research papers can be found describing the comparability of Parsum and laser diffraction measurements [35], investigating the effects of liquid feed pulsing during fluid bed granulation using volumetric information from Parsum [71] or analysing the granule size distribution during tabletting in order to detect segregation [72].

With increasing need of the pharmaceutical industry to prove enhanced process understanding when applying for submission of product in the context of the QbD initiative, more and more data is analysed by means of statistical methods. Not only particle size distribution information gained by Parsum measurements can be modelled for multivariate batch modelling, but also parameters measured by default as particle velocities, signal strengths, particle rate etc. These parameters indicate e.g. changes in fluidisation behaviour [34] or can be used together with other process parameters like product temperature to generate a batch progress fingerprint intended to shorten batch release time [73].

3.3 REFERENCE METHODS FOR PROCESS ANALYTICAL TECHNIQUES

3.3.1 Water content by Loss on Drying

The determination of mass lost during a drying process is determined according to the monograph 2.2.32. "Loss on Drying" part d) of the European Pharmacopoeia [45] and a internal Standard Operating Procedure (SOP) and is applied to assess the water content of granules.

This physical procedure implies the drying of the sample until a constant mass is reached [74]. The sample amount of 5 – 7 g is dried for 15 min on a halogen dryer HR 83 Mettler at 105°C. A mass balance measures the difference between the starting mass (m_{start}) and the final mass (m_{end}) of the heated sample.

Preliminary tests proved the assumption, that the total amount of water is dried out of the granulate during this time period without melting the granules.

The result of the LOD test is expressed as per cent mass/mass:

$$Loss\ on\ drying\ (LOD)[\%] = \frac{(m_{start} - m_{end})}{m_{start}} * 100\ \% \qquad \text{Eq. 12}$$

Appropriate pre-treatments are crushing for coarse samples and trituration for samples containing sugar in order to generate a smooth surface and avoid the formation of crusts. The reproducibility for this method is approximately 0.5 percentage points and hence quite high, permitting to use it as common reference method [33].

3.3.2 API content by High-Performance Liquid Chromatography

High-performance liquid chromatography (HPLC) is a widespread technique in analytical chemistry for separation of mixtures of substances and quantifying the analyte of interest. A mobile phase containing the test sample is pumped through columns packed with a stationary phase. The substances are separated due to different interactions between the compounds of the sample and the sorbent as stationary phase, resulting in different retention times of the compounds in the column [75]. The retention time of each compound is determined by passing a detector equipped with an UV spectrophotometer.

The API, analysed in the framework of the Project B of the present work, is extracted out of the tablets by a mixture of methanol and phosphate buffer (pH 1.5) and the extract is run in the reverse phase gradient mode on the HPLC column with a stationary phase consisting of silica of which the surface has been modified by alkyl-chains, in this case octyl-chains. The interactions between stationary phase and the sample are based on hydrophobic interactions. In general, reverse phase chromatography refers to a non-polar stationary phase and a polar mobile phase. The employed eluents are phosphate buffer (pH 3.0) as aqueous part and a mixture of acetonitrile and methanol as organic modifier. Detection was carried by means of a diode array detector at a wavelength specific for the API.
All HPLC tests were carried out in the analytical department of Boehringer Ingelheim.

3.3.3 Content Uniformity

Uniformity of dosage units is required by the European Pharmacopoeia [45], the United States Pharmacopeia [48] and the Japanese Pharmacopoeia [76] and is one of the harmonised chapters. The intention of this test is to ensure the consistency of dosage units: the drug substance content of each unit of a batch has to be within a specified narrow range around the label claim. The uniformity of dosage units can be either performed as content uniformity or as weight variation test. The test for content uniformity is required for film-coated tablets with a dose > 25 mg or a ratio of > 25 % of the active substance in the drug product. It refers to the assay of the individual content of drug substance(s) in a number of dosage units. Performing the content uniformity test implies the determination of the assay of ten individual tablets using an appropriate analytical method and the calculation of the acceptance value (AV) according to the equation below:

$$AV = |M - \bar{X}| + k * s \qquad \text{Eq. 13}$$

$\bar{X}$ is the mean of the individually determined contents and is equal to M in the present cases. Thus $k * s$ is the acceptance value, with k = 2.4 (for n = 10 tablets) and s representing the standard deviation of the sample. Moreover, the maximum allowed AV is 15.0 and the maximum value of a single dosage unit is to be smaller than $25.25 * M$ if not otherwise specified.

3.3.4 Temperature measurements by a PT-100 sensor

The temperature measurements referred to in this work are performed by a PT-100 sensor, which is a resistance thermometer. The electrical resistance of the sensor changes depending on the temperature. The integrated temperature-sensitive element is usually platinum. These temperature sensors can be installed directly into the fluid bed granulator and therefore measure directly the temperature of the product bed. PT-100 temperature probes are characterised by high accurate measurements in a wide operating range, but have a longer response time. This is acceptable, since the temperatures during a fluid bed granulation process also change relatively slowly.

3.3.5 Principles of particle size determination

3.3.5.1 Definition of particle size

The most intuitively understood parameters in particle size measurements are the length and the width of a particle. The length is defined as the longest diameter from edge to edge of a particle oriented parallel to the ocular scale and the width being the longest dimension of the particle measured at right angles to the length [77].

For exact spherical forms, the particle size of single particles is clearly defined as the diameter. For other forms, the information on the diameter can refer to plenty of different assumptions [78]. Each of them can be of interest depending on the specific issue. The most common ones are briefly described below.

The diameter can be understood as

- Side length of the smallest square, which encompasses the particle. This is the mesh width in case of sieve analysis.
- Edge length of the cube of which the volume is equal to the one of the measured particle.
- Diameter of the circle having an equivalent area to the projection area of the particle. This kind of particle size is often referred to when using laser light diffraction.
- Mean length of the three dimensions length, width and height.
- Ferret´s diameter: distance between two imaginary parallel lines tangent to a randomly oriented particle and perpendicular to the ocular scale [77].

- Martin´s diameter: diameter of the particle at the point that divides a randomly oriented particle into two equal projected areas [77].
- Determination of the chord length of the projected particle and being orientated in moving direction. This is the basis for Parsum measurements.

3.3.5.2 Types of particle size distributions

Particle size distribution (PSD) is a quite imprecise term, since beside of varieties in particle size determinations, there are also different ways of calculating their distribution. Powder samples that conform to the characteristics of a normal distribution are fully described by a mean particle size and the standard deviation. However, unless the range of particle sizes is extremely narrow, most particle size distributions do not follow the normal distribution function. Usually, the distribution is skewed towards the larger end of the particle-size scale. These powder samples can be described by the log-normal distribution, which is completely specified by two parameters: the geometric median particle size, pertaining to the 50 % value in the cumulative distribution, and the standard deviation in the geometric mean [77].

In general, there are different possibilities for calculating the distribution.

- Quantity-based distribution or Q_0 distribution:
  Each particle has the same valency and is sorted in the matching size class.
- Volume-based distribution or Q_3 distribution:
  Each particle is classified according to its volume. The transformation from Q_0 to Q_3 is effected class-wise by multiplication with the particle volume of the class or calculating the 3^{rd} potency. The weight of big particles is hereby distinctly increased, while fines tend to disappear. However, this corresponds to the general sense of quantity. Moreover, this distribution corresponds to the mass-based distribution which is the result of sieve analyses in case the density of the particles and thus the relation mass / volume is constant. Therefore, the Q_3 distribution measured by Parsum is compared to the PSD obtained by sieve analysis.

3.3.6 Particle sizing by sieve analysis

Sieve analysis is one of the oldest compendial method to classify dry powders and granules into size classes and hence to assess the particle size distribution. The procedures of sieve analyses are regulated in an internal SOP and in the European [45] and US Pharmacopeia [48]. Several woven-wire mesh sieves are stacked with ascending mesh-widths and the defined amount of sample – 100 g for the measurements of this work – is brought onto the top. The nest of sieves is then subjected to defined agitations (10 min, amplitude: 2 mm, interval time 10 s), after which the mass retained on each sieve is determined. The result of the test is expressed in mass percentage of each size class.

The analysed size parameter of sieve analysis is the size range of the smallest side length of each particle.

The mesh widths of the applied screens were selected as follows: 63, 90, 125, 180, 250, 355, 500, 630, 710 and 1000 µm.

3.3.7 Particle sizing by scanning electron microscopy

Scanning Electron Microscopy (SEM) is used to generate highly resolute images of small particles.

The irradiation of a sample by a thermionically generated electron beam induces interactions between the incident electrons and the sample giving information about the surface topography. The atoms of the sample produce several characteristic signals: secondary electrons, backscattered electrons, Auger electrons and X-rays. These signals are detected, pre-processed and displayed on the monitor as pixels of different brightness.

The finely focused electron beam scans the sample in a raster pattern and the irradiated part of the sample is visible on the display. The obtained magnification depends on the ratio of the horizontal width of the monitor screen to the width of the electron beam.

The analysed samples are pre-treated by gold-sputtering in order to increase the electrical conductivity of the sample surface.

3.3.8 Particle sizing by an image analysing system

The Occhio Zephyr (Occhio SA, Angleur, Belgium) used for this work is an image analysing system. The dedicated software Callisto for evaluation was also provided by Occhio SA.

In addition to the particle size distribution, the shape of the particles can be assessed by this technique. The particle size was assessed using the equivalent diameter, which gives the diameter of a circle with an equivalent area to the projection area of the particle.

The powder sample is dispersed by means of a combination of mechanical and vacuum dispersion and linear acceleration. A high-speed camera images the particle passing the measuring range. The measured sample size was 4 – 5 g of the respective granulate samples, corresponding to 3000 – 4000 particles which have been individually analysed.

4. RESULTS PROJECT A: FLUID BED GRANULATION

4.1 MANUFACTURING PROCESS

Project A implies the development of a film-coated tablet composed of two active pharmaceutical ingredients (API), API 1 and API 2, whereby the main manufacturing step impacting all further downstream process steps is a fluid bed granulation. The granulate consists of two APIs, a filler and an aqueous binder solution. The granulation process was characterised and optimised by means of several process analytical technologies, supporting process understanding by giving microscopic insight into the manufacturing process. Especially in-line moisture content and in-line particle sizing are considered to lead to an enhanced knowledge of the fluid bed granulation and particularly of the agglomeration behaviour.

The subsequent process steps are lubricating, compression into tablet cores and final film-coating. The unit operations performed during the manufacturing process are schematically outlined in the following flow chart (Figure 16).

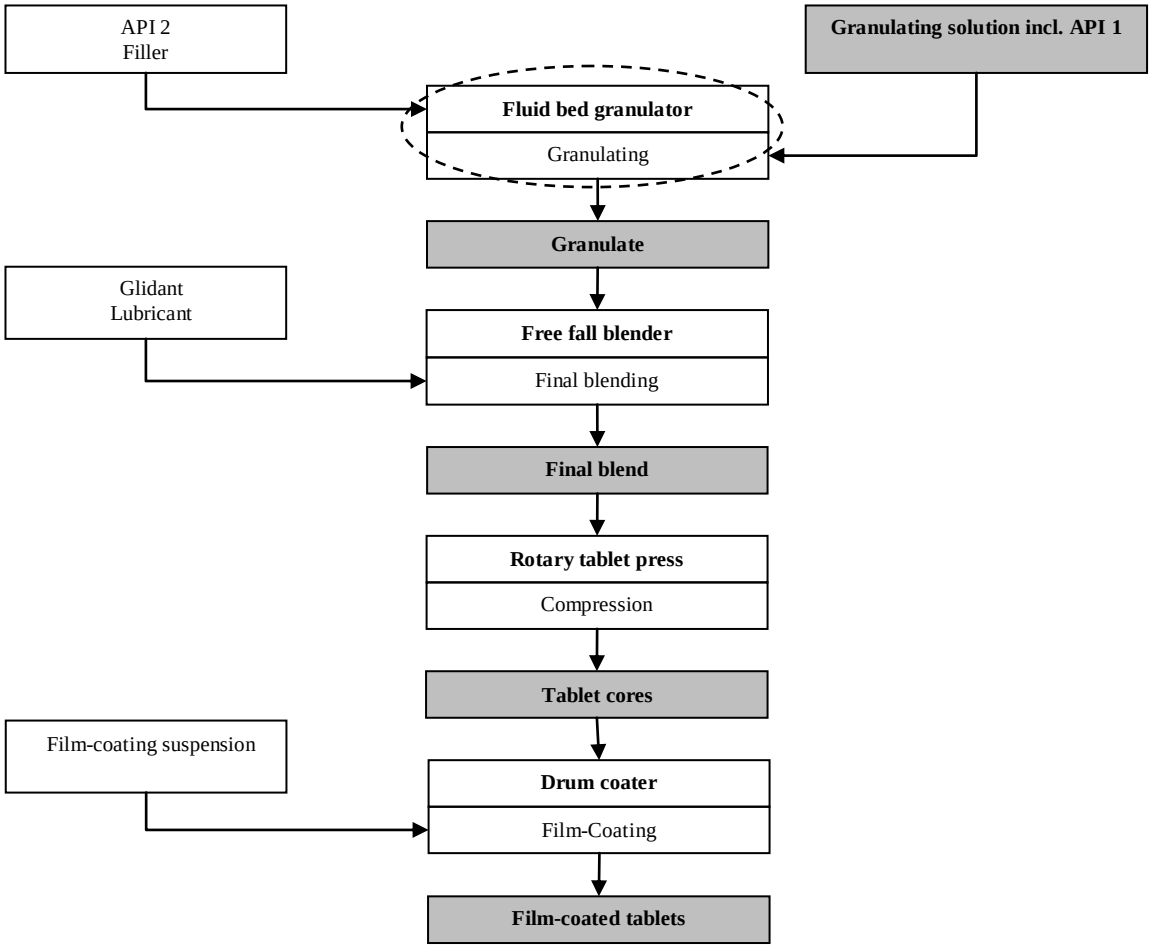

Figure 16 Flow chart of manufacturing steps comprised in Project A

Granulation is a widespread unit operation as it results in improved downstream processability and further on increases safety of the drug product by ensuring consistent dosing. Prevalent reasons for granulation of pharmaceutical compounds can be the ones addressed by Parikh [79]:

- Increase of the uniformity of drug distribution in the product
- Densifying of the material
- Improvement of flow properties
- Ease of metering or volumetric dispensing
- Reduction of dust and thus increase of workers safety
- More uniform appearance of the product.

Though there have been significant enhancements in the understanding of the principles of wet granulation, especially scale-up and control of the process is still problematic [15]. Iveson [80] even describes the practice of granulation processes to remain "more of an art than a science".

Thus process analytical techniques are needed to increase process understanding and allow controlling the granulation process in order to obtain consistently granulates of predefined quality.

4.2 PHASES OF A FLUID BED GRANULATION PROCESS

The granulation process consists of three phases, according to Iveson [80]: wetting and nucleation (a), consolidation and growth (b), and attrition and breakage phase (c). These phases are reflected in Figure 17.

The first phase, wetting and nucleation, describes the contact of the binder solution with the dry powder which results in forming nuclei granules. This phase is determined by the extent and the rate of wetting. The initial distribution of the binder liquid can have a distinct influence on the size distribution of the nuclei, which are formed from fine powder. Poor wetting properties can lead to coalescence of the binding fluid, resulting in few large nuclei and finally a broad granule size distribution. Nucleation implies the formation of liquid bridges between particles, which is sometimes called the pendular state. The pendular state changes into the funicular state when pore saturation increases, but still is not complete [79].

The next phase, consolidation and growth, mainly involves collision of particles, which bring about agglomeration. This includes coalescence of existing granules and layering of fines onto the surface of previously formed nuclei. Compaction of the granules by consolidation mechanisms reduces internal porosity and voidages.

The last phase of a granulation process is often characterised by breakdown of agglomerates.

All of these phases might also occur simultaneously [81].

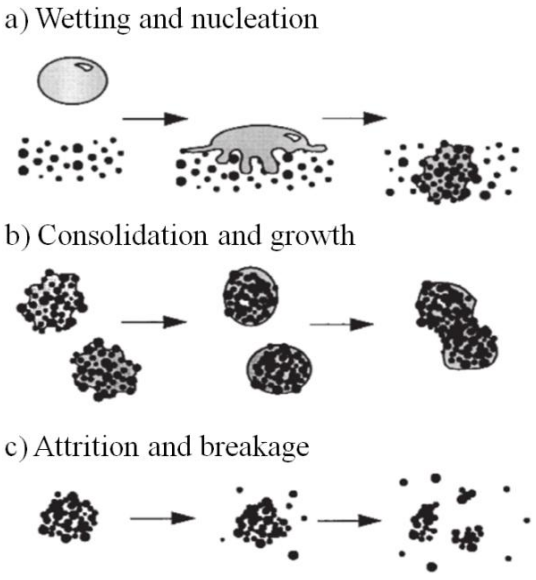

Figure 17 Phases of a wet granulation process (cf. [82])

4.3 RISK ANALYSIS OF THE MANUFACTURING STEP

Potential influencing factors are often summarised in an Ishikawa or so-called Fishbone diagram. This tool was used to identify sources of variability in the examined process step and is depicted in Figure 18.

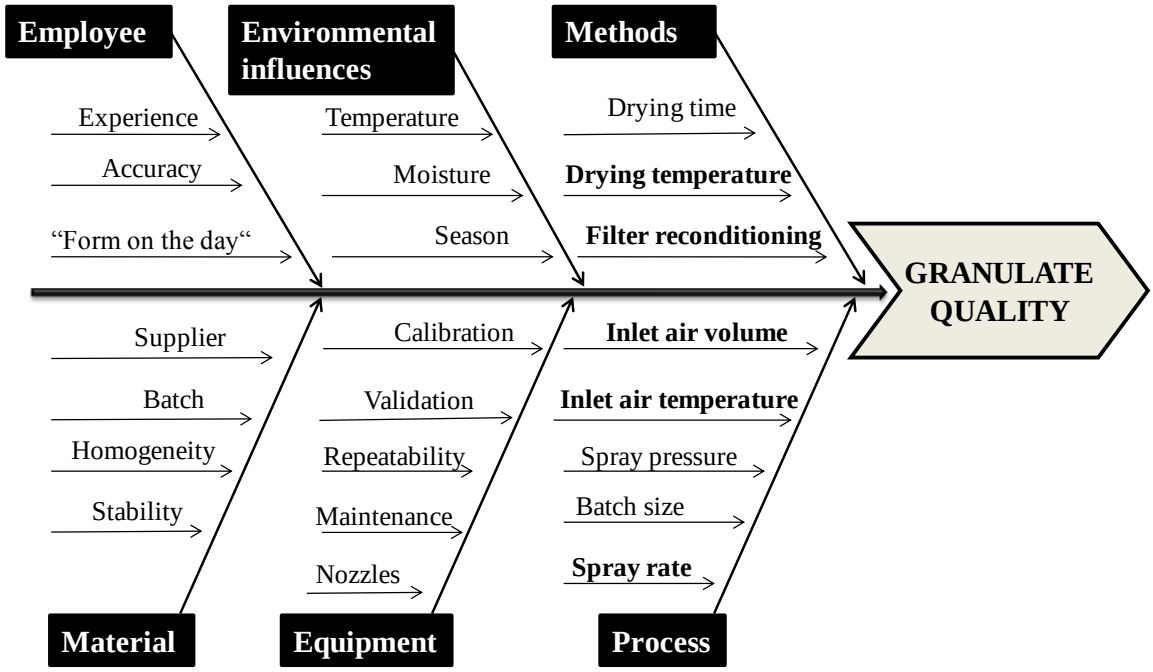

Figure 18 Ishikawa diagram for influencing factors on granulate quality

Plenty of these influencing factors are kept constant for the experiments described in this thesis e.g. suppliers of raw materials and the processed batches. Others are neither controllable nor measurable as is the whole branch termed "Employee". Furthermore, equipment related effects like maintenance were not included in evaluation of the trials.

The effect of filter-reconditioning was evaluated by comparing the effect of asynchronous and synchronous dedusting mode of the filterbags on granule structure (see chapter 4.5). Then several process parameters are evaluated and a Design of Experiments (DoE) was performed in order to estimate the effects of the most important process parameters and to find optimum settings (see chapter 4.6).

4.4 FULL SCALE DEVELOPMENT AT R&D SITE

The manufacturing process was developed in full scale meaning granulate batch size was approximately 75 kg. Several important process parameters and their influence on downstream processability were to be evaluated mainly by application of PAT tools.

The focus was set on particle size measurements during the granulation process and the development of appropriate statistical models to predict the final granule size and on real-time measurements of the moisture content in the granulate. The water content is important both during manufacture because it determines the behaviour of the agglomerates in the fluid bed and also at the end of the granulation process. The granulate moisture determines the water content of the final blend, since the outer phase consisted only of a glidant and a lubricant, both added in small amounts. In the end, the water content of the final blend has an important effect on its compression properties.

4.5 TRIAL ON THE EFFECT OF FILTER-DEDUSTING DURING FLUID BED GRANULATION

Two process options for fluid bed granulation were compared with regards to their effects on granulate morphology. The two filter bags in the fluid bed granulator were dedusted synchronously (process option I) or asynchronously (process option II) during the first 30 minutes of the spraying phase. The manufacturing processes were equal for the remaining process time, applying asynchronous dedusting. A replication of each variant was performed in order to confirm the results.

If both filter bags are dedusted synchronously, the inlet air stream and spraying of the granulation liquid is stopped and the fluidization is interrupted. Option I resembles an approach presented by several authors e.g. Ehlers [71], Närvänen [83] and Schaafsma [84], which is referred to as "pulsed liquid feed". The spraying of the binder solution is interrupted in regular sequences, allowing the granules to undergo short intermittent drying. Option I is a continuous granulation process, while the application of option II requires interruptions of spraying and at the same time of fluidisation, leading to a discontinuous process. The issue for the latter process option was to incorporate the fine fraction which tends to adsorb at the filterbags. The processes were compared by examining the effect on resulting particle size, granule size distribution and morphology. Both process variants are shortly presented in Table 1.

Table 1 Process parameters for fluid bed granulation

Process option	**I**	**II**
Batch	***a*** and ***b***	***c*** and ***d***
Dedusting mode (0 - 30 min spraying)	asynchronous	synchronous
Spraying time	60 s	300 s
Dedusting time	10 s	60 s
Inlet air volume during spraying / dedusting	on / on	on / off
Pump position during spraying / dedusting	on / on	on / off

4.5.1 Evaluation by in-line measurements applying the Parsum probe

In-line particle size distribution of the granulates were measured during fluid bed granulation by a Parsum probe. Predefined settings of the Parsum measurements are presented in Table 2.

Table 2 Settings for Parsum measurements

Parameter	**Value**
Particle range	10 – 3000 µm
Adjust factor	1.00
Adjust offset	0.00
Probability of stay	On
Coinc. check	On
Coinc. level	0.00 %
No. of particles in ring buffer	30000
Width of size class	1 µm
Interval for data log	30 s

All four granulate batches were manufactured without any problems, no particularities occurred. The Parsum probe measurements allowed a clear insight into the granulation process and revealed different granulation phases. The growth of particles is not linear over the whole spraying phase, but starts with the wetting and nucleation phase, which appears as a constant size level for the first approximately seven minutes of the spraying process. The further particle growth is not linear either, it approaches a saturation limit, where agglomeration and breakage occur at par and result in a constant median particle size. No attrition of the granules could be observed, since no additional drying step was carried out after having completed the spraying phase.

These general courses are similar for all manufactured granulate batches, however, the results of the Parsum probe showed clear differences in the course of particle growth between process option I and II.

Dedusting the filterbags in synchronous mode as for batches *c* and *d* led to a decrease in median particle size due to dust from the filters falling down onto the product. These short abatements in median particle size occur regularly every 5 minutes during the first half-hour. Afterwards, the filter-dedusting is carried out asynchronously; meaning the two

filters are shaken alternately for the rest of the manufacturing process. The effect of particle size reduction is overlapped by the overall measuring variation.

Alternate asynchronous dedusting of the filterbags, represented by batches *a* and *b*, does not lead to a visible pattern using in-line particle size measurements.

Nevertheless, the resulting median particle sizes at the end of the granulation processes are similar for all four batches and were not affected by the mode of dedusting the filterbags.

Figure 19 depicts the results of in-line measurements for batches manufactured with different dedusting modes during the first 30 minutes.

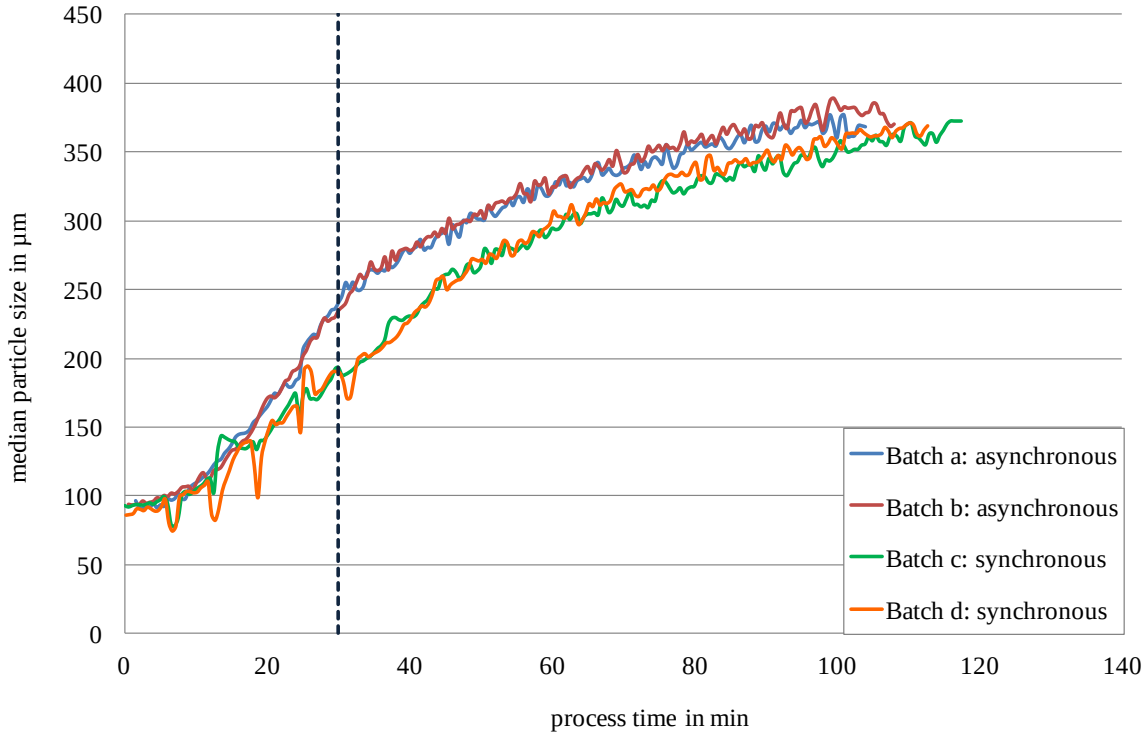

Figure 19 Particle growth during granulation affected by mode of dedusting the filterbags

Even when subtracting the time when the pump was turned off, the velocity of particle growth is still different. Despite the slower build-up of agglomerated granules, the resulting particle size at the end of the granulation process is equal. This situation is reflected in Figure 20, in which the spraying times are calculated for batch *c* and batch *d*, respectively.

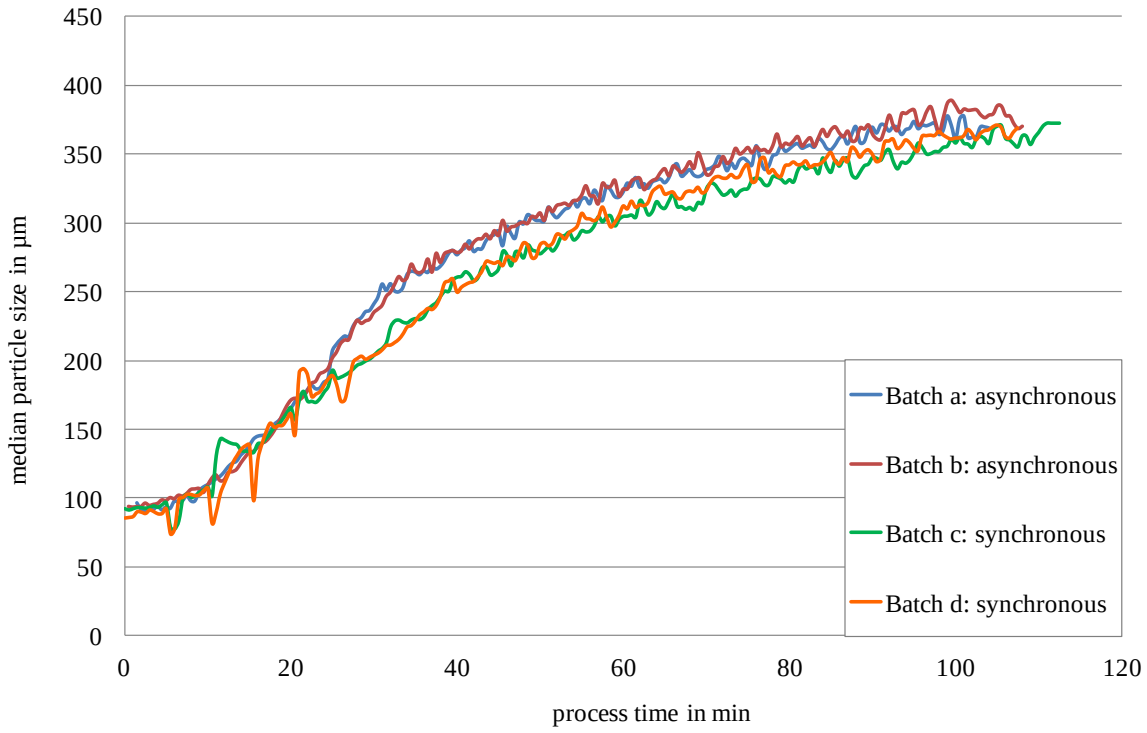

Figure 20 Particle growth during granulation affected by mode of dedusting the filterbags, only spraying time (pump on) taken into account

Batch *a* (asynchronous dedusting) and batch *d* (synchronous dedusting) result in the same granule size distribution at the end of the process. As has been revealed by in-line Parsum measurements, the agglomeration speed of granules is faster for asynchronous filter-shaking. This can be due to different wetting and nucleation behaviour. Synchronous filter-shaking, which was applied for batch *d*, effectively removes the dust adsorbed at the filterbags and forces it back into the spraying zone. This decreases the moisture of the fluidised product and reduces the probability of two nuclei to collide and agglomerate. This effect might be specific for this formulation which is known to have low absorptive capacity for water, but is equalized with rising water content in the course of granulation.

The results of final Parsum measurements are listed in Table 3. There is no obvious difference between the two ways of processing, neither in the median particle size D_{50}, nor in the relative width (RW) of the particle size distribution. The relative width of a grain size distribution is calculated using the following equation:

$$RW = \frac{D_{90} - D_{10}}{D_{50}} \qquad \text{Eq. 14}$$

Table 3 Results of Parsum measurements at the end of the granulation process for the batches investigated with regard to filter-dedusting

Batch	***a***	***b***	***c***	***d***
Dedusting mode	asynchronous (option I)	asynchronous (option I)	synchronous (option II)	synchronous (option II)
D_{10} [µm]	167	168	163	165
D_{50} [µm]	369	368	373	369
D_{90} [µm]	741	726	773	732
Relative Width (RW)	1.56	1.52	1.64	1.54

Although the results for D_{50} values at the end of the granulation process are very close for both process options, the slopes of increasing D_{10} and D_{90} quantiles, which are presented in Figure 21, show different behaviour dependent on the filter-dedusting mode. D_{10} and D_{90} of batch *a* reach a plateau phase at the end of the granulation, where no more particle agglomeration takes place. This steady-state in particle growth seems not to be achieved for batch *d*, which is manufactured with synchronous shaking during the first part of the granulation.

Furthermore, the graph reveals that the increase in D_{10} values, which represent the fine part at the beginning of the manufacturing process, is similar to the one of the D_{90} quantile. There are no agglomerated lumps, which disappear during the granulation process due to attrition or which occur during the process caused by partly blocked nozzles.

As was shown for median particle sizes, the absolute values for these quantiles are different during processing, but approximate each other at the end.

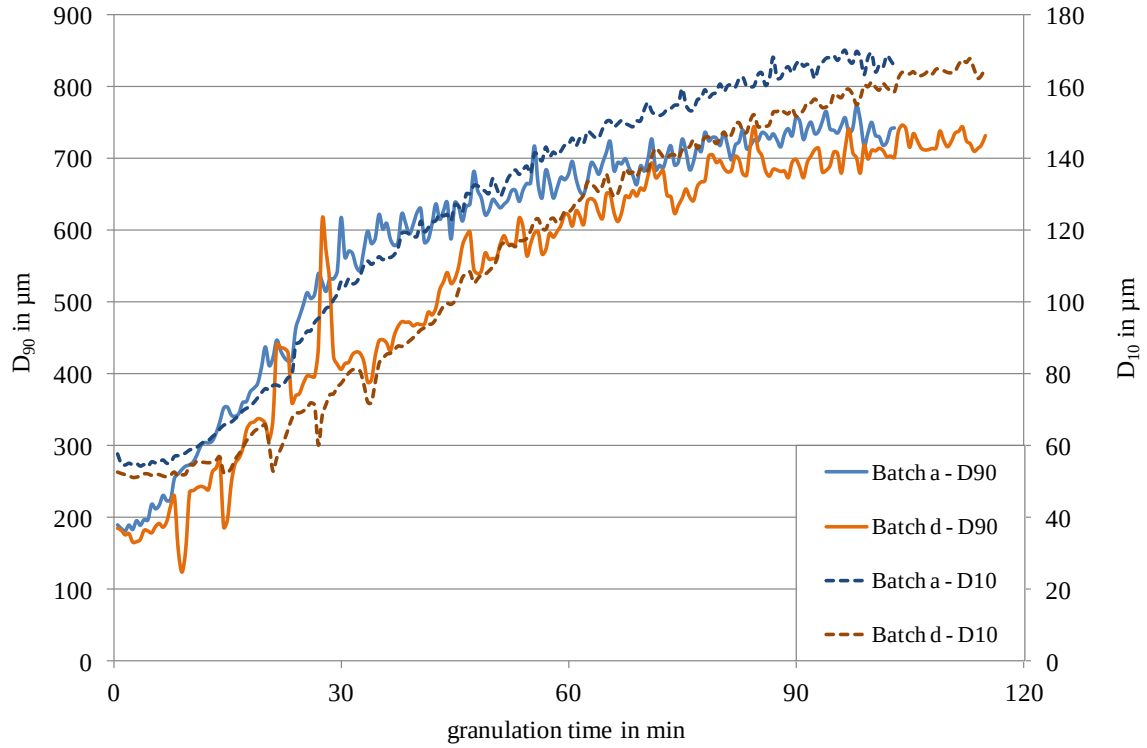

Figure 21 Increasing D_{90} and D_{10} values measured by Parsum probe for batch *a* (asynchronous) and batch *d* (synchronous dedusting)

4.5.2 Confirmation of Parsum results with further particle sizing methods

4.5.2.1 Comparison to sieve analysis and image analyser

Although the results of Parsum measurements are conclusive, the comparability of such a "new" tool with "old" broadly accepted compendial methods has to be proven. Therefore, the collected samples are subject to the standard sizing method sieve analysis, but also to another reference method, image analysing.

The same samples were subject to three different particle sizing methods: Parsum, sieve analysis and Occhio. The detailed procedures have been described before in chapter 3.3.6 and 3.3.8, respectively.

Particle sizing methods are often classified into two groups: stream scanning – analysing one particle at a time e.g. the Parsum probe and Occhio – and field scanning techniques which analyse simultaneously a collective of particles like for instance sieve analysis [69]. Thus the selected sizing methods represent distinct sizing approaches.

The exact values for the quantiles D_{10}, D_{50} and D_{90} resulting from these tests are summarised in Table 4.

Plenty of information is cumulated in the table, which allows comparing several items:

- Are the results of different sizing methods, expressed as absolute values for D_{10}, D_{50} and D_{90} respectively, similar? And are the methods thus exchangeable?
- Are there differences in particle size for batch *a* (process option I) and batch *d* (process option II) during granulation and at the end of the process?

Table 4 Overview of main results of three different particle sizing methods

Batch		***a* (asynchronous)**				***d* (synchronous)**			
Sample		20 min	40 min	60 min	end	20 min	40 min	60 min	end
D_{10}	**Parsum**	72	112	139	166	68	94	128	164
	Sieve analysis	83	126	166	204	78	115	157	210
	Occhio	121	153	212	271	128	141	173	243
D_{50}	**Parsum**	162	264	316	362	152	225	295	360
	Sieve analysis	166	247	301	352	152	226	286	366
	Occhio	232	296	374	449	252	285	318	420
D_{90}	**Parsum**	381	602	645	719	360	482	620	717
	Sieve analysis	309	373	474	557	292	343	450	559
	Occhio	425	497	643	728	574	491	523	680

Values of Parsum and sieve analysis listed in the table above are very close for the median particle size D_{50}, while D_{10} and especially D_{90} differ substantially. The difference between

Parsum and sieve analysis show good concordance, the deviation is lower than 17 µm for the D_{50} values. The results for D_{10} and D_{90} differ systematically. D_{90} values are higher for Parsum measurements, while D_{10} values are underestimated compared to sieve analysis. The absolute difference of D_{90} values resulting from both sizing methods is more than 40 µm for the D_{10} values and almost 230 µm for the D_{90}, corresponding to 21 % and 61 % relative deviation, respectively. This phenomenon is also distinct in Figure 22.

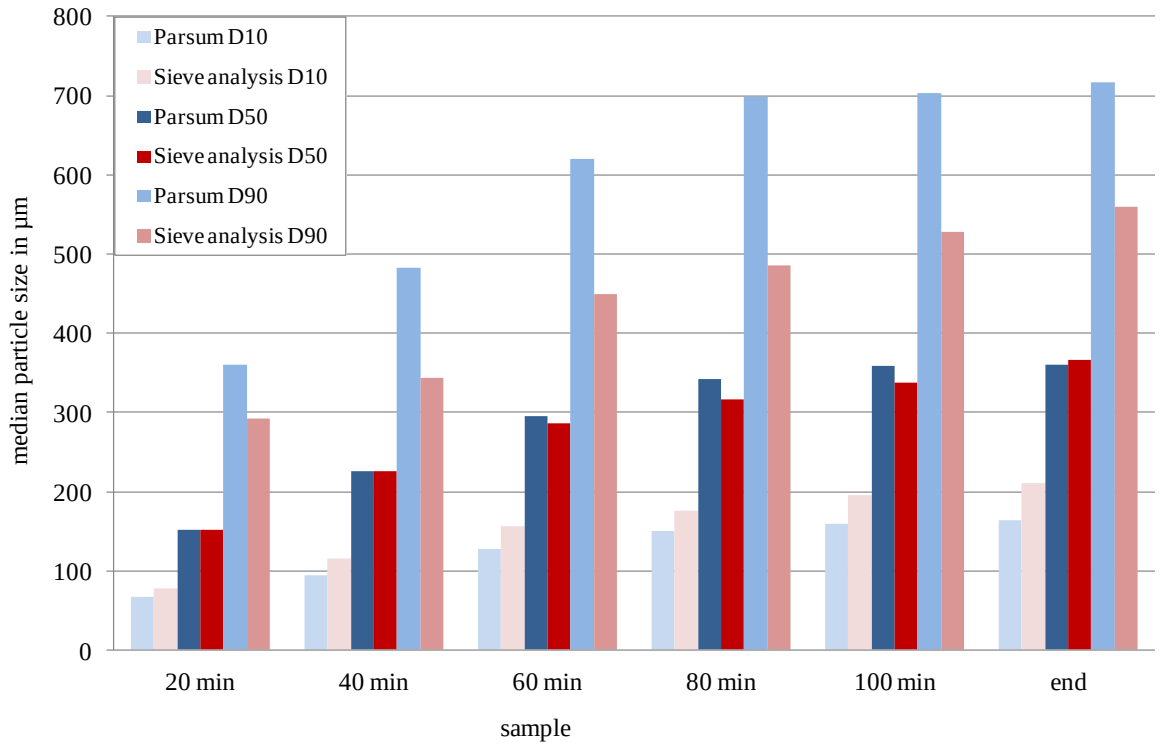

Figure 22 Comparison of Parsum results for characteristic quantiles to results obtained by sieve analysis; collected samples of batch *d*

A probable explanation is the different shear force which is applied during Parsum measurements and sieve analysis. Parsum in-line measurements use compressed air to induce a weak vacuum effect which makes the granules entering the measuring slot and passing the optics.

Sieve analysis on the other hand, is based on higher mechanical forces. The sieves made of metallic woven-wire meshes are exposed to intensive vertical shaking for 10 minutes. This procedure leads to attrition of bigger granules and thus results in increased D_{10} and lower D_{90} quantiles. On the other hand, the measuring range of the Parsum probe extends from 50 to 5000 µm. The amount of particles smaller than 50 µm is estimation only. In principle, the software for analysing Parsum results allows to adjust the results by

mathematical treatment of measured data. However, this was not considered necessary, as the median particle sizes correspond well during the whole granulation process.

The values obtained by the image analyser, Occhio Zephyr, show considerable deviations when comparing them to Parsum and sieve analysis. This is true for D_{10}, D_{50} and D_{90}, although the trends are the same.

Sieve analysis revealed the similar results to Parsum measurements when comparing the particle size distributions of granulates of both process options: Samples collected from batch *a* (blue) consist of bigger granules than samples of batch *d* (pink) during the granulation process, but almost the same distributions for the samples, which were collected close to the end of the manufacturing process after 120 minutes, as can be interpreted from Figure 23.

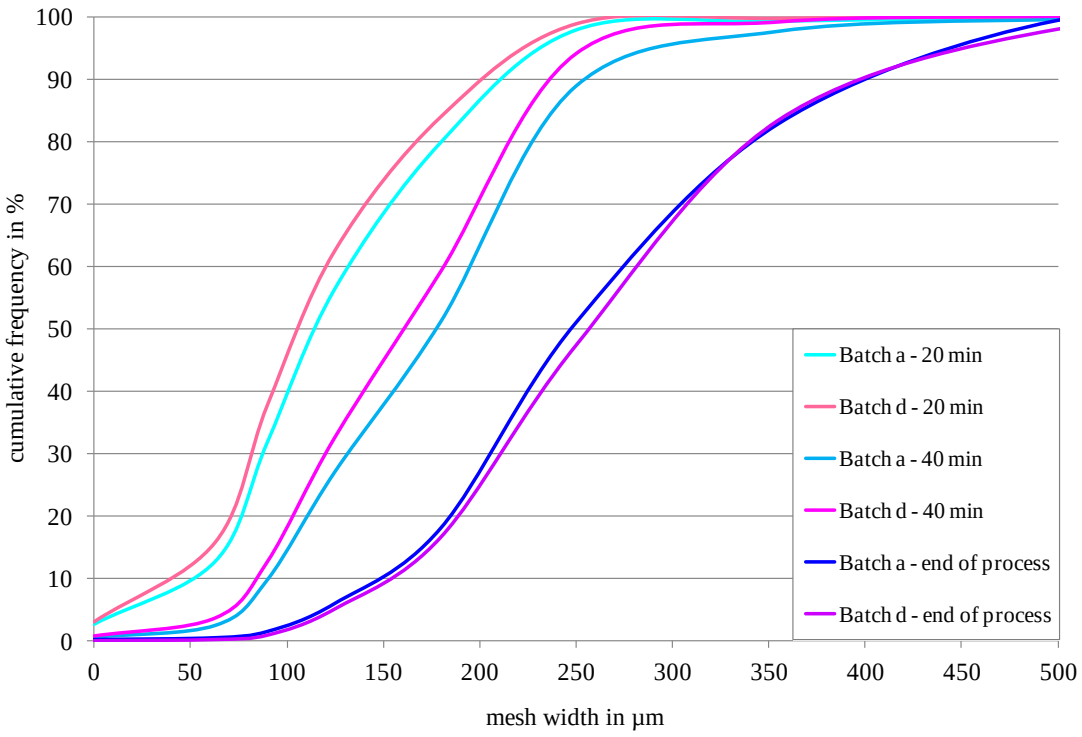

Figure 23 Comparison of cumulative undersize distributions of samples collected after 20 min, 40 min and at the end of granulation of batch *a* and batch *d* respectively obtained by sieve analysis

The results in PSD when using the Occhio were very sensitive to single bigger agglomerates, which tend to distort the cumulative frequency. It was not possible to obtain a clear picture with regards to differences in particle size as a result of the different process options (see Figure 24). Although there is a clear augmentation in the D_{50} quantiles

throughout the granulation process, the samples of batch *a* (blue) and batch *d* (pink) are only similar for the samples withdrawn after 40 minutes. The PSD of the samples of the other batches differ substantially.

One limitation of the method might be the comparatively small number of particles considered for calculating the distribution compared to the other two techniques: for Parsum, the size of 30000 individual particles is determined and taken into account for the distribution and sieve analysis is realised out of 100 g sample. In contrast, for the image analysing system about 4 g were tested.

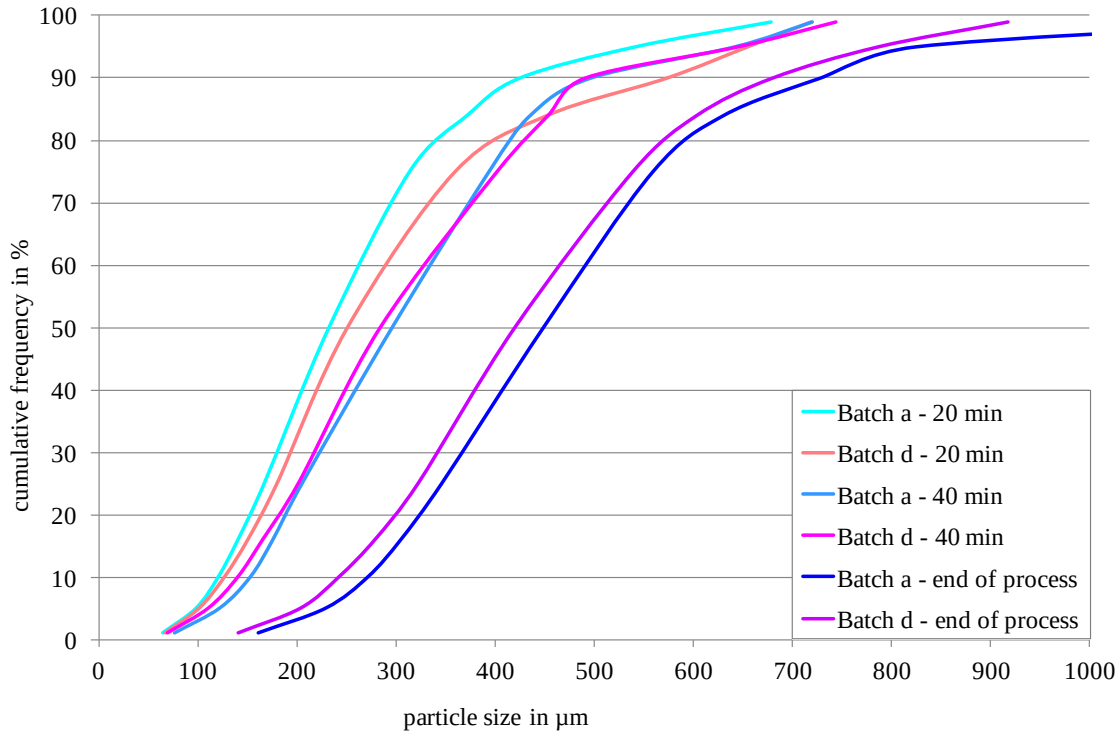

Figure 24 Comparison of cumulative undersize distributions of samples collected after 20 min, 40 min and at the end of granulation of batch *a* and batch *d* respectively obtained by Occhio

As a consequence, the application of the in-line measuring method Parsum probe is recommended, since the results for the median granule size is comparable to the conventional off-line sizing method sieve analysis. Whenever granule strength and the resistance towards attrition is a major issue, then sieve analysis can give additional information beside of actual grain sizes. The use of the image analyser is not recommended for sizing, because the results were not consistent with other methods and lack comparability. The advantage of image analysing is clearly in another field: analysing the morphology of samples.

4.5.2.2 Comparison to scanning electron microscopy

As Parsum measurements revealed differences in granule growth of the two process options concerning dedusting, scanning electron microscopy (SEM) is carried out in order to detect possible differences in granule morphology.

Scanning electron microscopy was realised by co-workers of the laboratory "Electron Microscopy". The investigated samples have been collected after 20 minutes granulation time. At this time point, the granulation process is performed in different ways. The samples represent the investigated batches batch *c*, which was manufactured when cleaning the filters synchronously, and batch *b*, produced while dedusting the filters in an asynchronous mode.

A slight difference in particle structure can be interpreted from the SEM images (Figure 25). But keeping in mind that SEM images represent only a quite small extract of the sample, interpretations of these pictures have to be done carefully.
More dust seems to be attached on the surface of the agglomerates on the left picture and the granules seem to be less glued when granulating with interruptions.

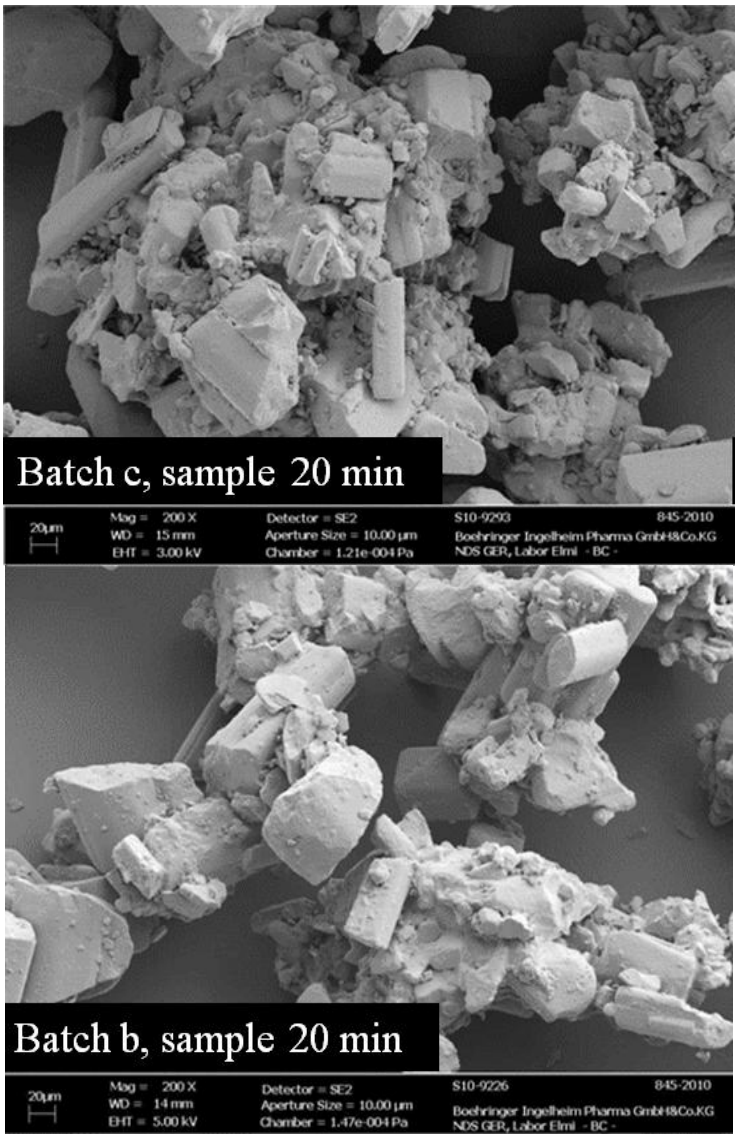

Figure 25 SEM images of batch *c* (above), sample after 20 min (LOD 0.70 %) and batch *b* (below), sample after 20 min (LOD 0.74 %)

Granulate samples of both manufacturing options are collected towards the end of the spraying phase and are also examined by SEM. No differences between the two samples regarding granule structure or particle size can be detected by microscopy. Examples of the recorded images of these samples are shown in Figure 26. Thus results of scanning electron microscopy correspond with particle sizing results of the final granulate which did not reveal a difference in PSD for final sample.

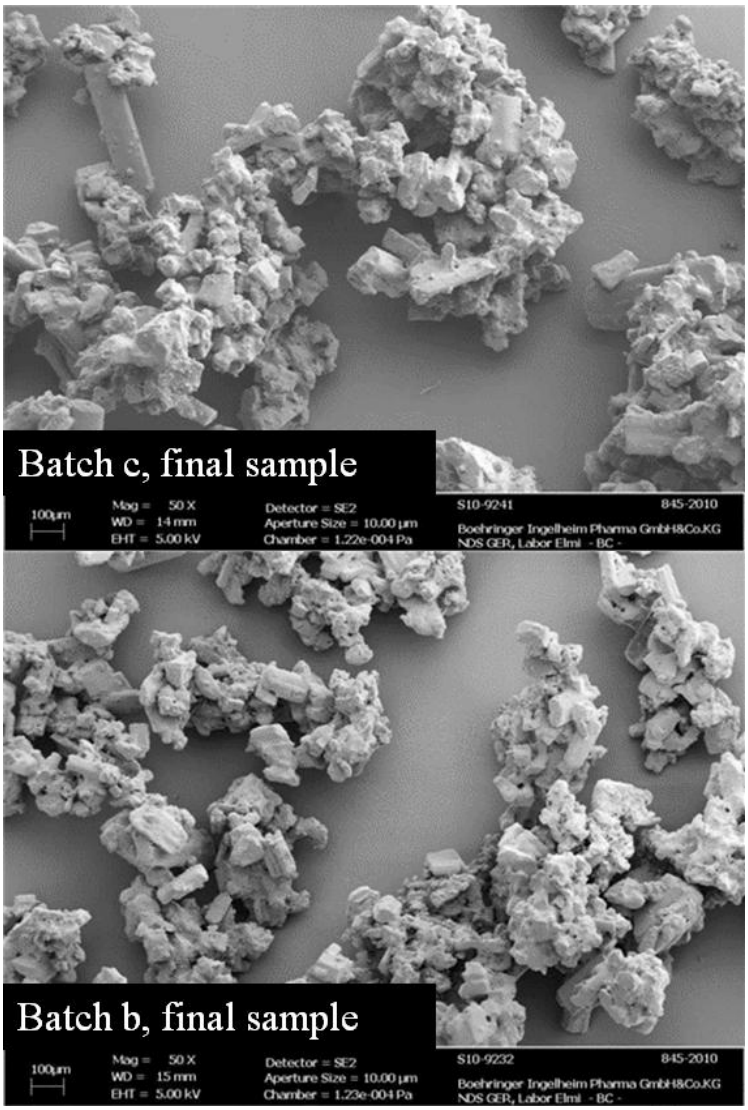

Figure 26 SEM images of batch *c* (above), final sample (LOD 1.30 %) and batch *b* (below), final sample (LOD 1.25 %)

The further process development was accomplished based on the continuous fluid bed granulation based on asynchronous filter-shaking. Although no differences of the final granulates manufactured either applying asynchronous or synchronous filter-shaking of the product filters in the fluid bed granulator could be detected, process option II was preferred because the continuous processing was considered to be associated with a lower risk of a collapsing fluid bed and thus potential loss of a whole batch.

4.6 DESIGN OF EXPERIMENTS ON THE EFFECT OF IMPORTANT PROCESS PARAMETERS DURING FLUID BED GRANULATION

In order to set up an appropriate process range for the fluid bed granulation step, a series of designed experiments has been performed. Due to the large number of influencing factors, the examined factors were limited to two main parameters having shown their importance in prior trials.

4.6.1 Experimental design

The variable factors are inlet air temperature and product temperature. The targeted product temperature is to be achieved by adjusting the spray rate in order to keep the product temperature constant.

The initial process ranges, called DoE A (inlet air temperature: 65 – 75°C, product temperature: 34 – 38°C), were set based on experience with previous products. These five trials are coloured in slight red in Figure 27. After having proven the processability of granulates with the mentioned factor settings, the design space was to be enlarged up to higher inlet air temperatures (75 – 80°C), in order to fasten the granulation process. This additional set of trials for DoE B is depicted in slight blue in Figure 27.

The eight manufactured batches can be evaluated as two separate full factorial designs with centre points, but due to the lack of iterations, the validity of statistical evaluation is low.
Median particle size of granules is measured by the in-line particle probe and interpreted as resulting parameter of the factor settings. Other influencing factors besides of inlet air temperature and product temperature were kept constant.

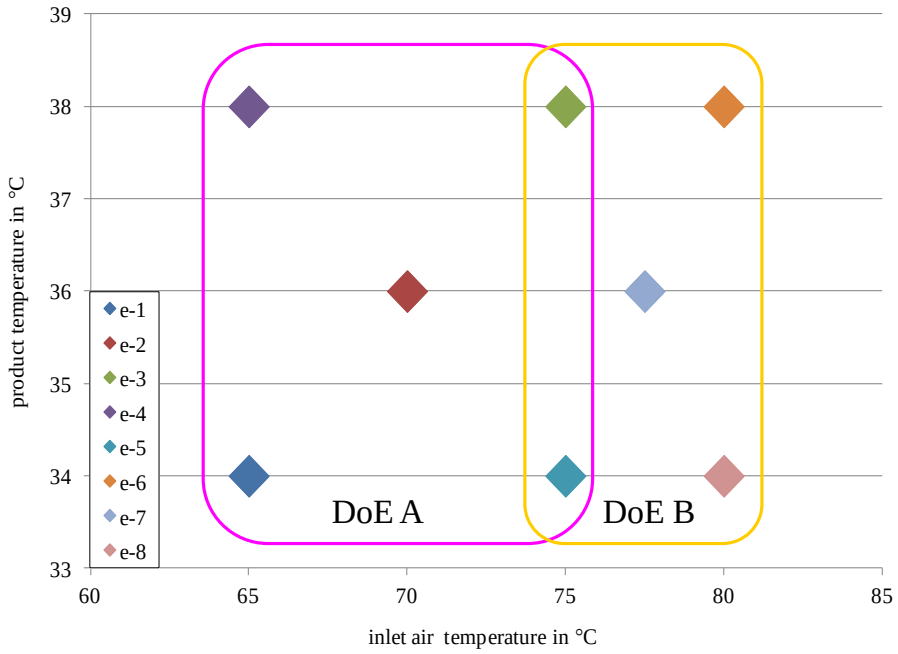

Figure 27 Experimental design for DoE batches

4.6.2 Results

The measured median particle sizes during fluid bed granulation process of all eight batches are depicted in Figure 28. Adjusting the spray rates in order to achieve a predefined product temperature, results in different granulation times for each batch. Furthermore, the in-line particle size measurements revealed differences in particle growth and in the final median particle size of the granules.

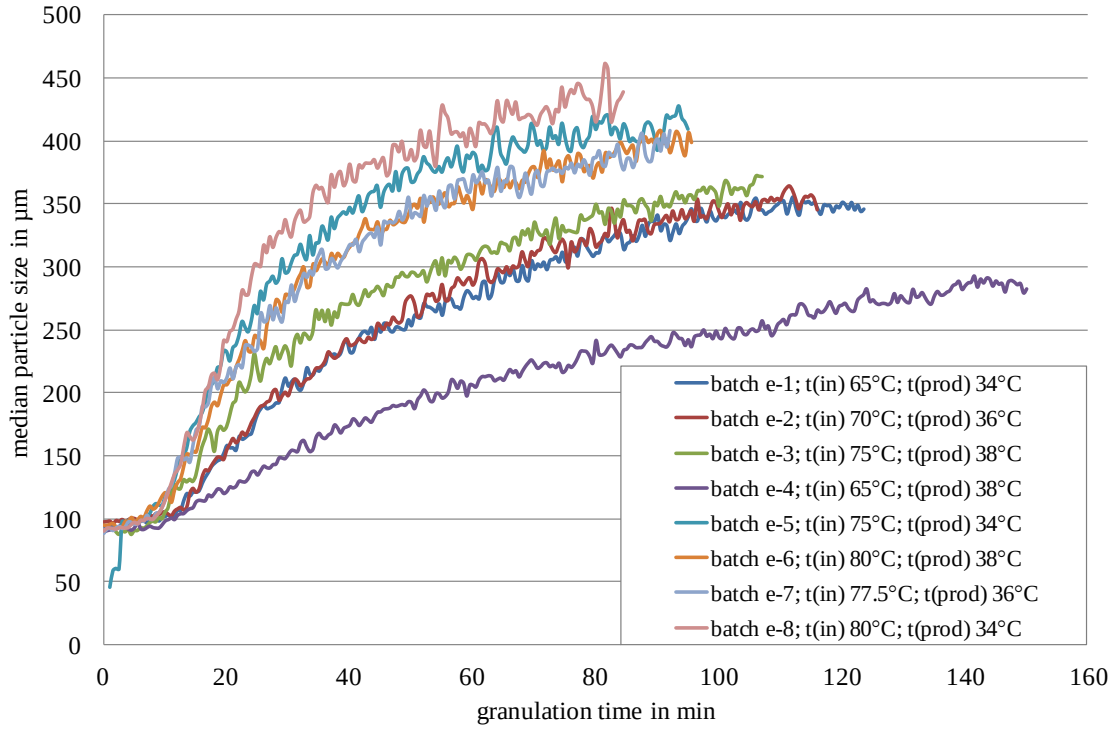

Figure 28 Median particle size during granulation – DoE batches

The variation of inlet air temperature and product temperature during granulation led to completely different median particle sizes at the end of the granulation processes. The exact values are given in Table 5.

Table 5 Factor settings for the DoE and responses

Batch	**Inlet air temperature [°C] = x**	**Product temperature [°C] = y**	**Median particle size D_{50} [µm] = z**
e-1	65	34	349
e-2	70	36	352
e-3	75	38	366
e-4	65	38	287
e-5	75	34	420
e-6	80	38	403
e-7	77.5	36	408
e-8	80	34	439

Three different approaches for evaluation of the results are pursued in order to gain maximum knowledge out of few experiments. The underlying design is a full factorial one with two factors and two levels (2^2).
All calculations were performed using the software Statistica 9.1 (StatSoft Inc., Tulsa Oklahoma, USA).

4.6.2.1 First approach – DoE A

This approach considers five of the manufactured batches in order to have the full 2^2 experiments plus a centre point.

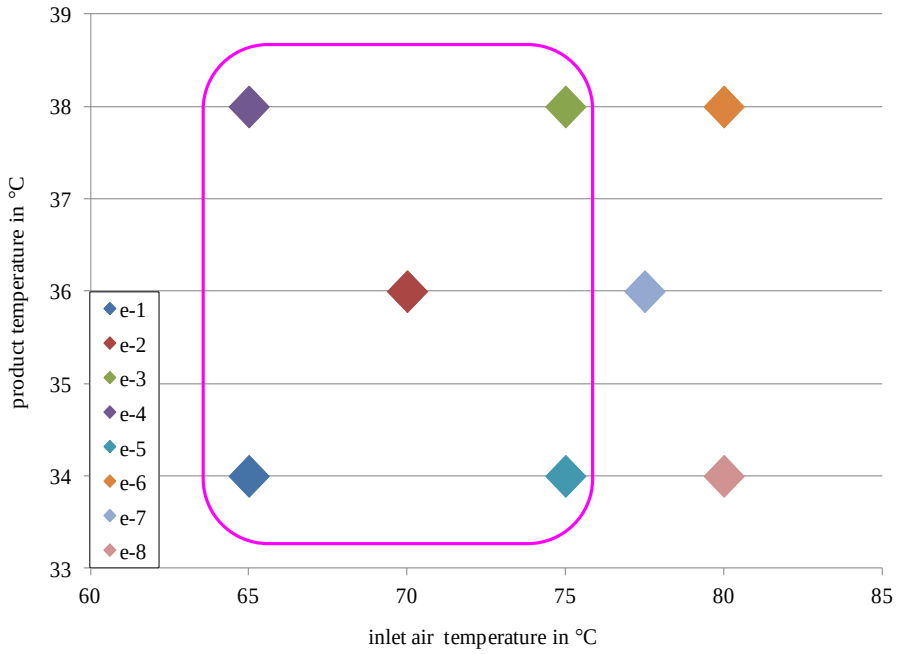

Figure 29 Experimental Design of DoE A

The remaining three batches are used as test points to challenge the performance of the model, keeping in mind that these batches are outside of the effective design space.
If it was possible to predict the particle sizes for the “test batches”, it should be possible to enlarge the design space.

The computation of a DoE prediction model includes the estimation of effects of the chosen factors using a statistical significance test. The applied calculation is based on ANOVA, meaning analysis of variance.

The null hypothesis H_0 states that there is no effect of the investigated factor on the response, i.e. median particle size of the final granules. If the estimation of the effect is lower than the significance level, the null hypothesis is rejected and the effect of the investigated factor is considered as significant. Otherwise, the experiment failed to reject the null hypothesis. The significance level p is set to 0.05. The effects of changes in inlet air temperature and product temperature were found to be significant, while the interaction of these two parameters was evaluated as insignificant. The detailed results are listed in Table 6.

Table 6 Estimation of effects of investigated factors

Investigated effect	**p (factor)**	**Relation to significance level**	**Consequence**
Inlet air temperature	0.026557	< 0.05	Rejection of H_0, significant effect
Product temperature	0.034328	< 0.05	Rejection of H_0, significant effect
Interaction of inlet air temperature and product temperature	0.422751	> 0.05	Failed to reject H_0, significance of the effect of the interaction cannot be assumed

The interaction, which was not revealed as significant by the statistical test, was removed from the ANOVA evaluation and the remaining factors were re-evaluated. The response z, D_{50} of the final granulate, is dependent from the factors x, inlet air temperature, and y, product temperature during granulation.

The evaluation of the DoE finally resulted in the compilation of this model equation:

$$z = 351.8 + 7.5\,x - 14.5\,y + 0 \qquad \text{Eq. 15}$$

The main effect is the product temperature (y) in the fluid bed, which increases particle size at lower temperature levels. This result is reasonable, since lower product temperatures are obtained by increasing the spray rate of the granulation liquid. Increased spray rates in turn lead to elevated levels of moisture and binder in the fluid bed granulator,

both augmenting the probability of particle agglomeration and thus increasing median particle size of the granules.

In contrast, inlet air temperature (x) has a positive effect on median particle size of the granulates, which means that higher temperatures of the inlet air promote granulation. Higher inlet air temperatures require elevated spray rates in order to maintain a defined product temperature. Higher spray rates of the granulation liquid support granule growth as prior described.

Concluding, the model equation can be explained by considering the respective effect on the spray rate. The model is illustrated in the prediction plot (see Figure 30), where the effects of the investigated independent factors on the dependent variable D_{50} are graphically depicted.

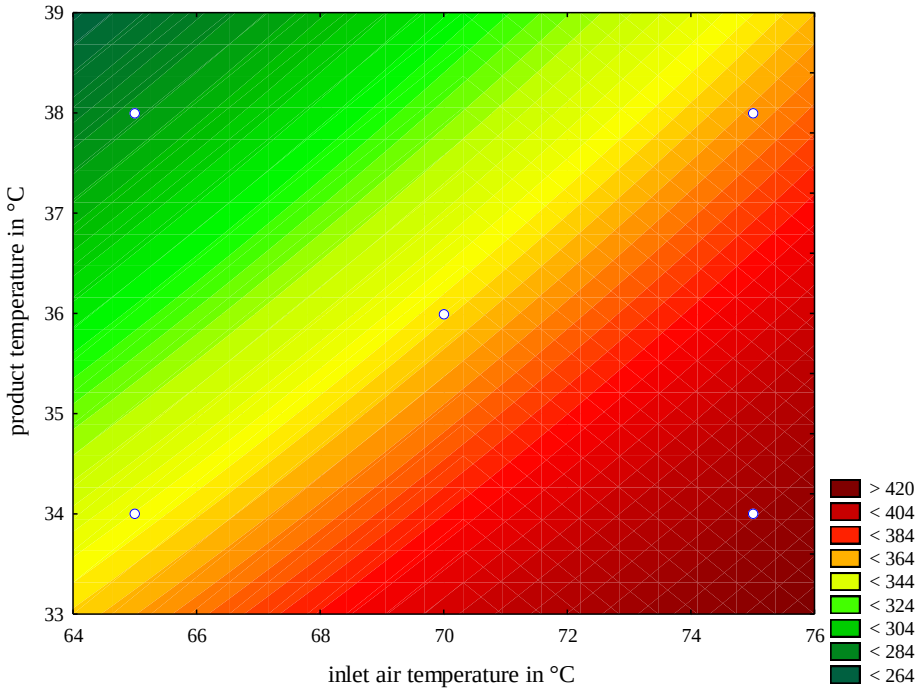

Figure 30 Prediction plot DoE A: dependency of granulate D_{50} values from inlet air temperature and product temperature

The test on normal distribution of the residuals is an important prerequisite for the validity the compiled model. The graphical evaluation is presented in Figure 31.

As can be seen, the residuals for DoE A are normally distributed showing no deviating trend from the depicted straight line for observed vs. predicted values.

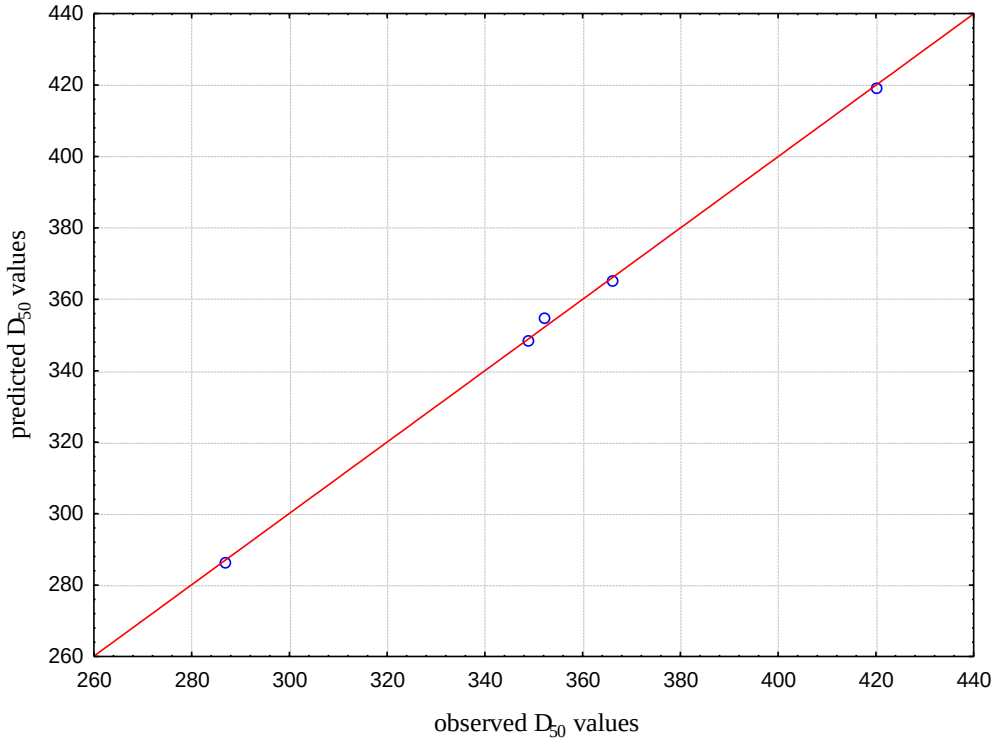

Figure 31 Normal distribution plot of residuals for DoE A observed vs. predicted values

In order to evaluate the validity of the model, it is verified by predicting the responses of the batches not included in the model. The predicted and measured median particle sizes of the granulates are summarised in Table 7. This approach was followed only for test purposes; it is not possible to claim validity by testing it for trials out of the design space.

Table 7 Comparison predicted and measured responses for batches not included in DoE A

Inlet air temperature [°C] = x	**Product temperature [°C] = y**	**D_{50} predicted [µm] = z**	**D_{50} measured [µm]**	**Deviation [µm]**
77.5	36	411	408	-3
80	34	459	439	-20
80	38	401	403	2

The predicted and measured median particle sizes for three other batches correspond quite well, except for the value for even being outside of the actual design space of the model calculated for DoE A.

4.6.2.2 Second approach – DoE B

DoE B includes the trial runs with a range from 75 – 80°C of inlet air temperature. Batch *e-7* is regarded as centre point in this full factorial 2^2 design.

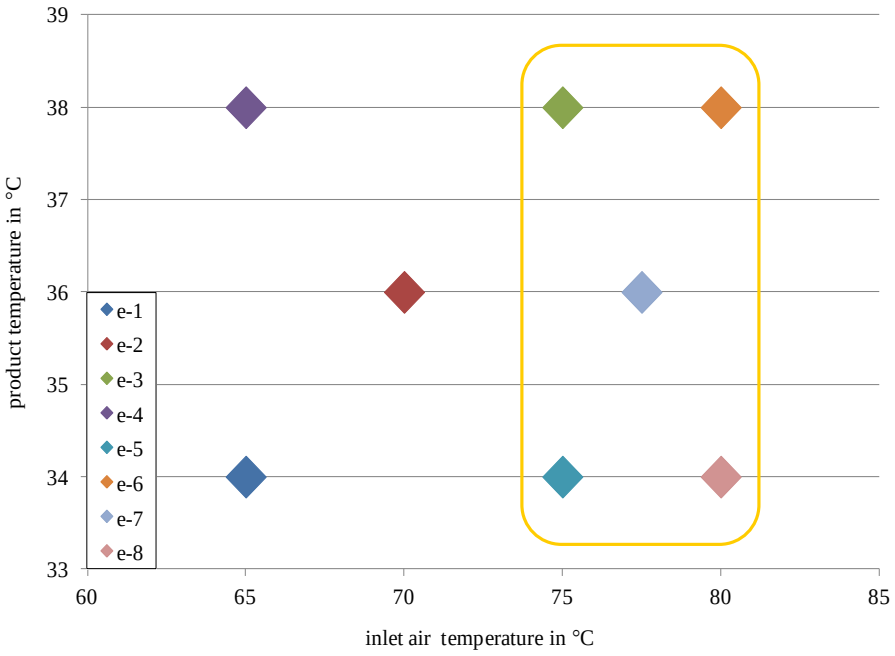

Figure 32 Experimental Design DoE B

The model compilation was again accomplished using Statistica software and applying ANOVA.

The model compilation ended up in the following equation:

$$z = 378.2 + 5.6\,x - 11.25\,y + 0 \qquad \text{Eq. 16}$$

This equation again is similar to the one of DoE A. This emphasizes the assumption that the design space can be extended over the whole investigated range.

The design space of this model spans the inlet air temperature range of 77.5 ± 2.5°C and is thus comparatively narrow, while the three test batches are all outside of this range. Nevertheless, they were used as test batches to verify the model. The predictions were not as close to the measured values like for the previous two models, but still in an acceptable range (see Table 8). The highest deviation was obtained for batch *e-4*, which was manufactured at 65°C inlet air temperature and 38°C product temperature. The predicted D_{50} was nearly 30 µm smaller than the actual median particle size.

Table 8 Comparison of predicted and measured responses for batches not included in DoE B

Inlet air temperature [°C] = x	**Product temperature [°C] = y**	**D_{50} predicted [µm] = z**	**D_{50} measured [µm]**	**Deviation [µm]**
70	36	365	352	-13
65	34	360	352	-8
65	38	315	287	-28

4.6.2.3 Third approach – DoE C

This model consists of data obtained from the extreme batches concerning inlet air temperature and product temperature: only the extreme points are used for model calculation. This design corresponds to a 2^2 full factorial design without centre point.

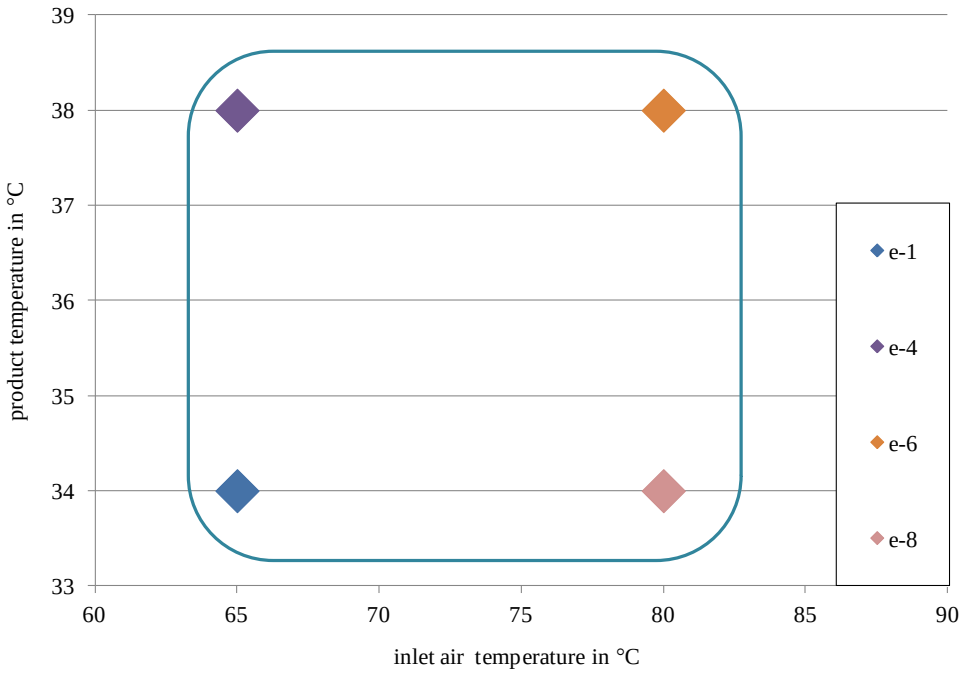

Figure 33 Experimental Design DoE C

The trials were evaluated again applying ANOVA in the way previously described. The interaction between the two factors is again found to be insignificant and was removed. Moreover, the normal probability plot of the residuals did not reveal any peculiarities.
The calculations ended up in this model equation for DoE C:

$$y = 312.667 + 6.867\,x - 12.25\,y + 0 \qquad \text{Eq. 17}$$

Both the effects and their ratio have the same order than found for DoE A and DoE B. The way affecting they affect median particle size was already explained for the previous DoE approaches.
This can be understood as confirmation of the previous DoEs, and also for the legitimacy to expand the investigated design space.

This model for DoE C is also tested by comparing the predicted responses for batches not included in the calculation with measured D_{50}values. The predictions were nearly identical to the measured median particle sizes for four test points as is shown in Table 9.

Table 9 Comparison predicted and measured responses for batches not included in DoE C

Inlet air temperature [°C] = x	**Product temperature [°C] = y**	**D_{50} predicted [µm] = z**	**D_{50} measured [µm]**	**Deviation [µm]**
70	36	352	352	0
75	38	362	366	4
75	34	411	420	9
77.5	36	404	408	4

4.6.3 Conclusions of DoE of fluid bed granulation process

The examined range of the critical process parameters inlet air temperature and product temperature during fluid bed granulation are 65 – 80°C and 34 – 38°C, respectively. The resulting median particle sizes of the granulates ended up between 287 – 439 µm.

It was possible to predict the median particle sizes of the manufactured granulates by the compiled model equations based on product temperature and inlet air temperature as latent variables. Three different models for different ranges of product temperatures were developed. The obtained equations were very similar, showing that product temperature is the more important effect than inlet air temperature. Product temperature has a negative

effect on particle size, meaning that lower product temperatures support granule growth and lead to higher D_{50} values of the granulates. Inlet air temperature had a positive effect, i.e. higher inlet air temperatures result in bigger granules. Both effects can be explained by their influence on the spray rate: lower temperature of the fluid bed can be achieved by increased spray rates, and higher inlet air temperatures also result in higher spray rates, because the product temperature was to be maintained during the whole granulation process. However, the interaction of both variables was assessed as insignificant applying ANOVA.

The original DoE, DoE A with inlet air temperatures from 65 – 75°C, could be reproduced without any problems during the granulation processes. Moreover, the shift of DoE A towards higher inlet air temperatures from 75 – 80°C was successful. It was even possible to span the design space over the whole investigated temperature range from 65 – 80°C. This model equation of DoE B delivered the best predictions for median particle sizes with lowest deviation to the actually found values, although it does not incorporate a centre point run.

Yet, the reproducibility of the results and thus the robustness of the model are to be evaluated by repetition of several trial runs. Furthermore, the transferability to another scale and associated, to another equipment, is not immanent but would have to be verified.

4.7 IMPROVEMENT OF PROBE POSITION IN THE GRANULATOR

The location of insertion of probes into the equipment is crucial for a good quality of the in-line measurements. The probe insertion and its orientation have to be reproducible in order to deliver constant measurements and results. Furthermore, the kind of insertion has to fit the requirements related to workers safety e.g. for explosion protection and pressure shock resistance.

In general, the particle sizing results are affected by the height of the probe location: a fluid bed is typically not perfectly homogeneous and tends to segregation according to the mass of the individual particles. Additionally, it has been described in literature that there are flow patterns which are distinct to conical fluid bed granulators [85].

It was shown by tracking a radioactive particle mimicking a granule moving in the bed that the velocity of particles near the wall is not the same than the one of particles in the core of the fluid bed. The distinct pattern implies faster particles rising in the centre of the product bed, while the outer ones are falling slowly [86]. Therefore, besides the height, also the immersion depth of the particle probe is of importance in order to achieve reliable in-line data.

When using a top-spray granulation approach, care has to be taken that the probe is not directly touched by the spraying cone of the nozzle. This would enlarge the risk of material stuck on the inlet of the dispersing unit of the probe.

Figure 34 depicts schematically the construction of the used fluid bed granulator. The fluid bed granulator consists of a product container and an expansion chamber and has windows for assessing the fluidisation of the product.

The measurements during manufacture of the granulates in the framework of the DoE were used to find optimum conditions for the insertion of the Parsum probe. The location was selected to be at a similar height than the sample thief. This is a prerequisite for comparing in-line measured data to results of off-line tests e.g. sieve analysis. The middle of the product container was supposed to fit best to the requirements of having constantly product in front of the probe when the bed is fluidised and prevents excluding big and dense particles, which are more likely to be located at the lower part of the fluid bed. This would have been the case for measurements carried out in the expansion chamber.

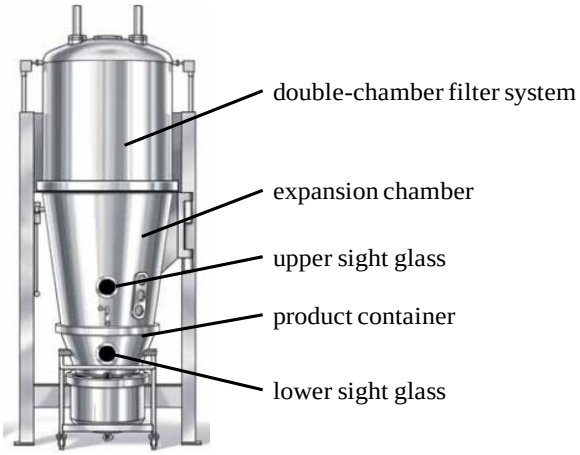

Figure 34 Schematic illustration of the used fluid bed granulator; based on [87]

Previous trials yielded in the definition of an immersion depth of approximately 10 cm into the fluid bed granulator since this delivered most reproducible results. Moreover, the inlet of the dispersing unit of the probe was not oriented vertically, but in an angle of 30° in order to assure that particles are dispersed by the pressurised air of the probe to avoid a too dense particle flow.

Figure 35 depicts the two alternatives for insertion. The first set-up of probe insertion was to substitute the lower sight glass by a home-made plate equipped with flanges for the PAT probes (set-up a). The advantage of this location is the close proximity to the sample thief, but no visual control of the fluid bed granulation is possible any more. Therefore, the insertion of the probe by means of flange (set-up b) was tested as alternative. This set-up allows simultaneously visual evaluation of the current fluidisation behaviour of the product.

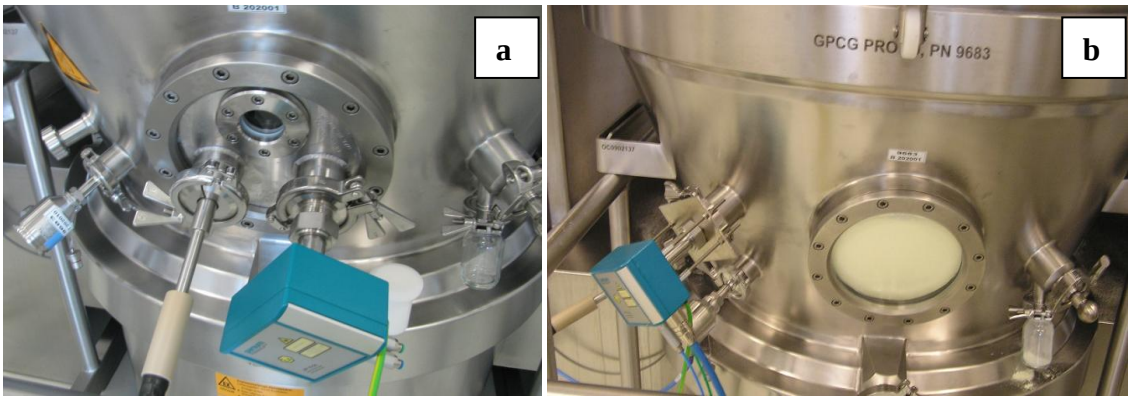

Figure 35 Insertion of the Parsum probe into the product container through the sight glass (a) and by a welded-in flange (b)

The two described locations of the particle probe were considered as equal. This was proven by measuring the particle size distribution during the fluid bed granulation processes of two granulate batches of identical dosage strength. All process parameters were kept constant, except for the installation of the PAT probes.

The particle size data measured in-line by the Parsum probe of both batches is depicted in Figure 36 and allows comparison of set-up a and set-up b. Set-up a, which is based on replacing the sight glass by a home-made plate equipped with flanges (dashed lines), can be compared to the new probe position (set-up b), which is a welded-in flange near to the temperature probe (continuous line).

The particle size measurements were only started after the first seven minutes of granulation of the batch using set-up a. Nevertheless, the particle size data allow the conclusion that the two probe locations are interchangeable without affecting the results of the measured particle size distributions.

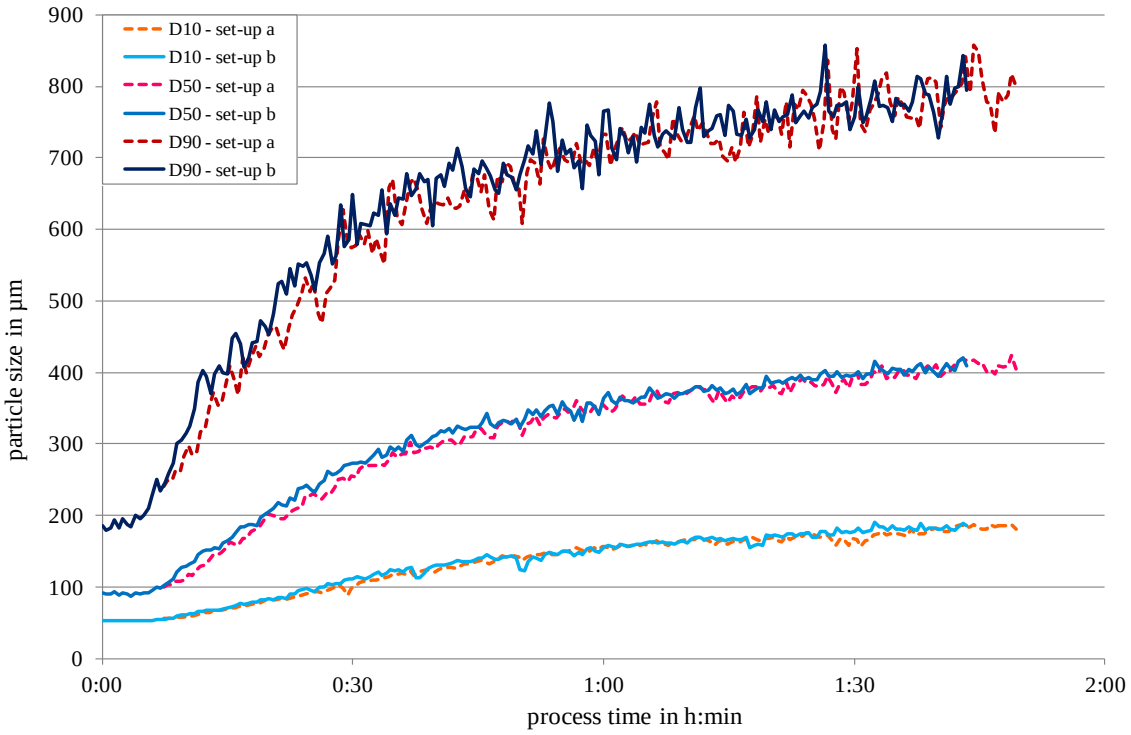

Figure 36 Comparison of in-line particle size measurements in dependence of the probe locations in the fluid bed granulator

4.8 IN-LINE DETERMINATION OF WATER CONTENT BY NEAR INFRARED SPECTROSCOPY

Near infrared spectroscopy is an indirect measuring method requiring reference values for the compilation of a calibration model. The following chapters describe the measuring settings and the details of acquiring NIR data, the reference method and the development of the calibration models.

4.8.1 Measuring settings

An in-line NIR probe, connected to the near infrared spectrometer, which is described in chapter 3.1.3.3, is inserted into the product bowl of the fluid bed granulator GPCG 60 (Glatt, Binzen; Germany).

4.8.1.1 Acquisition of NIR spectra

In-line NIR spectra are recorded as described in detail in Table 10. The acquisition time for single spectra was chosen to be short in order to detect changes in the process in real time.

Table 10 Adjustments for in-line NIR-measurements using the fibre optic probe

Parameter	**Value**
Measuring mode	Diffuse reflection
Wavenumber range	12500 – 4000 cm^{-1}
Resolution	8 cm^{-1}
No. of scans per spectrum	4
Preamplifier gain	B
Detector	Indium-Gallium-Arsenide
Measuring cycle	15 s

4.8.1.2 Calibration samples

Samples for reference measurements of approximately 100 g each are collected every 20 minutes during the spraying phase of the fluid bed granulation process. The sample thief for removing these samples from the product is located at the same height of the granulator bowl than the PAT probes, i.e. NIR and Parsum probe. This set-up was chosen to ensure that granulate having the same properties is sampled than the one being measured by the NIR and the particle probe. At the same time, the granulation process is neither interrupted nor is the fluid bed in front of the probes interfered due to sampling.
The time of sampling is noted in order to correlate relating NIR spectra, particle sizes and important process parameters, e.g. product temperature and spray rate. The reference measurements LOD and sieve analysis are carried out in the way described in chapter 3.3.1 and 3.3.6, respectively.

4.8.2 Compilation of NIR calibration model for in-line moisture determination

The moisture quantitation model includes calibration spectra out of more than 30 granulation batches and was applicable for all six granulates covering drug loads from 0.43 – 2.15 % of API 2.
The NIR model for in-line moisture determination is intended to monitor and control the whole fluid bed granulation process. This implies the requirement, that moisture can be determined independent of changes in chemical composition due to the addition of granulating solution containing API and binder, but also the model being insensitive versus changes in particle size. These changes occur on the one hand during each granulation process, starting with a powder of approximately 100 µm as median particle size and ending up with granules from 300 – 400 µm, and on the other hand as the result of deliberate variations in certain process parameters, e.g. DoE trials (see chapter 4.6) or the trials on modes of dedusting the filterbags (see chapter 4.5).
Outlier values are recognised automatically by the software and are removed before generating the calibration model.

4.8.2.1 Selected wavenumber ranges

The PLS model for moisture determination is intended to quantify specifically water. Therefore, wavenumber ranges are selected, where the absorption of water is high in order to discard irrelevant wavelengths. This approach is advised e.g. by Blanco [88].
Typical absorption peaks of water molecules in the NIR range can be found in literature: the absorption peaks of water are the overtone vibration, the peak maximum of which is around 1420 nm (corresponding to 7040 cm^{-1}) and the combination vibration at approximately 1920 nm (5200 cm^{-1}) [89]. These absorption bands are very distinct, especially the combination band of the O-H-vibrations.

4.8.2.2 Selected pre-processing techniques

The effect of different chosen pre-processing techniques is described as follows.
Figure 37 depicts NIR raw spectra out of one fluid bed granulation process in the wavenumber range of interest between 7500 cm^{-1} and 4200 cm^{-1}. The offset of the spectra increases with progress of the granulation. Other differences are difficult to realise in this visualisation.

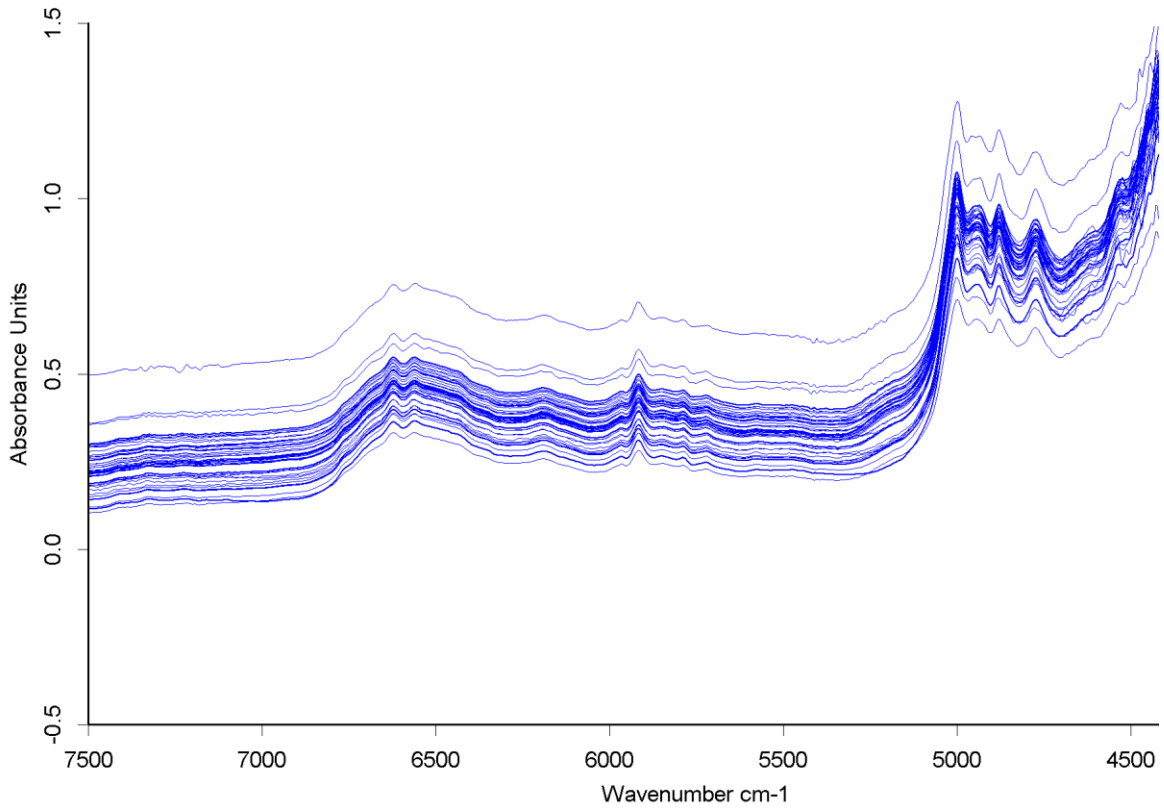

Figure 37 NIR spectra of one fluid bed granulation batch, raw data

The first pre-processing technique applied is an offset correction which removes the baseline offset. This shift in the baseline is often due to changes in physical conditions, either due to temperature or particle size changes. The spectral differences in the region of 5200 cm^{-1}, related to the combination vibration, become more apparent in the off-set corrected spectra as depicted in Figure 38.

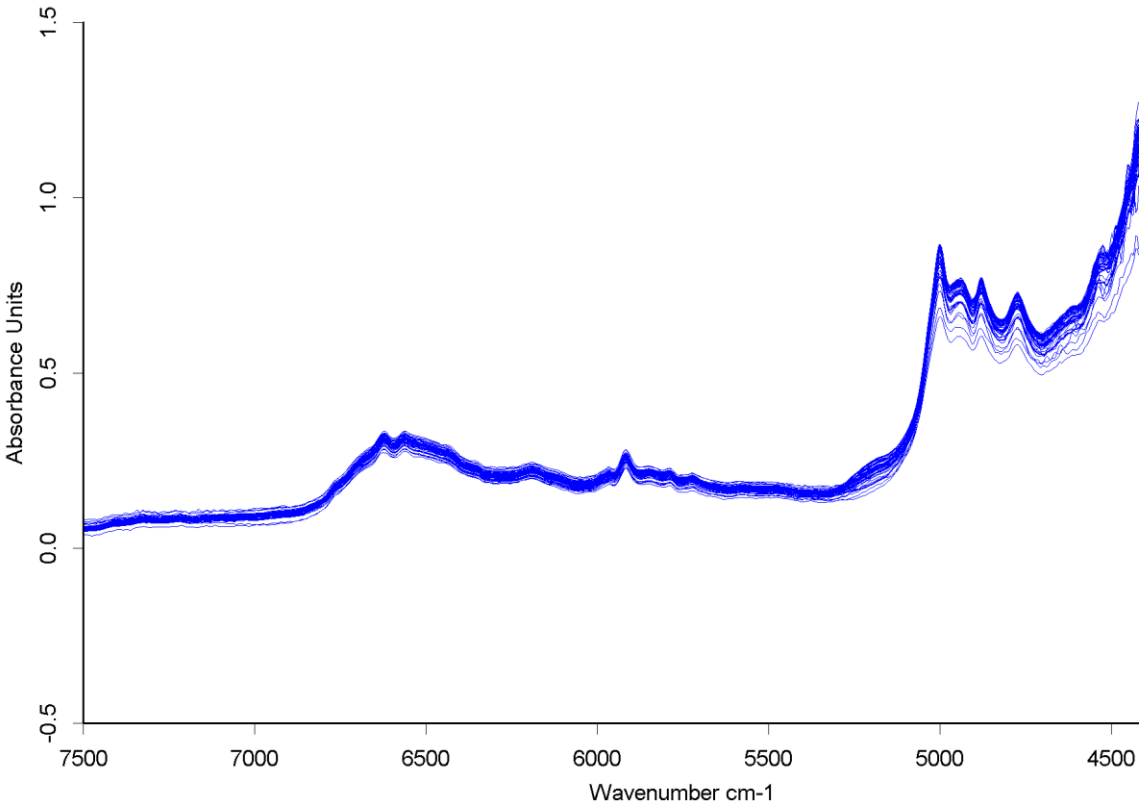

Figure 38 Pre-processed NIR spectra of one fluid bed granulation batch, offset corrected

Calculating the first derivation of the spectra reveals the typical water absorption peak: the distinct combination vibration at 5200 cm^{-1}, presented in Figure 39. The 1st derivation of the spectra was calculated after Savitzky-Golay with 25 smoothing points, followed by Standard Normal Variate transformation.

The overtone vibration at 7000 cm^{-1} is still not obvious. Eliminating or minimising physical influences on the spectra reduces noise and improves the prediction accuracy of the calibration model. This pre-processing technique was chosen for developing quantitative calibration models.

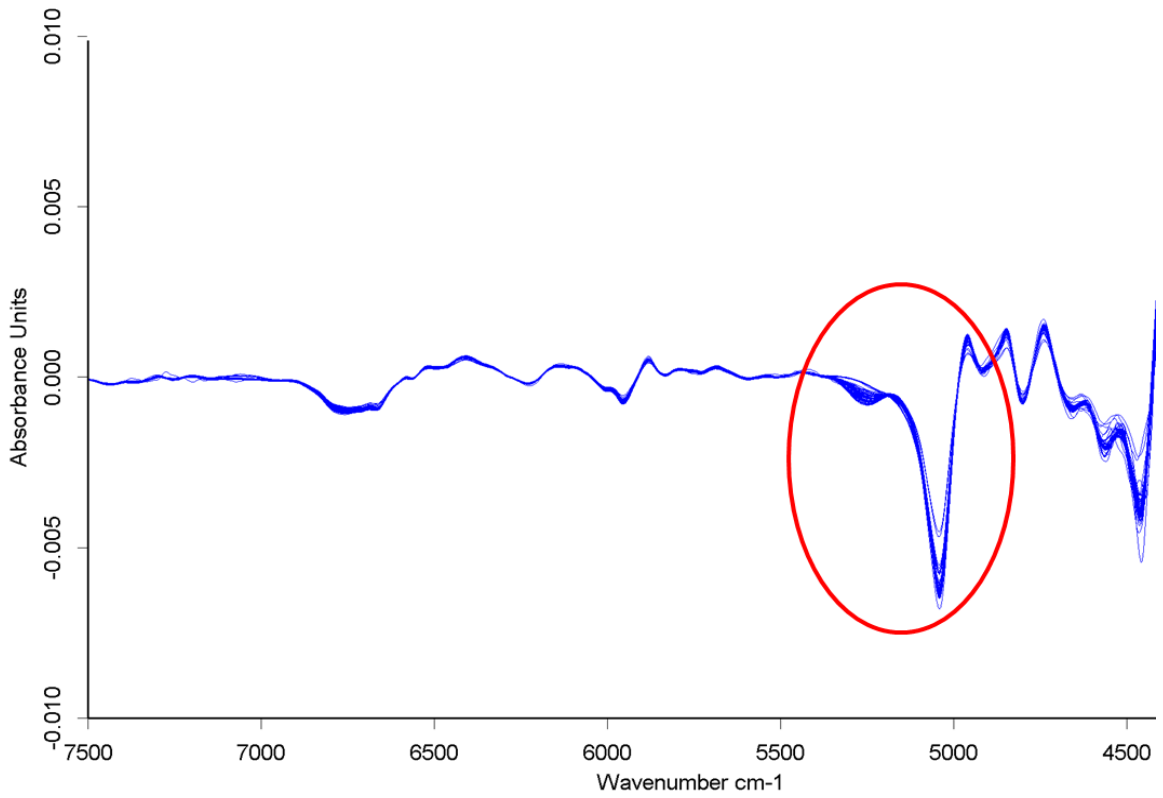

Figure 39 Pre-processed NIR spectra out of one batch, 1st derivation followed by SNV

The section marked in red in Figure 39 was further investigated by means of a drying experiment. The granulate was subject to fluid bed drying directly after the granulation spraying phase had been completed. NIR spectra recorded at the start (orange) and end (blue) of the spraying process, as well as spectra from two further moisture levels (green and red), were selected to illustrate the distinct features in the first derivation of the spectra (see Figure 40).

The minimum at approximately 5270 cm^{-1} corresponds to the combination vibration of surface water, while the area around 5140 cm^{-1} is due to the combination vibration of bound water. These findings correspond to the phenomenon reported by other authors (e.g. [89]), who were able to differentiate surface and bound water in derivations of NIR spectra.

The combination vibration of bound water at 5140 cm^{-1} is very close for all samples except of the orange-coloured start sample. This indicates that the water binding capacity of the product is small and is quickly saturated during the granulation process. Further water is adsorbed at the surface of the granules. This surface water decreases during a subsequent

drying process. Therefore, the minimum at 5270 cm^{-1} is less distinct the lower the water content and thus the amount of surface water is.

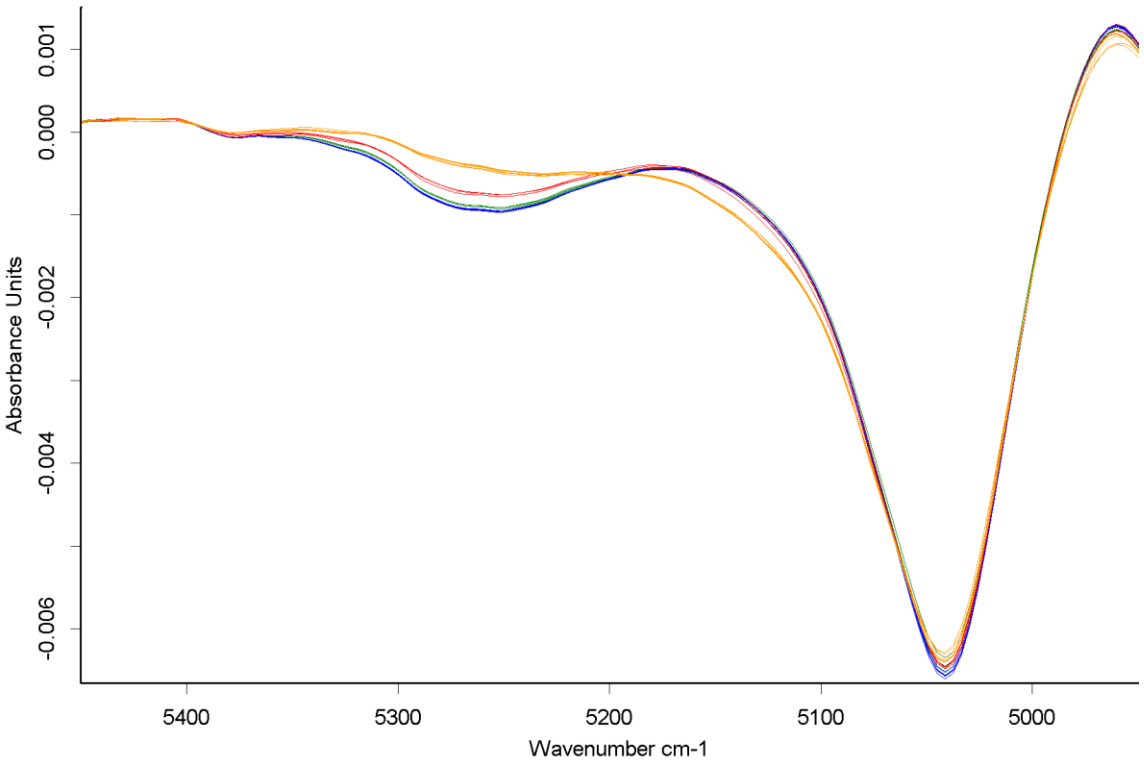

Figure 40 NIR spectra at different moisture levels: orange: start of granulation ≈ 0.7 %, blue: end of granulation: ≈ 1.6%, green: drying until ≈ 1.4%, red: drying until ≈ 1.1% , pre-processed by 1st derivation

4.8.2.3 Comparison of developed calibration models

The calibration work took place simultaneously to the process development of this drug product. Therefore, the initial PLS calibration models include only few calibration spectra recorded during the manufacture of only a small number of batches. With increasing number of calibration spectra corresponding to different batches and up to six different drug loads, both the accuracy and the robustness of the PLS calibration model were excellent. The robustness of the method even allowed compiling one single calibration model for prediction of the water content for all granulates in six different drug loads.

Different calibration models are presented in Table 11, which allows directly comparing three final methods.

Table 11 Comparison of calibration parameters for developed PLS models

Parameter	**Method 1**	**Method 2**	**Method 3**
No. of batches included	32	32	31
No. of calibration spectra included	505	501	491
Calibration range [% LOD]	**0.34 – 1.64**	**0.34 – 1.64**	0.57 – 1.64
Data pre-processing technique	No pre-processing	**1st derivation + SNV**	**1st derivation + SNV**
Selected wavenumber range [cm^{-1}]	**7309 – 6757** **5345 – 5064**	**7309 – 6757** **5345 – 5064**	5345 – 5064
R^2 [%]	97.18	97.13	96.72
RMSECV [%]	0.039	0.039	0.040
Bias	0.00016	-0.00009	0.000017
Offset	0.030	0.030	0.034
Rank	6	3	2

Initially, the calibration models summarised in Table 11 contain the same set of calibration spectra and reference values, but depending on the pre-processing technique applied and the wavenumber range selected, other spectra are recognised as outliers by the software. Spectral outlier detection was performed by determining the Mahalanobis distance between the respective spectrum and the calibration set. The Mahalanobis distance is a statistical technique often applied in combination with multivariate data analysis and gives the distance between points in a multi-dimensional space. Thus spectra which display different spectral features than the spectra of the calibration set are recognised. The identified spectra have been removed before performing full cross validation, the procedure which is described in chapter 3.1.5.4.2. Exemplarily, Figure 41 depicts the result of full cross validation of Method 3 for illustrative purposes. The correlation between values predicted

by the calibration model and the reference values is very high and no clear trend with regards to the residuals can be observed.

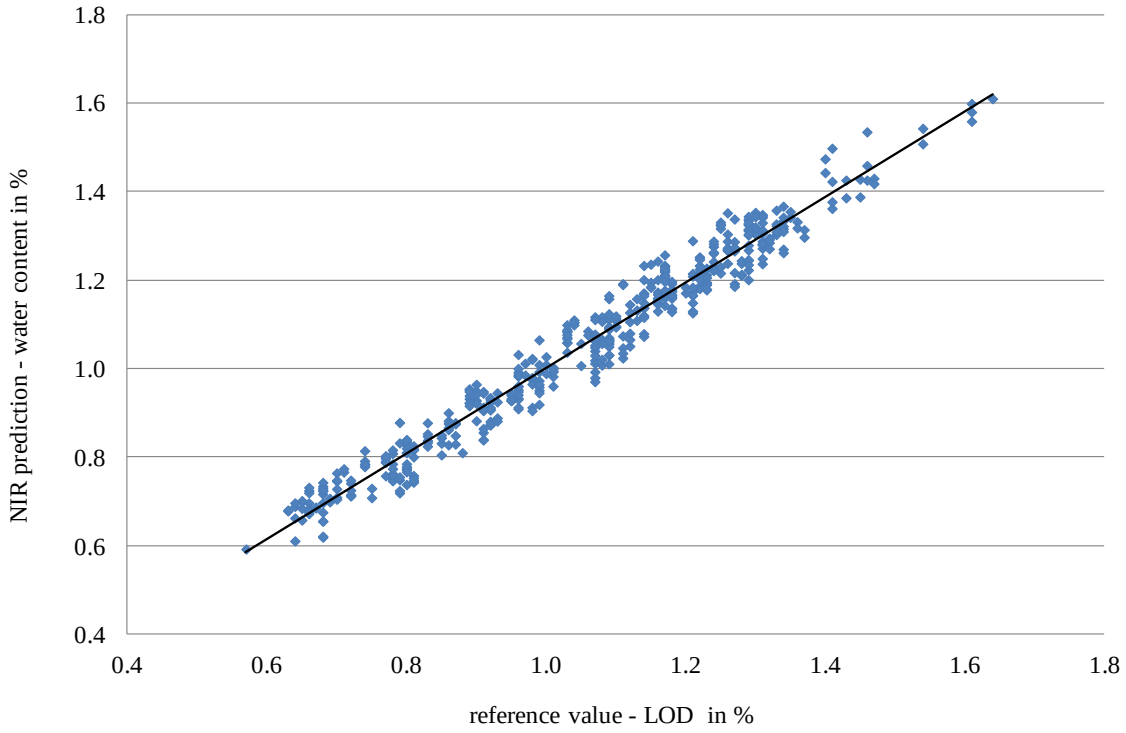

Figure 41 Cross validation of NIR method for in-line moisture determination

Method 1 and Method 2 (see Table 11) consist of calibration data of the same wavenumber ranges, involving both the 2nd overtone vibration at around 6900 cm^{-1} and the combination vibration of water at approximately 5200 cm^{-1} [52]. Method 3 covers only data of the combination vibration wavenumber region.

However, the methods differ in the applied pre-processing technique, the effect of which has already been discussed in section 4.8.2.2. 1st derivation was chosen for eliminating baseline corrections, while SNV transformation centres and normalizes the spectra and removes scatter effects. Method 1 was compiled without pre-processing the spectral data, while Method 2 and Method 3 are based on firstly derivative spectra which were additionally pre-processed by SNV. Data pre-processing by 1st derivation and SNV delivered best results.

Beside of the variation in water content, a lot of variation present in the spectra is due to the fact of in-line-measuring. The sample is a moving particle bed in front of the probe and a lot of information, which is not caused by chemical changes, is captured in the NIR spectra, requiring data pre-processing.

The coefficient of prediction (R^2) obtained by cross validation of the calibration model is > 96 % for all of the presented methods. This is an indicator of goodness of fit, since more than 96 % of the variability in the calibration data is accounted for in the predictive model. Correspondingly, the RMSECV values are ≤ 0.040, which is very small and indicates itself good modelling. Moreover, both bias and offset are almost zero and thus have no inadvertent effect on the model with regards to linearity and fit of the regression.

All three methods are similar in the key performance indicators R^2, RMSECV, bias and offset. However, the calibration models differ in the rank, which is the number of principal components considered to establish the PLS models. The higher the rank, the higher is the risk of overfitting the model. Overfitted models are characterised by low values for RMSECV, yielding excellent results for cross validation, but poor predictive ability for new samples. This phenomenon was already stated by other authors, who point out to the paradox, that the method with the smallest apparent error is not necessarily optimal for process monitoring. This is particularly valid for in-line measurements in solid systems, which are prone to heterogeneity [90].
Therefore, Method 3 was chosen as the most promising model which could also be applied during routine manufacturing of this product.

4.8.2.4 Development of model performance

The performance of the model changed over time by including more and more samples collected during granulation of different batches with different process parameters into the calibration. Therefore, the samples differ not only in the amount of water which they contain, but also in attributes like particle size distribution, composition due to different drug loads of the batches, temperature and others. The calibration model was developed synchronously to the process development, thus the model performance increased at the same time than did process understanding.
The root mean square error is an indicator of the quality of the calibration model when predicting new samples. The RMSEP gives the mean deviation between predicted NIR values and respective reference values for a number of samples; the lower its value, the closer are the predicted values and the values determined by the reference analysis and, as a consequence, the more accurate is the model.

Samples of each succeeding batch were included into the calibration model and the model was applied for monitoring of the following batch. The deviations between predicted and found LOD values for all samples of one batch are summarised in the RMSEP, which is depicted in Figure 42 dependent on the number of batches included in the calibration model. For comparability reasons, the calibration parameters, e.g. wavenumber ranges and data pre-processing, were the final ones of calibration method 3 for these calculations.

a) The RMSEP for the model, which is based on calibration samples out of one batch, is comprehensibly high, because the succeeding test batch had a different drug load.
b) The following values are similar, except of the one for the model built up on seven batches. The test samples for this model were part of a batch of which the moisture content was higher than for the trials before and which was partly overwetted. But including these samples into the calibration model, lead again to lower RMSEP values.
c) The model compiled on fifteen batches was used to predict the water content during fluid bed granulation of one of the batches (batch *e-5*), which are part of the DoE; this one manufactured at low inlet air temperature and lowest product temperature, resulting in high moisture levels during the process.
d) The batch, which was monitored by means of the NIR calibration model built upon eighteen calibration batches was another extreme batch of the DoE (batch *e-8*), granulated applying maximum inlet air temperature and minimum product temperature, leading to the highest median particle sizes, which might have affected NIR predictions.

After having included all batches, which were part of the DoE, into the NIR calibration model, the performance of the calibration model was similar for all other batches. The RMSEP levelled off at a small value below 0.04 % water content, which indicates excellent goodness of the model.

This evaluation proves that for development of a robust NIR calibration model batches with varying process parameters are needed. For this special formulation, the resulting changes in physical attributes like particle size and moisture where even more important as interfering factors than different drug loads. Therefore, the calibration efforts for multivariate models have to be implemented into the process development phase.

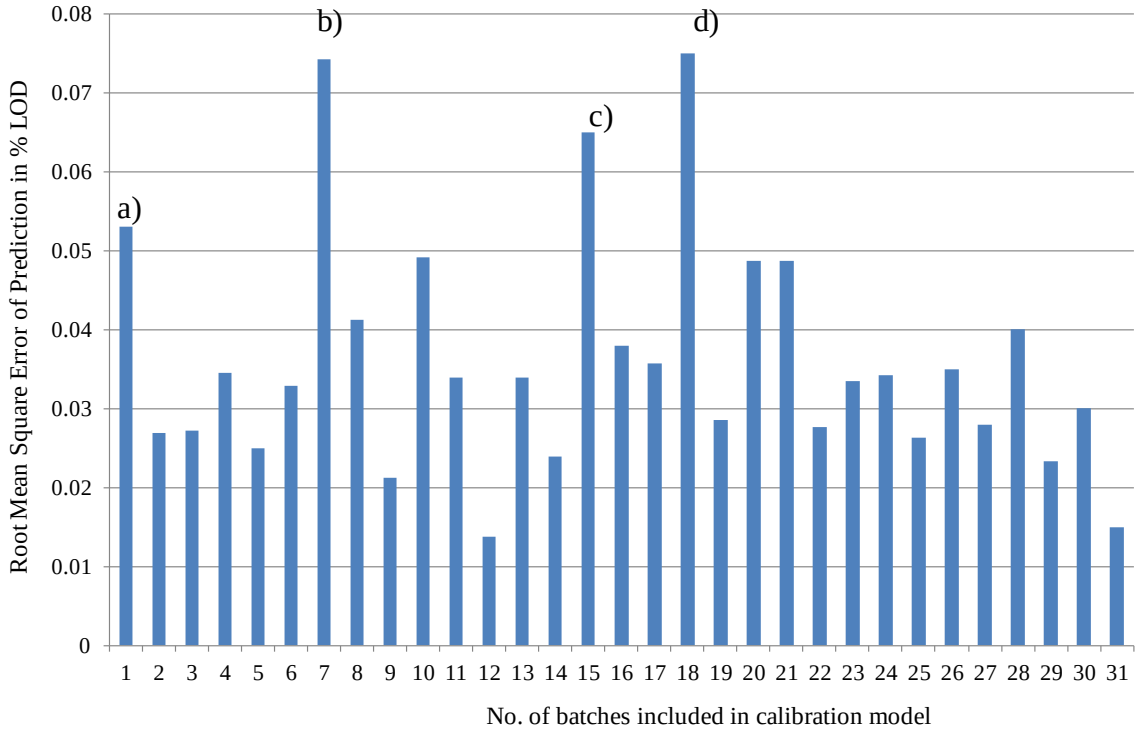

Figure 42 Development of NIR model performance by reference to RMSEP with increasing number of batches included in the calibration model

4.8.2.5 Principal component analysis

Principal component analysis (PCA) is a chemometric method to extract information of interest from a tremendous amount of data and to condense the variation, which is present in the data, into a reasonable number of principal components. The mathematical background is explained in chapter 3.1.5.2.

A principal component analysis was performed on all spectra of Method 3, which was the final calibration model for in-line moisture determination. The parameters selected for the PLS model were used for the PCA. NIR spectra pre-treated by 1st derivation after Savitzky-Golay with 25 smoothing points in the wavenumber range 5345 – 5064 cm^{-1} were used for the analysis.

A clear differentiation with regard to water content is achieved using the scores on the first and the second principal component, of which the loading plots are given in Figure 40. Moreover, the samples of similar moisture collected after 60 minutes of spraying and during the second drying step have close scores on the second principal component, which is related to the water content.

The principal component analysis confirms the selected parameters of the PLS model, since it allows ranging the spectra according to their moisture level.

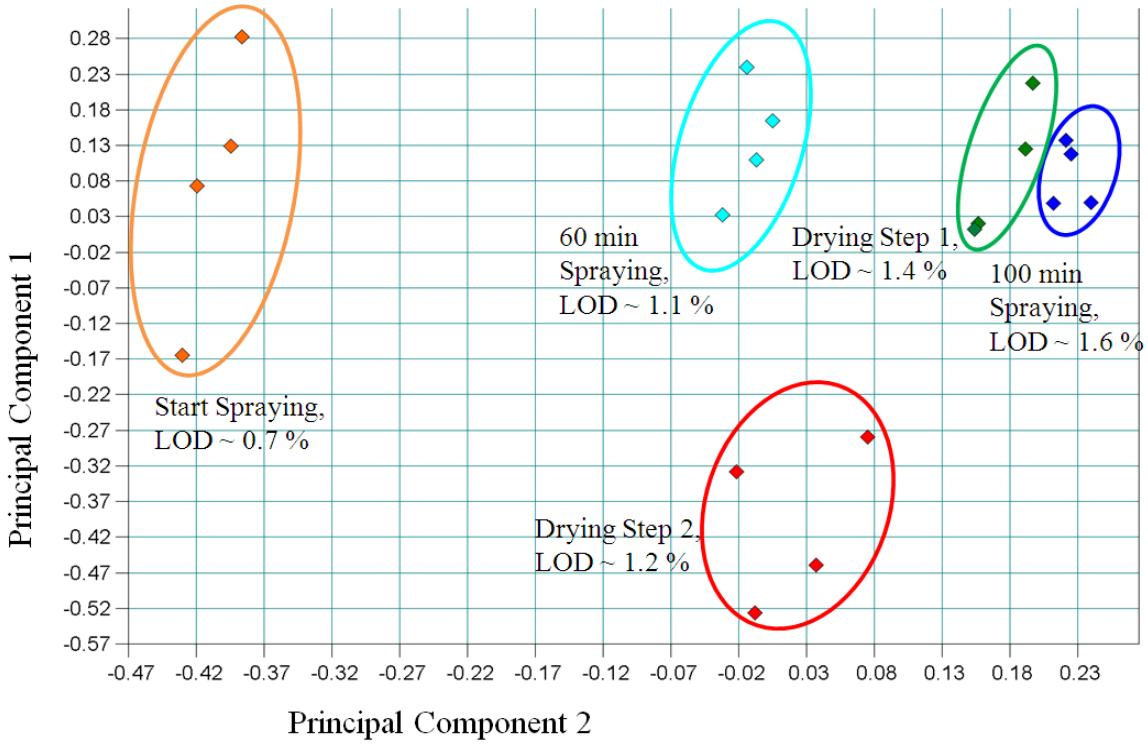

Figure 43 Principal component analysis of samples of different moisture levels, 1st derivative spectra in the selected wavelength range

Most of the variability of the calibration spectra can be expressed by a single principal component, which accounts for 95.72 %. The second principal component enhances this value for another 1.00 %. The loadings of these two vectors are illustrated in Figure 44.
The first principal component (blue) resembles the 1st derivative spectrum of pure water. The second one is noisier, showing a similar form to the first one, but is shifted to higher wavelengths. Shifts of absorption maxima can be due to different properties regarding the strength of water binding properties.

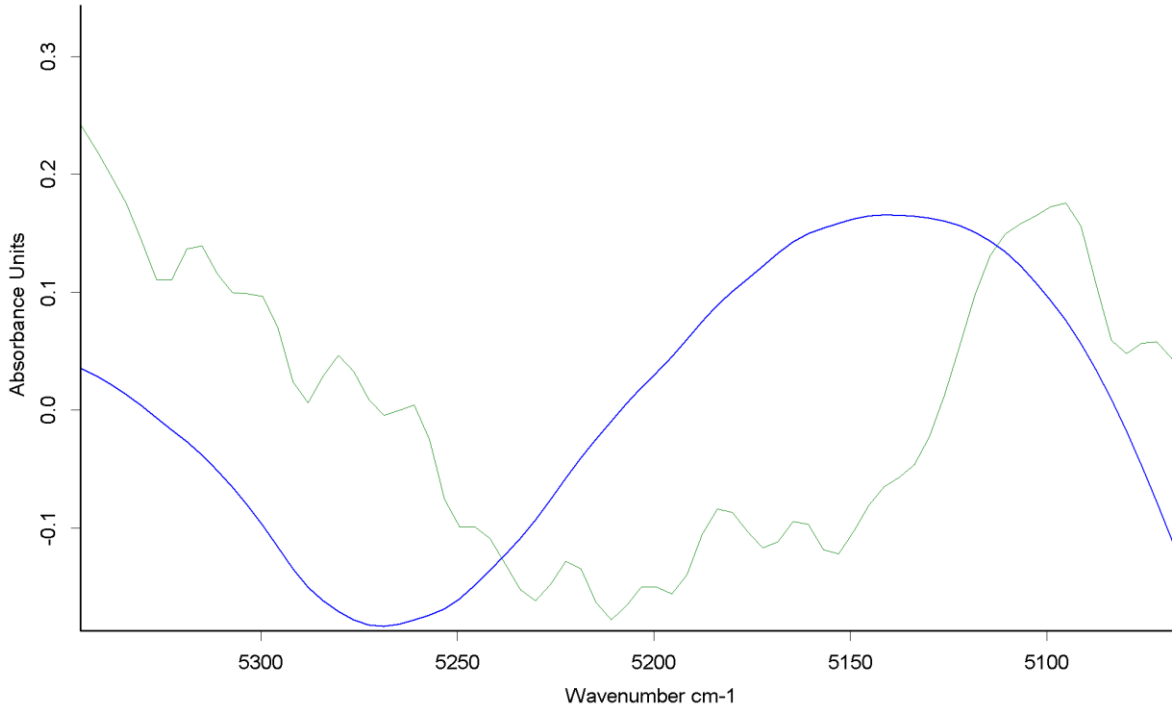

Figure 44 Loadings obtained by PCA; blue: PC1, green: PC2

Moreover, Partial Least Squares regression, which includes the reference values in order to find the principal components, was performed. PLS regression revealed that subsequent principal components increase the coefficient of determination and improve the RMSECV only slightly. However, this amelioration is not considered as significant, since more principal components increase noise signals in the PLS model and the risk of overfitting raises. Overfitted models deliver high values for the coefficient of determination and the Root Mean Square Error of Cross Validation, but result in poor robustness and therefore often in deviating prediction values.

4.8.3 Performance of NIR calibration model

4.8.3.1 Accuracy of NIR model

The performance of a calibration model can be assessed by applying the method for moisture prediction of a new batch, which has not been used for calibration purposes. The accuracy of the calibration model is evaluated by comparing in-line measured NIR values of certain timepoints to traditional off-line LOD-measurements by means of a halogen dryer of samples collected at the respective timepoints. The values for batch *f* are provided in Table 12.

The in-line NIR-measurements are very close to the reference values; thus the developed calibration model was successful. The highest deviation between NIR and LOD was 0.29 % for the first sample; all other values are much closer. The next higher deviation was found to be 0.07 % water for the second sample; all further predictions are even closer.

Table 12 Comparison of NIR predictions and LOD values for batch *f*

Process time [min]	**NIR prediction [%]**	**LOD [%]**	**Deviation [%]**
0	0.78	0.49	0.29
20	0.86	0.79	0.07
30	0.93	0.95	-0.02
40	1.01	0.97	0.04
60	1.08	1.09	-0.01
70	1.16	1.17	-0.01
80	1.19	1.16	0.03
90	1.27	1.24	0.03
100	1.32	1.27	0.05
104	1.34	1.34	0.00
105	1.33	1.36	-0.03
106	1.34	1.29	0.05
107	1.34	1.30	0.04
108	1.34	1.31	0.03
109	1.33	1.29	0.04
110	1.32	1.30	0.02

The residuals obtained were highest for the beginning of the granulation process as is presented in Figure 45. For a process time longer than 20 minutes, the residuals are less or equal than 0.05 %, showing no clear trend. This is even less than the variation of the reference method LOD, which was given to be ≤ 0.1 % (red line), expressed as absolute deviation of moisture content.

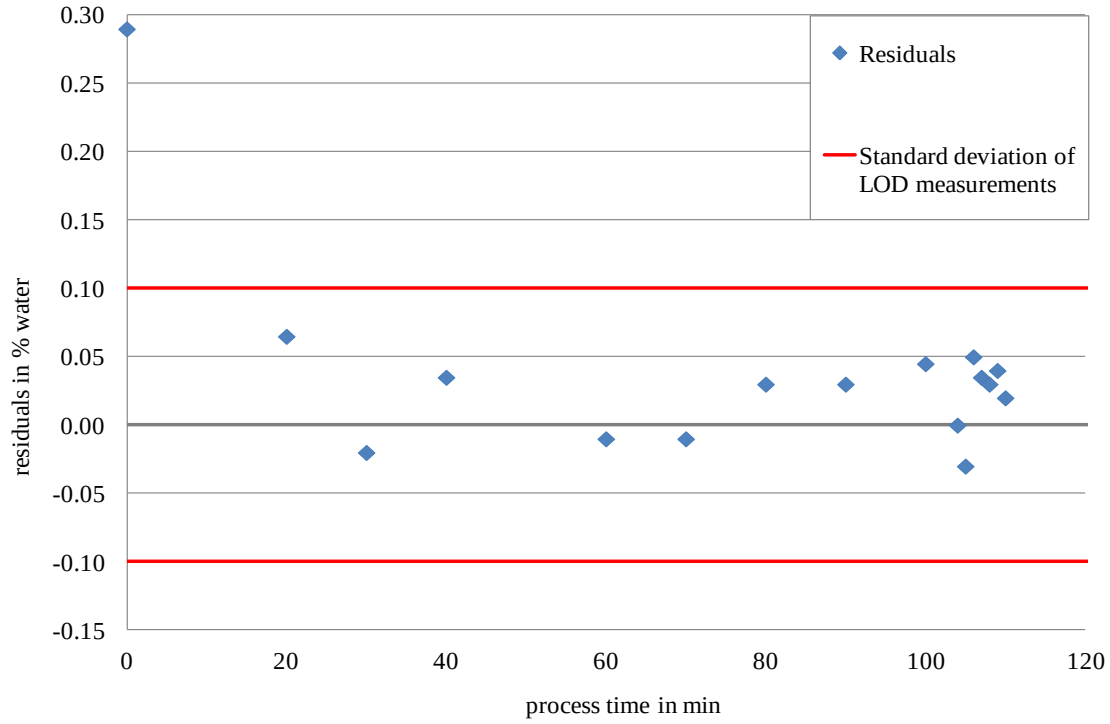

Figure 45 Correlation of process time and residuals of NIR predictions vs. reference values of batch *f*

4.8.3.2 Precision of NIR model

Moreover, the NIR-measurements allow monitoring the complete granulation process. This is not possible when using a halogen-dryer, since only the moisture for single time-points can be controlled and the result is available soonest after 15 minutes. The moisture content during the whole granulation process and the confirming LOD values are depicted in Figure 46.

This graph also allows assessing the precision of the NIR predictions, since the variation in subsequent measurements is apparent. Linking the variation of subsequent in-line measurements to the precision of a test method implies that the measured product does not change between consecutive measurements. This can not be guaranteed in a fluid bed process, but the changes are assumed to occur with low speed. Besides, each NIR spectrum itself is averaged of several scans and thus is not related to a specific part of the continuously moving sample. This fact was already reported by Green et al., who found out that heterogeneity played a major role in determination of apparent prediction accuracy for in-line measurements of solid systems [90].

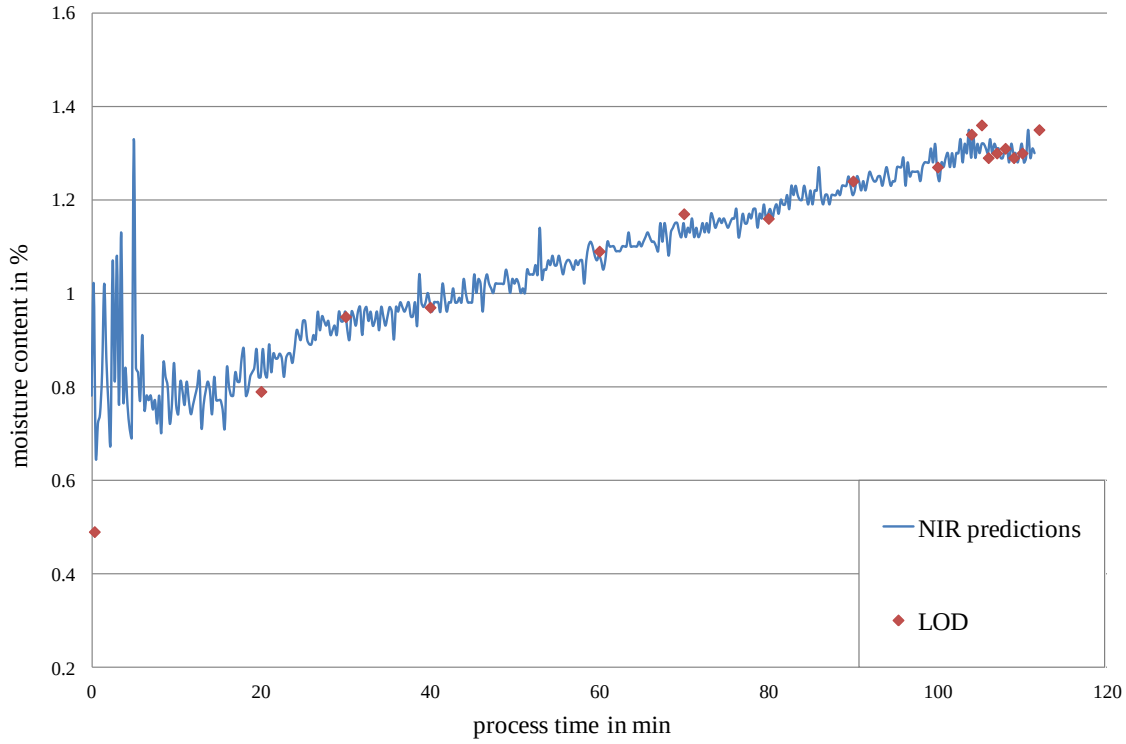

Figure 46 Water content during fluid bed granulation of batch *f* measured by NIR spectroscopy and LOD

4.8.3.3 Assessment of NIR model

The developed calibration model is applicable for monitoring the whole fluid bed granulation process. The higher deviations in the early granulation phase can be explained by two phenomena: On the one hand, smaller particles, which are mainly present at the beginning of the process, produce much more straylight than bigger agglomerates, and on the other hand, the nucleation and wetting phase is characterised by inhomogeneous distribution of moisture in the fluidised powder bed. Moreover, the location of the probe, which is installed in the middle of the granulator bowl, can play a major role, when the water is only present in some single nuclei. The probability that wet nuclei are in the lower part of the GPCG is high, since their mass is higher compared to drier particles. Hence the probability that these particles pass the NIR probe is higher.

The following trial was set up in order to confirm the assumption, that the NIR model for in-line moisture determination allows even controlling subsequent drying steps of the granulate.

4.8.4 Trial on the application of the NIR calibration model for gradual drying

This trial was performed in order to examine whether the compiled NIR calibration model for water determination during the granulation process would also be an appropriate PAT tool to monitor potentially needed re-processing like subsequent fluid bed drying.
The regular granulation process lead to a granulate of 1.6 % LOD. This batch was subject to further fluid bed drying, in order to decrease the moisture content onto 1.4 % for the first drying step and to 1.2 % LOD for a further drying step respectively.
Both granulation and drying were accompanied by NIR-measurements. The drying process was stopped as soon as the real time measurements revealed that the intended LOD was reached. Then samples were collected to confirm the PAT-results by LOD values.
NIR- and reference values depicted in Figure 47 indicate very good agreement and hence the direct applicability of the calibration model for potentially necessary post-drying processes.

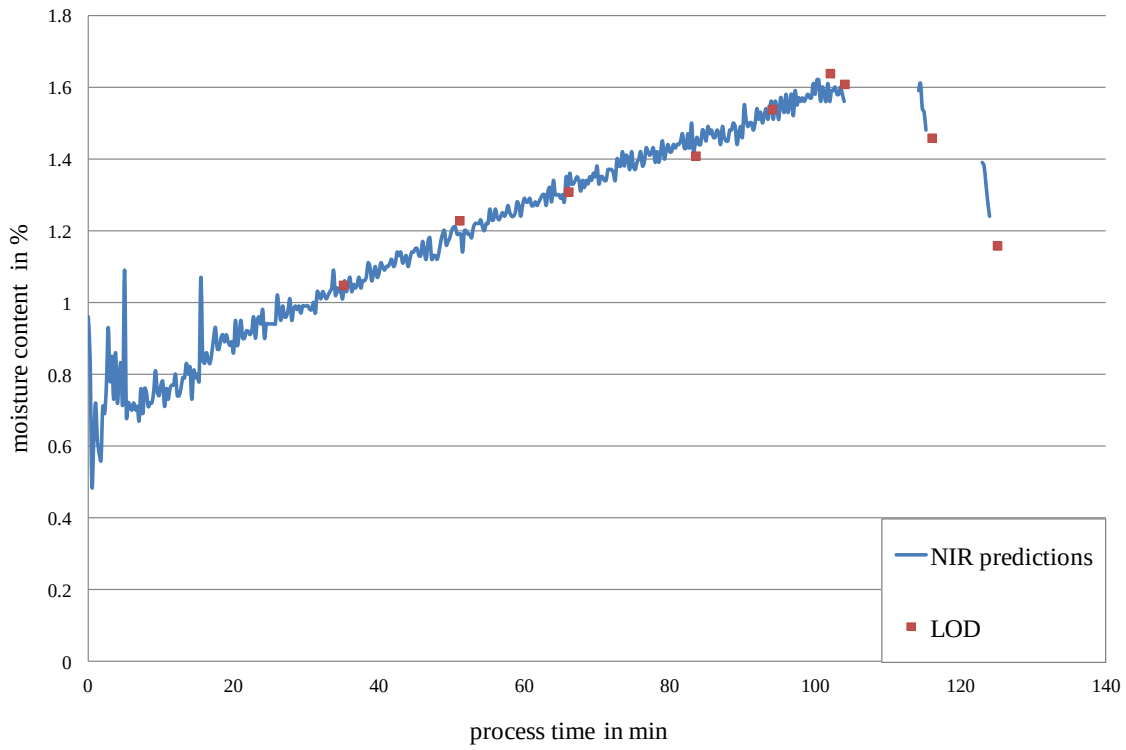

Figure 47 Moisture content during fluid bed granulation and subsequent gradual drying

4.8.5 Verification of NIR model during scale-up to commercial scale

The developed NIR model for in-line moisture determination during granulation in full scale was to be verified on its applicability for commercial scale for fluid bed granulation in a WSG 300 (Glatt, Binzen, Germany). This scale is achieved by a scale-up factor of almost four.
Another FT-NIR-spectrometer was applied for recording the NIR spectra during the fluid bed granulation processes in commercial scale. The spectrometer type was Matrix F (Bruker Optics, Ettlingen, Germany) equipped with a fibre optic probe, which is identical to the one used during process development in full scale.
The transfer of the calibration model is supposed to work without problems, since both types of NIR spectrometers contain a laser beam for precise wavelength measurements.

The focus was particularly set on the verification of the full scale NIR calibration model for in-line determination of water content during fluid bed granulation in commercial scale. Although the method was developed to achieve high robustness and performed well for granulations in full scale, its applicability for processes in other scales and changed equipment is to be proven. Challenges for moisture quantitation by NIRS are mainly changes in the physical attributes of the samples, which are e.g.

- Altered particle size distribution of the granules due to changed spray pattern of the used nozzles or massing effects due to scale-up, therefore
- Changes in density of the fluid bed in front of the NIR probe
- Further temperature effects
- Other sampler and thus probably changed sample composition
- Modified NIR probe location and its orientation relative to the sampler.

4.8.5.1 Testing procedure

Six granulate batches were manufactured in commercial scale representing three different drug loads of API 2 (0.43 – 2.15 %) and a confirmation trial of each drug load. The testing procedure was identical to the approach in pilot scale:
During the fluid bed granulation process, in-line NIR spectra are collected in order to assess the moisture of the granulate. Granulate samples of approximately 50 g respectively

are removed from the product container. Off-line LOD reference analyses are carried out on a halogen dryer and the results are compared to the NIR predictions.

4.8.5.2 Performance of NIR calibration model for manufacture in commercial scale

The values for water content obtained by near-infrared spectroscopy in real-time allowed monitoring granulate moisture during the complete granulation processes. An example of one fluid bed granulation process of a successfully manufactured batch in commercial scale is depicted in Figure 48. The moisture content during granulation predicted by near infrared spectroscopy is consistent with collected samples, of which the LOD values were determined off-line. Succeeding NIR values vary in a range smaller than 0.05 %, which indicates good precision of the calibration model in the larger scale. Moreover, the conformance of NIR values and reference values prove that the accuracy, which has been claimed in the smaller scale, is still valid in commercial scale.

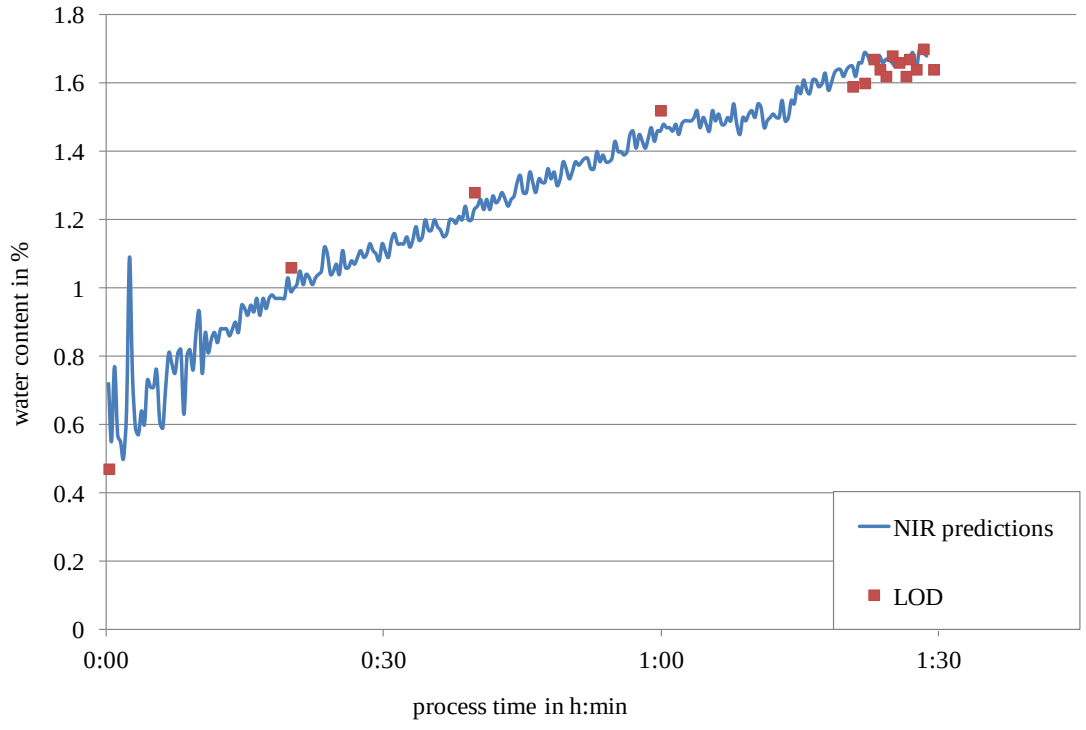

Figure 48 Performance of NIR model in commercial scale

The application of NIRS during manufacture in commercial scale revealed its ability for trouble-shooting purposes as illustrated in Figure 49.

For nearly one hour (phase I), the fluid bed granulation worked out as expected with continuously rising moisture content of the granulate and good correlation between NIR and LOD values. Then one of the nozzles was blocked and the spray rate suddenly decreased, thus the granulate was subject to drying for some minutes (phase II) and directly expressed in the NIR values. The fluidisation was stopped immediately and the spray nozzles were removed and cleaned (phase III). The NIR predictions during this time are constant, since the product is static and in direct contact with the NIR probe. The values are slightly higher than for fluidised product which is an effect of higher density of the measured material. This is an explanation for the drop in NIR values with beginning of re-fluidisation and continuing spraying in phase IV. The LOD values in phase IV differ for approximately 0.1 % (m/m) of water, which is still in an acceptable range since it is in the range of variation of the LOD method, but is higher than before the process was interrupted. Hence, near infrared spectroscopy allowed real-time monitoring of the manufacturing process and supported prompt answering to process disturbances and prevented re-processing of this batch.

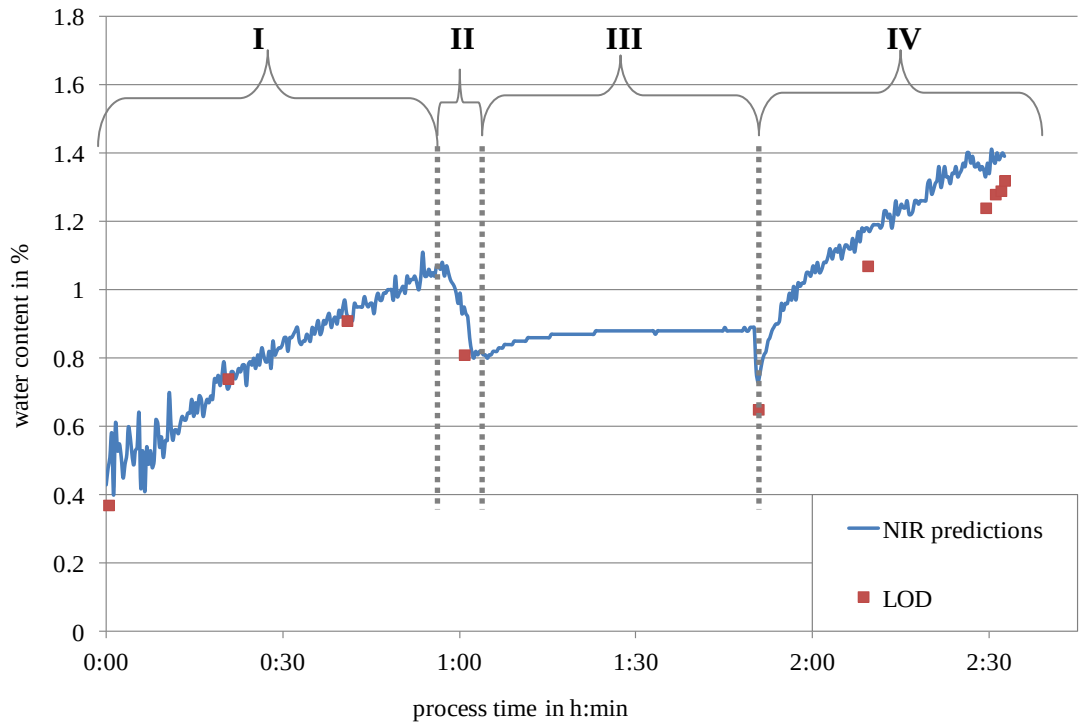

Figure 49 Performance of NIR model and support of trouble-shooting during manufacture in commercial scale

4.9 CONCLUSION PROJECT A AND ADDITIONAL VALUE OF APPLICATION OF PROCESS ANALYTICAL TECHNIQUES

The application of process analytical techniques allowed gaining valuable insight into the manufacturing process. This was realised by means of simultaneous in-line moisture determination and in-line particle sizing during the fluid bed granulation process. This unit operation has been identified as the main manufacturing step which influences downstream processability and quality attributes of the final drug product. Therefore, the importance to create a thorough knowledge base during process development and scale-up was considered as crucial.

Parsum measurements for particle sizing revealed different phases during fluid bed granulation: wetting and nucleation as well as agglomeration and steady-state could be observed. Moreover, the impacts of varying process parameters on the final granules could be assessed by this PAT tool. The moisture content of the granulate at the end of the manufacturing step was even more critical with regards to compression properties and stability of the API; such being the case for implementing extensive in-line moisture monitoring during granulation in the process design project phase.

At first, the effect of different dedusting modes, synchronous and asynchronous filter-joggling, during the first granulation phase was found not to result in differences in D_{10}, D_{50} or D_{90} values of the granulates after the process had been completed. The results of in-line particle size measurements using the Parsum probe were compared to further off-line particle analyses. The results for median particle sizes were consistent to sieve analysis results of samples of samples collected at defined time points throughout the granulation process, but differed slightly for D_{10} and D_{50} quantiles. The comparability shown is restricted to D_{50} values of granulates in the investigated particle size range and might be product-specific, since the applied shear forces for sieving and spatial filter velocimetry and the sensitivity of the product towards them might not be the same. The measurements realised by the image analysing system Occhio and the Scanning Electron Microscopy images are not particularly suitable for the evaluation of particle sizes; other applications e.g. assessment of granulate morphology are more pronounced. Even if the actually obtained particle size results of all these measurements techniques are not identical, they yield comparable relations. The in-line determination of the entire particle size distribution during granulation lead to enhanced process understanding, since effects of changed process parameters on the particle size could directly be observed and

supported significantly process knowledge. Finally, this knowledge ended up in the establishment of a predictive model for median particle size of the granulate based on the process parameters product temperature and inlet air temperature.

Additionally, the granulation processes were accompanied by NIR measurements, which allowed real-time determination of water content during the granulation process. It was possible to develop a calibration model based on Partial Least Squares, of which validity both in full and in commercial scale could be demonstrated. The successful establishment of NIRS for moisture monitoring did not only facilitate process development activities by reducing the risk of loosing batches, but also effectively supported transfer activities to another manufacturing site and further scale-up to commercial scale.

Although there is currently no need to implement all these technologies for routine manufacturing, their application during development phase turned out to be beneficial.
The added value of application of PAT during process development in this project did not save development time, but increased the required understanding of the (inter-) relationships between process parameters and attributes of the produced granulates. Based on this knowledge, reasonable specifications for routine manufacturing can be selected by minimising the risk of out-of-specification results and process windows or design spaces for single unit operations can be implemented.

5. RESULTS PROJECT B: ACTIVE FILM-COATING

5.1 MANUFACTURING PROCESS

Project B implies the development of a film-coated tablet (FCT) composed of two APIs, whereby one is contained in the tablet core, while the second one is suspended in the film-coating.

In general, this API-layering technique allows combining two intrinsically incompatible APIs in one single drug administration. If the therapeutic doses of the APIs differ substantially, the content uniformity of both actives may be achieved by applying API-layering of the lower dosed API on a tablet core containing the higher dosed API. Another advantage is the possibility to combine drug substances with different pharmacokinetics. An immediate release agent in the film-coat can be administered in a single dose with a modified release drug substance enclosed in the tablet core, which itself may be subject to functional coating.

This formulation approach implies a lot of challenges, which may also be assessed as CQAs. Content uniformity of the final product is of high criticality; especially if the API applied during the coating process is not or only partly soluble in the spraying liquid and may be prone to sedimentation. Moreover, the determination of the spraying endpoint is problematic, since the conventional methods like determination of weight gain [91] or height measurements of the film-coated tablets are not appropriate. Besides of the deficient validity of the results, these are indirect methods which are not able to quantify directly the API but only a more or less linked attributes. Furthermore, it is necessary to measure the functional parameter in real-time, meaning in-line or at-line, in order to determine the endpoint.

Recently published articles describe the application of Terahertz pulsed imaging for in-line determinations of coating thickness in pan coating processes [92], [29], [25]. Working without calibration and unaffected from formulation changes is advantageous, but the detection limit of this technique is higher than for NIR spectroscopy [30].

For this work, NIR spectroscopy was chosen as at-line technique for endpoint determination of the active coating process. This was mainly due to the fact, that NIRS is able to quantify directly the applied content of API and does not rely on any more or less related parameter and is therefore able to indicate immediately potential manufacturing issues.

The flow chart of the unit operations of the manufacturing process of Project B is depicted in Figure 50. The application of NIR spectroscopy as PAT tool for feasibility tests is restricted to the active coating process (dashed line).

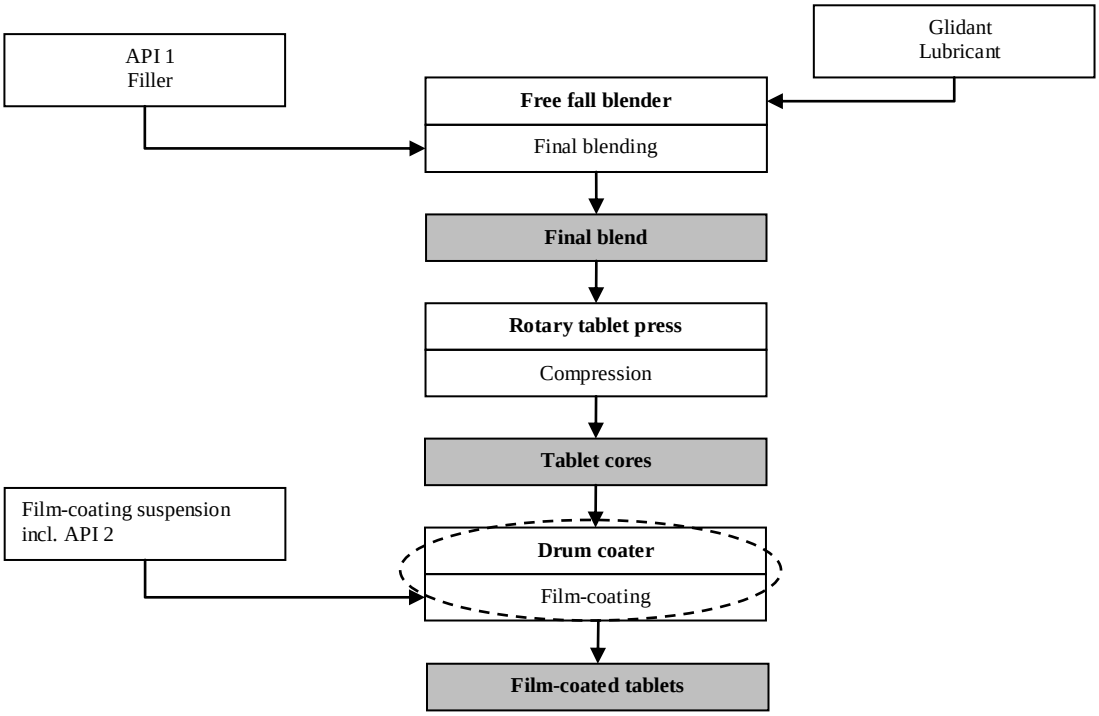

Figure 50 Flow chart of manufacturing steps comprised in Project B

The feasibility of the API layering process was evaluated using placebo tablet cores of dimensions 21.0 x 9.6 mm and an average mass of 1100 mg. Beside of API, the coating suspension contains a film-forming agent, a plasticiser, a stabiliser, a glidant and water. The amount of film-coat to be applied on each tablet is 60 mg correlating to 2.5 mg API 2. This is equal to 0.2 % API 2 (m/m) in the final film-coated tablet.

5.2 INVESTIGATED BATCHES

Table 13 lists the batches and the respective intention for their manufacture. The common goal of all these batches was to examine the feasibility of an active coating process in pilot and full scale and the potential of near infrared spectroscopy for monitoring the active coating process.

All calibration and validation procedures which are described in the following chapters are based on these batches.

In total, the film-coating processes of 13 batches in pilot scale (10 kg tablet cores) and one batch in full scale (75 kg tablet cores) have been accompanied by at-line NIR-measurements. Moreover, a batch of blanks was produced which were manufactured equally to the active tablets, but without API in the film-coating suspension. These tablets are to be detected by the NIR quantitation method.

Table 13 List of batches of FCT measured by NIRS

Batch	**Scale**	**Purpose**	**Calibration samples in NIR model**			
			B-1	**B-2**	**B-3**	**B-4**
N1	Pilot scale	DoE	x	x	x	x
N2		DoE	x	x	x	x
N3		DoE	x	x	x	x
N4		DoE	x	x	x	x
N5		DoE	x	x	x	x
N6		DoE	x	x	x	x
M1		Reproduction of DoE			x	x
M2		Reproduction of DoE			x	x
M3		Reproduction of DoE			x	x
M4		Reproduction of DoE			x	x
M5		Reproduction of DoE			x	x
O	Lab scale	Blanks (for validation purposes)				x
P	Full scale	Feasibility test				

5.3 DESIGN OF EXPERIMENTS ON THE EFFECT OF IMPORTANT PROCESS PARAMETERS DURING API-LAYERING

The first NIR calibration model is based on tablet samples collected during the coating-process of six batches. These batches were manufactured in the framework of a DoE.

5.3.1 Experimental design

The trials were designed and performed as fractional factorial DoE by varying rotation speed of the coating drum, varying spray rate and solid content of the coating suspension. The settings are referred to as high (+), low (−) and medium (0). The measured response was defined as the relative standard deviation of the CU test results of ten film-coated tablets (see Table 14). The order of the trial runs was randomised by the DoE software and is also given in the order in which the trials were run.

Table 14 Factor settings and responses for the coating trials

Batch	Solid content	Drum speed	Spray rate	s rel of CU test (n=10) [%]
N1	−	−	+	5.3
N4	+	+	+	6.7
N2	+	−	−	4.6
N6	0	0	0	3.4
N3	−	+	−	2.6
N5	0	0	0	4.8

The endpoint for these initial feasibility batches was defined as solid weight gain of 60 mg. This means that the uptake of water is not considered as weight gain. Sets of samples were collected referring to the sprayed amount of theoretically needed coating suspension as described in chapter 5.4.1.

The experiments are designed based on a $2^{(3-1)}$ fractional factorial design (resolution III) with two centre point runs (N5 and N6) and is depicted in Figure 51.

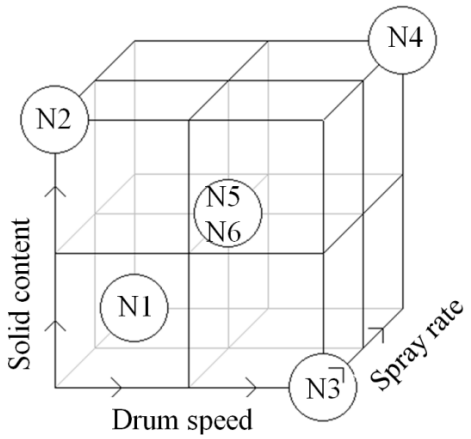

Figure 51 Design of the coating trials

5.3.2 Results

The effects of the process parameters drum rotation speed, spray rate and solid content in the coating suspension were evaluated using the statistics software Statistica 9.1 (StatSoft Inc., Tulsa Oklahoma, USA).

The fractional factorial $2^{(3-1)}$ design is mainly appropriate for screening of influencing factors on the process; the quantitative model may not be sound. The resolution of III implies that main effects and interaction of two factors are merged. Thus the model can not differentiate if the effect is induced by the main effect or the interaction of two other main effects. Therefore, the exact model equation is not considered in detail, but the effects of the investigated process parameters are assessed.

For this active coating process, the goal is to achieve minimal variation in the content uniformity of the film-coated tablets and therefore a small relative standard deviation of the CU values of the ten tested tablets. Hence, the combinations of factor settings which lead to a small relative standard deviation have to be selected for further trials e.g. the settings for batch N3 which are summarised in Table 14.

The effect of the factors can be interpreted from a main effects plot (see Figure 52), which standardises the influence of the factor settings high (+) and low (-) on the mean response (dashed line). The main effect on the response, the relative standard deviation of the content uniformity test, was found to be the spray rate. The effect of varying drum rotation speeds affects content uniformity less in the investigated range than the solid content in the suspension.

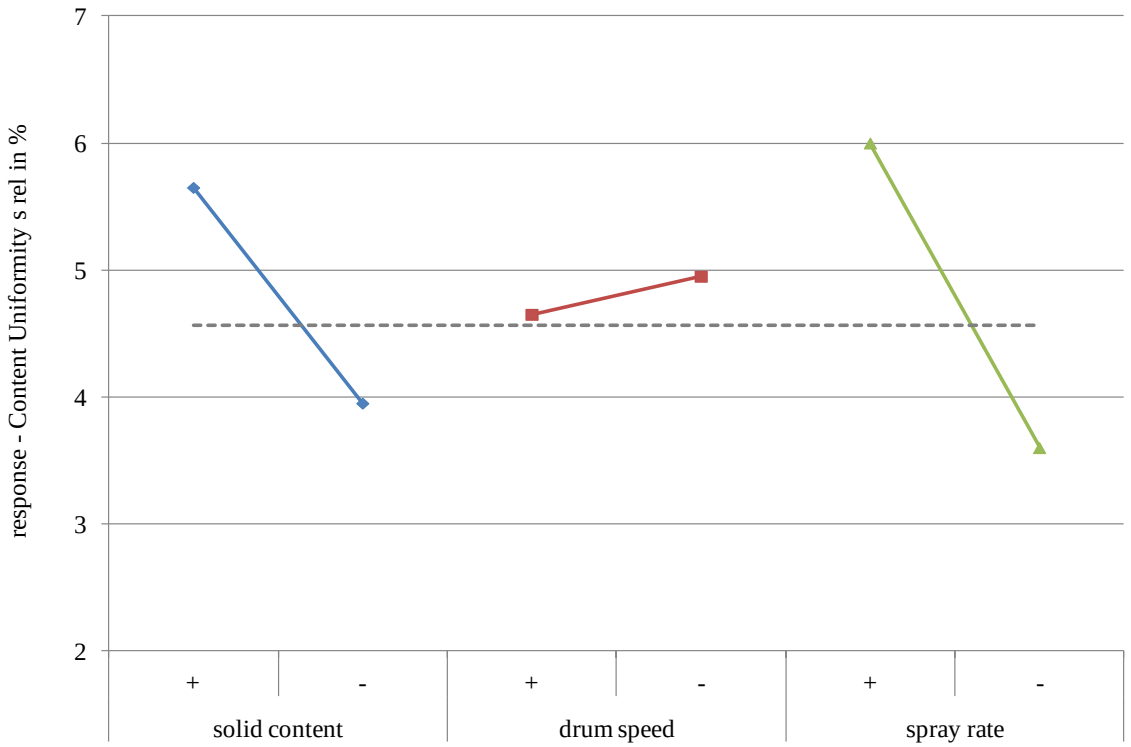

Figure 52 Main effects plot of the investigated factors solid content, drum speed and spray rate

The contour plots shown in Figure 53 illustrate the influence of two process parameters on the response while the third factor is set to the centre point level. Green areas indicate factor settings leading to lower variation of API in the film-coated tablets and hence to smaller values for the relative standard deviation of the CU test. This possibility to define parameter settings by means of the results of a small number of trial runs is of particular interest in process optimisation since further experiments can now be carried out to quantify the respective effects.

Further observations can be derived from the contour plots:

- Higher rotation speed of the coating drum improves the content uniformity. This is easily comprehensible, because the result of higher rotation speed would be an improved mixing of the product in the coating drum by raising the velocity of each single tablet. This increases the frequency of each tablet to pass the spraying zone with different sides upwards.
- Lower spray rates enhance the content uniformity. The effect of lower spray rates is time-related, since longer process times are needed in order to apply the same amount of API on the tablets. Slower spraying distributes the coating liquid and thus the API more uniformly onto the moving product bed.

- Furthermore, best results would be achieved by additionally decreasing the solid content in the coating suspension, the effect of which is again a prolongation of the spraying process.

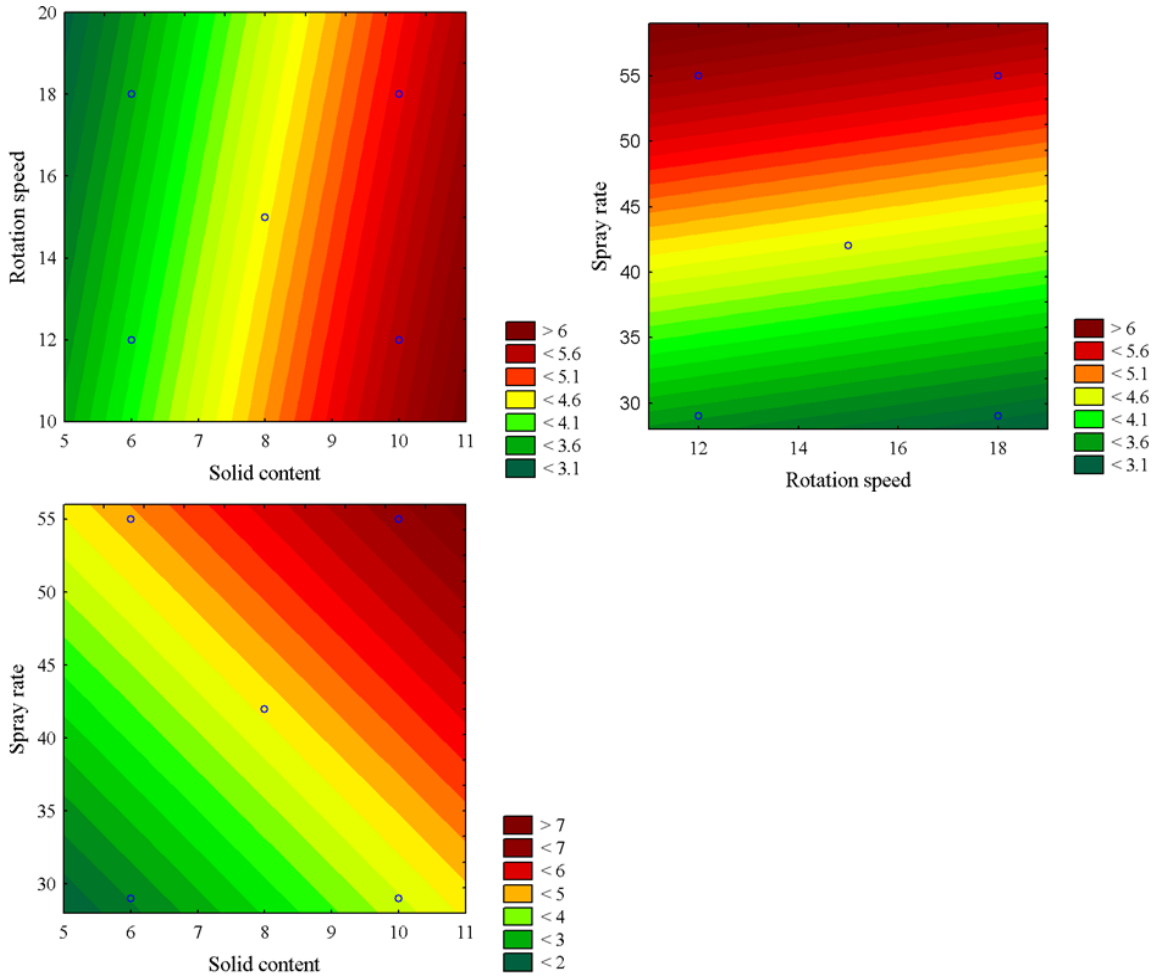

Figure 53 Contour plots of the effect of investigated process parameters on the variation in content uniformity

5.4 AT-LINE QUANTITATION OF API CONTENT DURING FILM-COATING PROCESS

The small amount of API contained in the coating suspension necessitates the need for a precise endpoint detection tool. It is not possible for film-coating processes in a drum coater to determine the coating liquid applied on the tablets by simply putting the vessel with the liquid on a balance. This approach would not consider the spray loss which is present when coating solution is not caught by the product but lost when captured e.g. by the drum wall. Applying the weight gain method is neither an option because the absolute weight gain is small compared to the mass of the tablet cores and the relative standard deviation of this initial mass. Moreover, the tablet cores tend to absorb water which additionally complicates the determination of the applied mass of film-coat. Therefore, the feasibility of applying NIR spectroscopy as endpoint determining tool was assessed.
Ideally, the NIR probe would be inserted directly into the coater and in-line spectra would be recorded. However, this was not an option because the drum coater GC 750 (Glatt, Binzen, Germany) is not equipped with the necessary flange for the fibre-optic probe. Therefore, an at-line application had to be evaluated whereby samples are manually removed from the coater and then measured. An important prerequisite of any at-line analysis is the representativeness of the collected samples. Despite, at-line measurements are supposed to deliver sufficient results to assess the general applicability of this method for the intended purpose.

5.4.1 Testing procedure

At pre-defined points of the spraying process, sample sets of approx. 30 tablets were removed from the drum coater. The samples were collected referring to the amount of film-suspension which had been sprayed until the current time-point, according to the sampling plan given in Table 15.

Table 15 Sampling plan of film-coating process

Sample Name	Sprayed amount of theoretically needed suspension [%]
Start	0
1	25
2	50
3	75
4	80
5	85
6	90
7	95
8	100
9	105
10	110
11	115
12	120

Each tablet was measured at-line using the fibre optic probe of the NIR.

The tablet samples were individually put in sample boxes and analysed by means of HPLC/UV. This procedure allowed the assignment of the respective reference assay value to each average spectrum calculated out of three individual spectra. The API content is expressed as percentage of the nominal value.

The water contents of the sample sets were determined on a halogen dryer (Mettler HR 83; 105°C, 15 min) immediately after weighing and grinding in order to determine the amount of film-coat applied without considering uptake of water.

5.4.2 Measuring set-up

In general, NIR-measurements of tablets are realised in transmission mode in order to measure a large part of the tablet. This is not possible for the present tablets, since the height of even the uncoated tablet core is 7.5 mm and thus too thick to detect any transmitted NIR radiation. Therefore, the measurements are carried out in diffuse reflection mode using the fibre optic probe. It has been described in literature before that tablets can also be measured by applying a reflection probe [93]. Diffuse reflection determines the

radiation which is not absorbed by the material but is reflected to the detector. The extent of reflected radiation varies due to chemical and physical properties; whereas the composition of a sample mainly determines the absorption and the physical attributes like porosity and density primarily influence scattering. Measurements of tablets in reflection mode assume that the API is distributed equally on the tablet surface. Deviating situations may lead to the published fact that reflection spectra of tablets are less repeatable than transmittance spectra [94].

The first challenge for at-line measuring of these tablets was to find a suitable and reproducible measuring position. The commercially available tablet holders fix the tablet in a certain position, but require round shaped tablets and are not appropriate for measurements using the fibre optic probe. The oblong tablet form of the tested tablets inhibits using the tablet holders. The following measuring set-up was found to results in the most reproducible spectra: The NIR probe is vertically fixed by means of a stand, while the tablet is placed and centred directly below the probe and being touched by the metal casing. Thereby, the distance between tablet and reflectance probe is minimal in order to reduce the detection of straylight. All measurements were realised with the non-embossed side of the tablet oriented upwards in order to further minimise potential influencing factors.

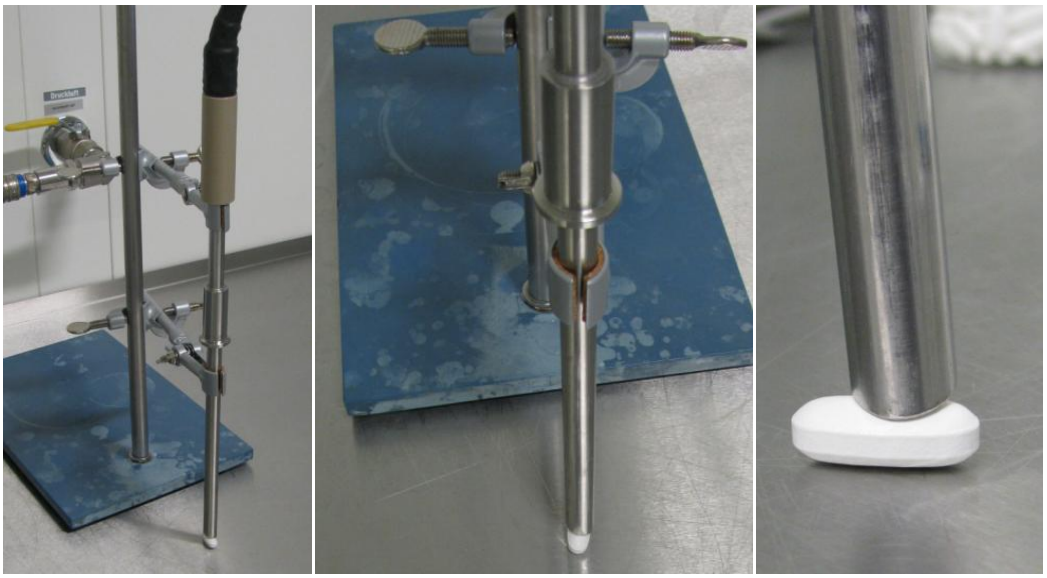

Figure 54 Measuring set-up for single tablets in diffuse reflection mode

The dependence of noisy straylight from the distance between probe and sample was assessed in preliminary tests: Both the intensity of the signal and the degree of noise in the

recorded NIR spectra increase when raising the distance between probe and tablet surface, as can be concluded from Figure 55. The lowermost NIR spectrum (red) was recorded with the settings described above. These settings were chosen for all further measurements of single tablets in diffuse reflection mode. The other spectra are measured when the distance between probe and sample was enlarged gradually.

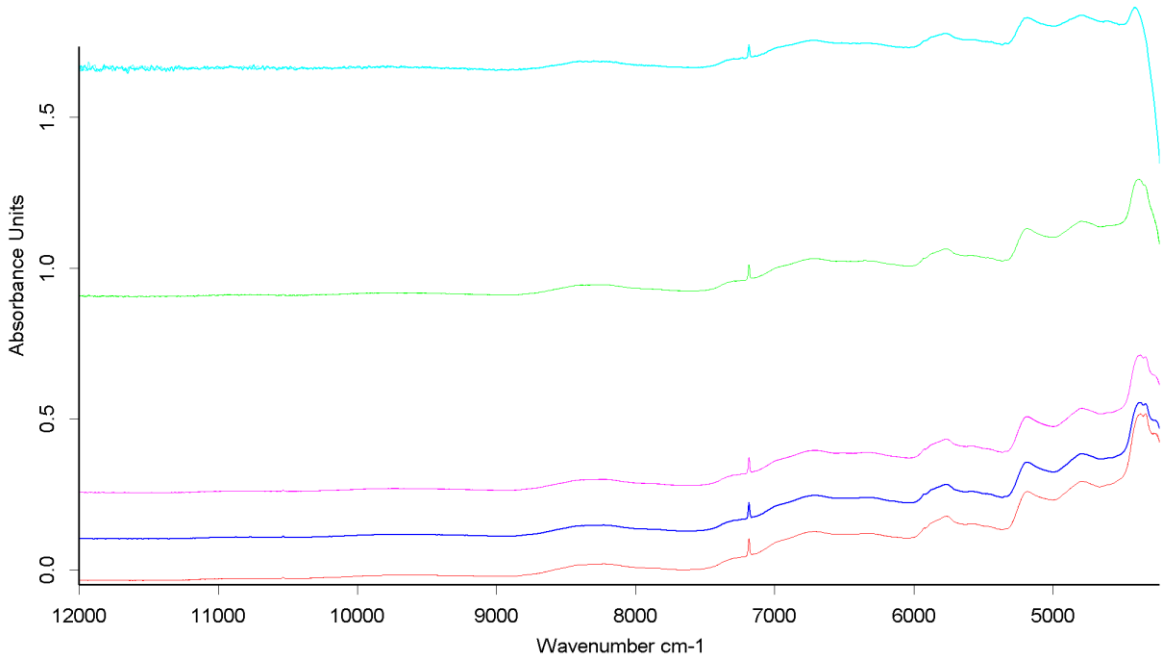

Figure 55 Effect of distance to probe on the resulting spectra (red: probe touching the tablet surface, blue: 0.5 cm, pink: 1 cm, green: 2 cm, cyan: 4 cm distance between tablet and probe)

Beside of fixing these "hardware" settings, the "software" adjustments for measuring the NIR spectra are specified as summarised in Table 16. Three single NIR spectra were taken from each tablet and averaged into one spectrum. The measuring time for one spectrum is with approximately 25 s, due to the higher number of scans, longer than the settings for the in-line measurements during fluid bed granulation (cf. Table 10). The longer measuring times were preferred because the resulting spectra are more reproducible. Moreover, the at-line measurement of a static sample can be more easily defined and reproduced than measuring a moving product bed.

Table 16 Adjustments for at-line NIR-measurements using the fibre optic probe

Parameter	**Value**
Measuring mode	Diffuse reflection
Wavenumber range	12500 – 4000 cm^{-1}
Resolution	8 cm^{-1}
No. of scans per spectrum	32
Preamplifier gain	B
Detector	Indium-Gallium-Arsenide

5.4.3 Compilation of first NIR calibration model B-1

5.4.3.1 Effect of film-coat on NIR spectra

At first, the localisations of absorption ranges which are specific for the applied film-coat were selected. For this purpose, NIR spectra of tablet cores, of pure film-coating solution and of final film-coated tablets are compared. Three wavenumber ranges are obviously influenced by components of the coating suspension as is shown in Figure 56. The peaks at 10500 cm^{-1} and at approximately 7200 cm^{-1} marked in orange are features due to the coating suspension (green spectrum), which are not present in the spectrum of the tablet core (blue spectrum) but in the NIR spectrum of the film-coated tablet (red spectrum). Furthermore, the spectral characteristics between film-coating suspension, tablet core and film-coated tablet are clearly distinct in the range from 6080 – 5500 cm^{-1} (marked in orange).

The large absorption peak at 5200 cm^{-1} (marked in cyan) is caused by vibrations of water molecules of which the effect is particularly evident in the spectrum of the coating liquid.

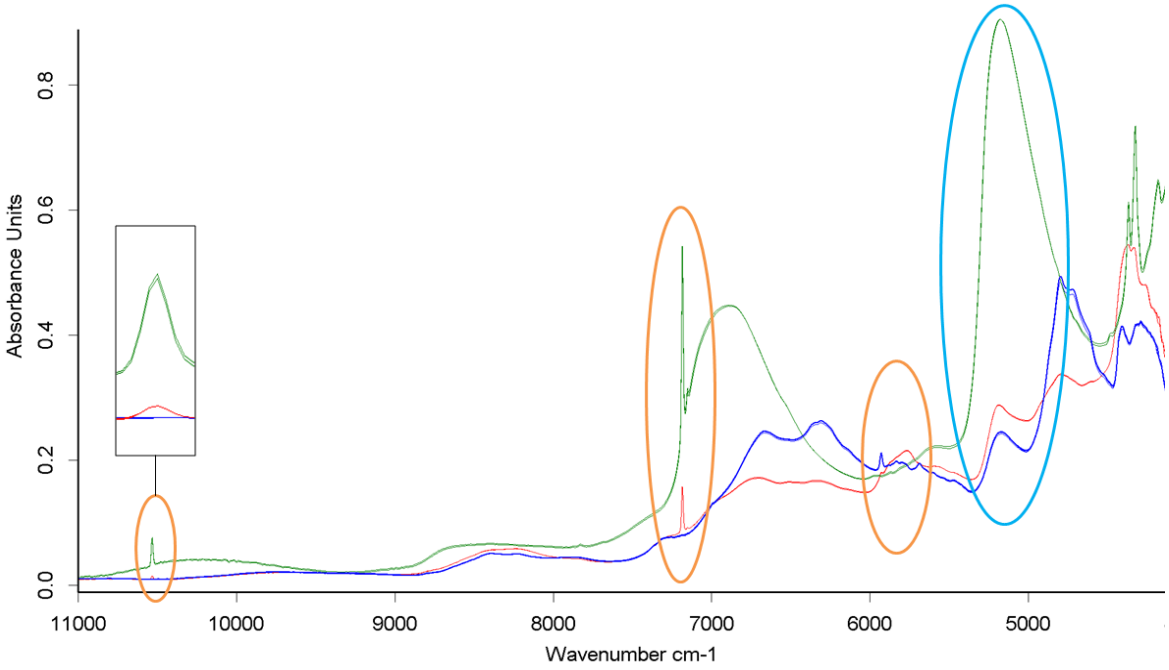

Figure 56 Offset-corrected NIR spectra of tablet cores (blue), coating suspension (green) and FCT (red)

5.4.3.2 Parameters of first NIR calibration model B-1

At first, a NIR calibration model was established based on the three wavenumber regions marked in orange.

Table 17 Parameters of calibration model B-1

Parameter	**Value**
No. of batches included in calibration	6 (N1 – N6)
No. of calibration samples	301
Scale of calibration batches	Pilot scale (10 kg)
Calibration range	0 – 117.5 %
Data pre-processing	1st derivation (smoothing: 5 pts)
Selected wavenumber ranges	A: 10579 – 10499 cm^{-1} B: 7262 – 7158 cm^{-1} C: 6082 – 5457 cm^{-1}

As a first estimation, a principal component analysis (PCA) of the model was realised. The result is depicted in Figure 57. Considering the score plot of the first and second principal component, the scores are discriminated according to the amount of coating

applied and thus to the progress of the coating step. This is a promising result because it is a prerequisite to establish near infrared spectroscopy as tool for endpoint detection.

However, the score plot of the PCA reveals another interesting observation: the calibration spectra are classified according to the level of solids content in the coating liquid which was varied in the framework of the DoE described in chapter 5.3. The points representing calibration samples of batches with high solid content are coloured blue, the ones representing samples of batches manufactured at medium level are coloured green and the pink ones represent batches with low solid content. More precisely: not the amount of solids in the coating liquid is captured in the model, but the corresponding level of moisture during the coating process. The amount of solids in the suspension is correlated to the moisture level during the process since the spray rate is expressed as mass per volume. When maintaining the spray rates, an increase in the solids content results in a lower input of water into the product.

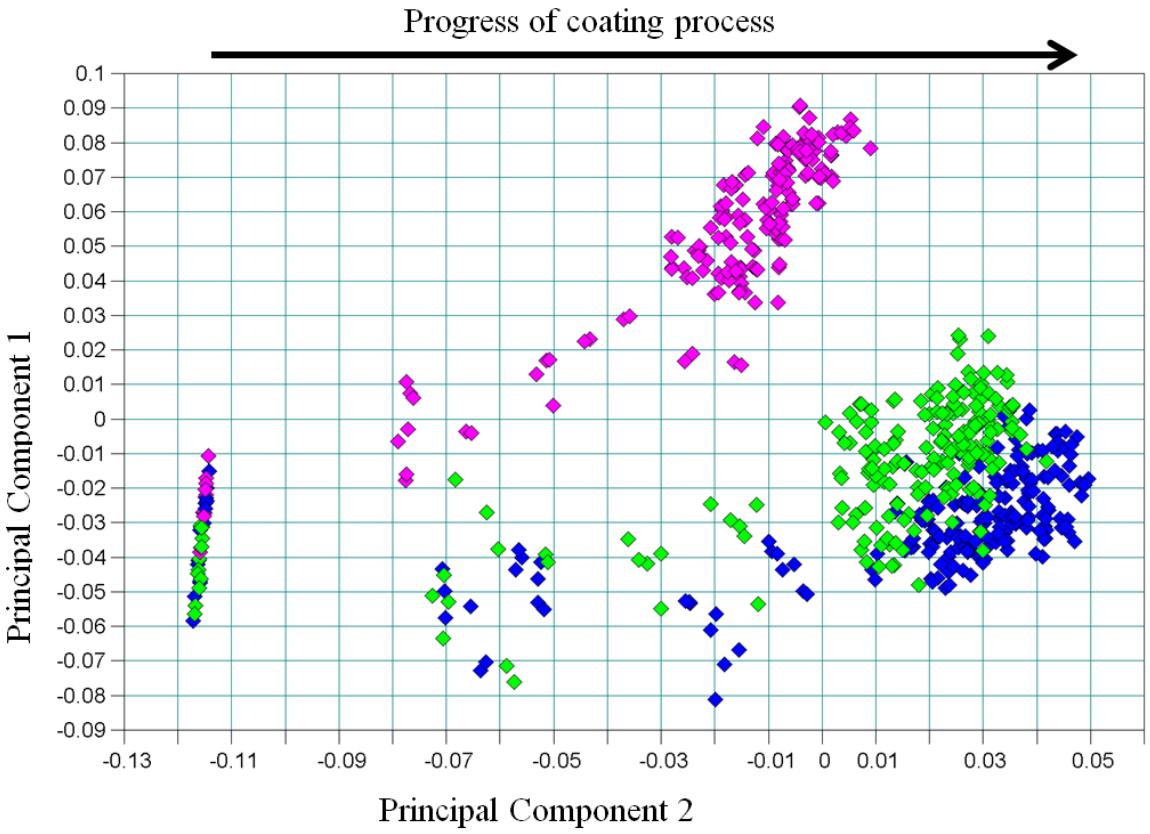

Figure 57 PCA of calibration spectra: Differentiation of DoE batches with high (blue), medium (green) and low (pink) solid content in the coating liquid

Conclusively, the peaks of the selected wavelength regions are mainly generated by talc particles and can be used to differentiate coated and uncoated tablets, but are not appropriate to quantify the amount of the API in the film-coat. Thus other wavelength regions have to be selected for the NIR calibration model.

5.4.4 Development of NIR calibration model B-2

Beside of selecting suitable calibration samples and performing reliable reference analytics, the selection of the proper wavelength range is one of the most crucial decisions for a successful development of a NIR method. For quantification of water, the regions of overtone and combination vibrations are well known and often distinctly and visible in the spectrum. Yet, for the determination of a new active, much more efforts are necessary to find out specific peaks.

5.4.4.1 Rationale for the selection of NIR region for the calibration model B-2

A NIR spectrum of the pure API was recorded in order to find characteristic peaks with high absorption of NIR radiation. This spectrum is compared with a synthetically generated subtraction spectrum. This synthetic spectrum was calculated by subtracting the NIR absorption of a blank film-coated tablet, which did not contain any API, at each single wavelength from the one of a regularly film-coated tablet containing the full amount of API 2. Hence, the blank and the regular film-coated tablet differ only in the API content. The difference of the spectra should thus match the NIR spectrum of API 2, even though further attributes e.g. the level of residual moisture or physical parameters like hardness and smoothness of the surface area affect the NIR spectrum.

Both spectra are given in Figure 58. Several characteristic shapes are recovered in the subtraction spectrum and are indicated by the exact positions of the peak maxima.

It is not possible to find a common scale for the depiction of both spectra in one graph since the absolute absorption values are too different and a common scale would not allow the comparison of the subtraction spectrum (blue) and the spectrum of pure API (red). This is a consequence of the different magnitudes of API in the measured samples respectively.

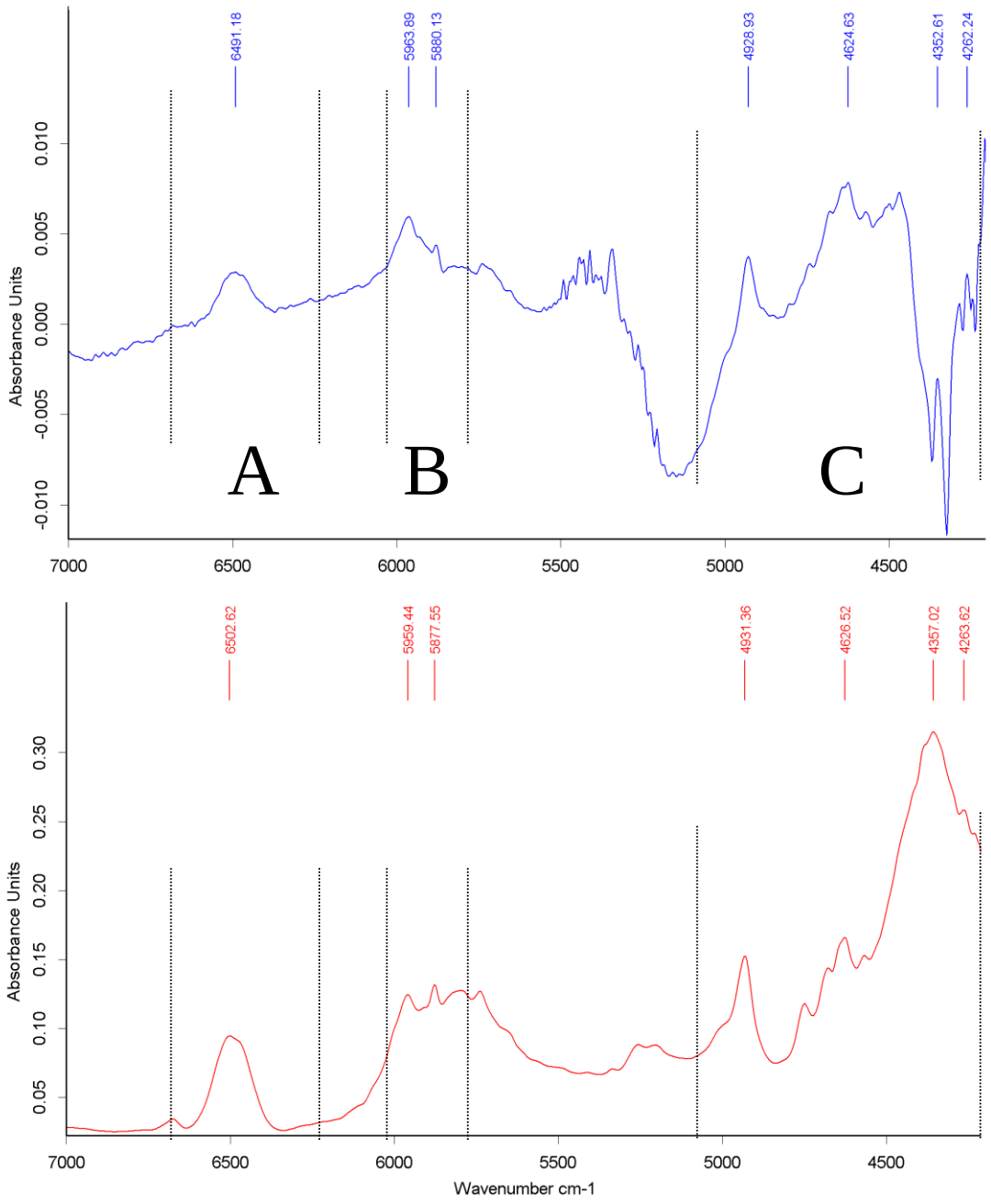

Figure 58 Recovery of API 2 peaks (red) in the subtraction spectrum (blue)

NIR spectra of tablets, which have been withdrawn consecutively during manufacturing, differ obviously and reflect the course of the film-coating process. This is illustrated in Figure 59, where the first derivations of spectra of different samples are presented. The plotted ranges A, B and C represent the wavenumber ranges which have been selected for the calibration model based on the peaks indicated in Figure 58.

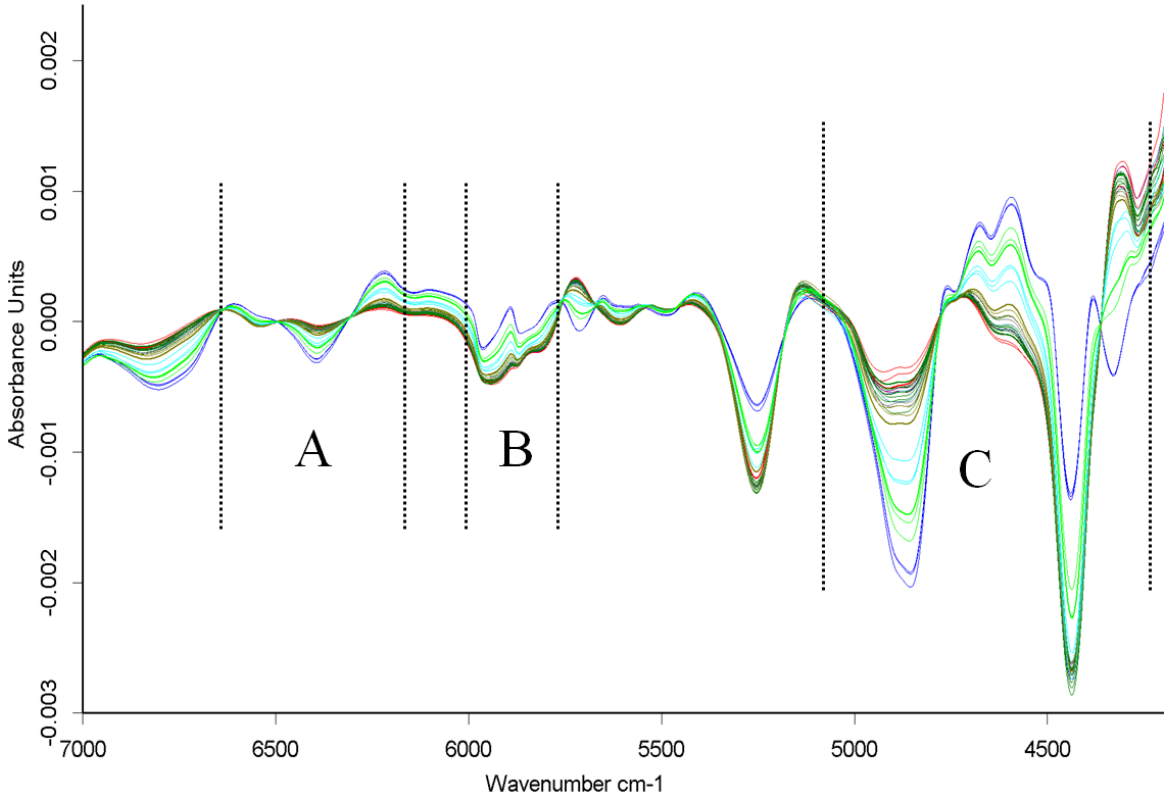

Figure 59 NIR spectra of tablets at different stages of the film-coating process (pre-processing: 1st derivation, 5 sm.pts);
FCT at the beginning of coating process: blue;
FCT during coating: other colours;
FCT at the end of the coating process: red

5.4.4.2 Further parameters of the calibration model B-2

Having defined the calibration samples and the wavenumber regions, the appropriate pre-processing technique had to be chosen. The effect of 1st derivation of the spectra has already been shown in section 4.8.2.2. The effect of eliminating baseline drifts is again desirable, since due to the measuring set-up, different amounts of straylight are present in the calibration spectra. Moreover, the physical attributes of the measured tablets such as hardness, which itself can have an effect on the reflectance, is not in the focus of the present work. The NIR spectra of the tablets were measured with a resolution of 8 cm^{-1} and 32 scans per spectrum. Therefore, the smoothing according to Savitzky-Golay is not as distinctly needed as for the in-line recorded spectra of Project A; an interval of 5 smoothing points is sufficient.

Further parameters of the calibration model B-2 are summarised in Table 18.

Table 18 Parameters of calibration model B-2

Parameter	**Value**
No. of batches included in calibration	6 (N1 – N6)
No. of calibration samples	323
Scale of calibration batches	Pilot scale (10 kg)
Calibration range	0 – 117.5 %
Data pre-processing	1st derivation (smoothing: 5 pts)
Selected wavenumber ranges	A: 6703 – 6190 cm^{-1} B: 6009 – 5831 cm^{-1} C: 5052 – 4169 cm^{-1}

5.4.4.3 Performance indicators of the calibration model B-2

The performance indicators of the calibration model B-2 are given in Table 19. The coefficient of determination (R^2) is the proportion of variability in a data set that is accounted for by the statistical model. Its value is 97.96 % and hence quite good. The rank gives the number of principal components used for computation of the calibration model. Seven principal components are needed here, which is a higher number than usual compared to other determinations such as the determination of water. This can be due both to the low concentration of the API 2 in the film-coated tablet and / or to different physical and chemical attributes of the samples.

The Root Mean Square Error of Cross Validation (RMSECV) of 4.2 % is comparatively high but corresponds well to the relative standard deviation of the CU determinations of the film-coated tablets.

Table 19 Performance indicators of the NIR model B-2

Parameter	**Value**
R^2 [%]	97.96
RMSECV [%]	4.2
Rank	7
Bias	0.00579
Offset	1.505

The results of the cross validation procedure are depicted in Figure 60 allowing a comparison of the predicted value and the reference value for each calibration sample.

The broad calibration range can be encompassed in a single calibration method, but the deviation between predictions and reference values is obvious. Moreover, the predictions for all calibration samples are too low for the sample sets collected at approximately 20 % applied amount of API and for the film-coated tablets with a reference value higher than 110 % API 2. The higher values seem to reach a plateau in NIR predictions.

Nevertheless, the predictive ability of this model developed in order to evaluate the general feasibility of at-line monitoring of the active coating process by means of NIR spectroscopy is tested by measuring further batches, which are not included in the calibration. This approach can be considered as an external validation procedure.

The deviation of values below 50 % API content as reference value is not regarded as failure of the NIR model, since even the linearity of the reference method using HPLC was only assessed for API contents higher than 50 %. Yet the slope of the regression line (black) within Figure 60 is 0.99, which is close to 1.00 and the y-intercept is with 1.5 acceptably low.

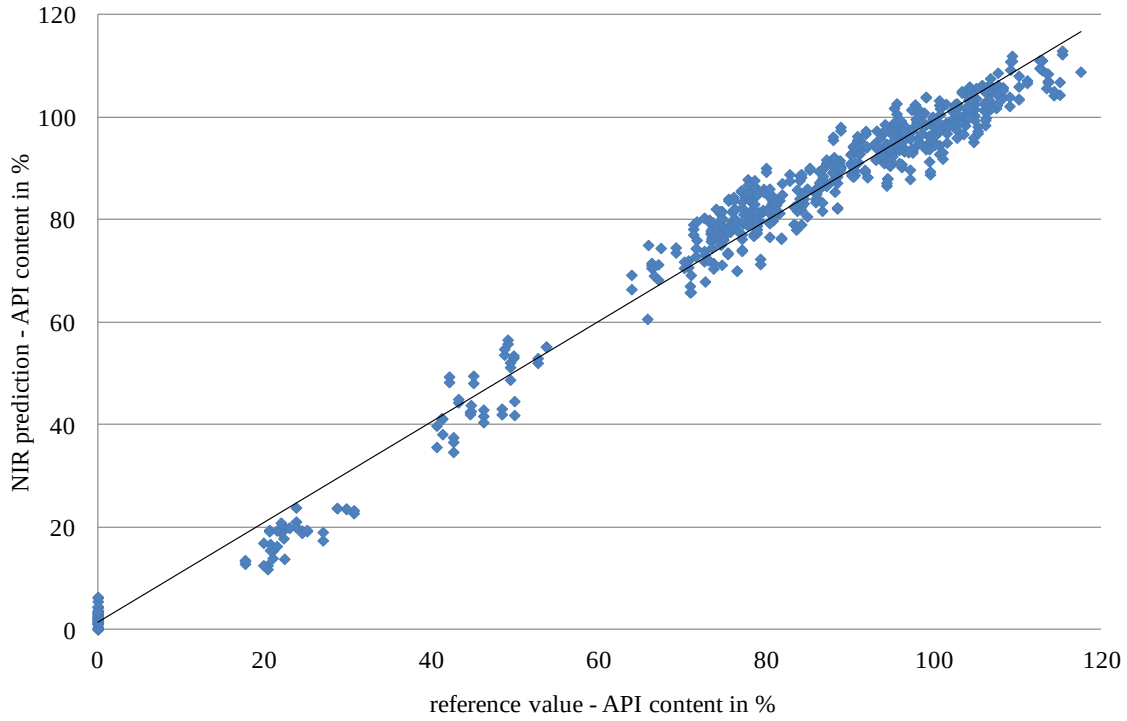

Figure 60 Cross validation of calibration model B-2

5.4.4.4 Predictive ability of NIR model B-2 for endpoint determination

The most efficient way to investigate the predictive ability of a NIR calibration model is to perform a test set validation. For this purpose, all calibration samples related to batch N5, one of the centre point batches manufactured in the framework of the DoE on important process parameters, were removed from the calibration. All other selected calibration parameters were maintained. By this means, the presented NIR calibration model was applied to monitor the active coating process of one complete batch without wasting one of the extreme batches, which would not be considered any more in the calibration.

Each single tablet of a sample set was at-line measured by NIRS and afterwards analysed by HPLC as reference analysis.

Figure 61 depicts the mean values both predicted by NIR spectroscopy and the mean API content determined by HPLC. Obviously, the course of the coating process of batch N5 can be monitored, but the accuracy is not yet acceptable. This is not necessarily due to an insufficient calibration model, but also to a manufacturing process, which is only at the beginning and which does not yet lead to a drug product with a uniform content of API. The absolute intra-variation in each sample set increases during the manufacturing process, indicating that the uniformity of the applied API is not sufficient. This is probably due to poor mixing capacity of the used Glatt Coater.

The range of predicted NIR values in one sample set coincides with the range of single CU values, which confirms the established model for at-line API quantitation. However, the model in this form can not be applied as endpoint detecting tool, the deviation between mean NIR and mean CU value is too high towards the end of the process.

Nevertheless, the feasibility to apply NIRS as PAT tool for endpoint detection is considered feasible for a more optimised active coating process.

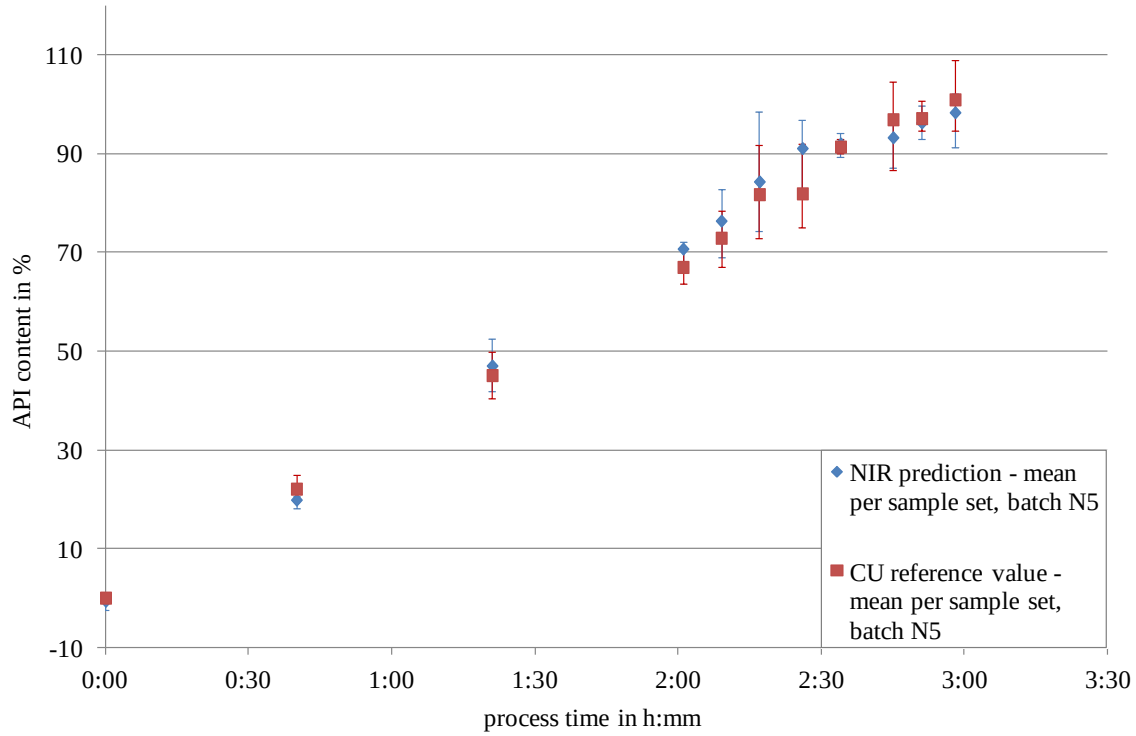

Figure 61 API content on tablet samples measured by NIR and HPLC during the coating process of batch N5

5.4.5 Enhanced NIR calibration model B-3

The second set of feasibility trials in pilot scale comprised five batches (M1 – M5, see Table 13), which were used to enhance the NIR model. The calibration samples were collected focusing on increasing the precision of the NIR model when approaching 100 % API 2 content and thus improve its performance for endpoint prediction.

The therefore modified sampling plan for these trials is given in Table 20. Ten tablets of each of the samples numbered 4, 5, 6 and 8 were analysed by NIRS and, for purpose of reference, CU was tested by HPLC.

Table 20 Modified sampling plan for second coating trial set with reduced number of samples

Sample name	Sprayed amount of theoretically needed suspension [%]
Start	0; after pre-heating
1	25
2	50
3	75
4	90
5	95
6	100
7	105
8	105; after drying

The inclusion of these calibration samples into model B-2 led to the model B-3 based on 511 calibration spectra in total. Although all other parameters were kept constant, the performance parameters of the model declined. This is most obvious for the increased number of needed principal components of 10, compared to rank 7 in case of model B-2. Besides, R^2 decreased for almost 3 % while the RMSECV raised by almost 2.

Table 21 Comparison of performance indicators of the models B-2 and B-3

Parameter	Model B-2	Model B-3
R^2 [%]	97.96	95.02
RMSECV [%]	4.2	6.11
Rank	7	10
Bias	0.00579	-0.0277
Offset	1.505	4.366

The specificity of the calibration models were assessed as follows. Beside of the DoE batches (N1 – N6) and a second set of repetition trials (M1 – M5), a batch of blank film-coated tablets was manufactured as analytical placebo. Therefore, the blank tablets are processed in the same way than the previous coating batches, but are coated by a

suspension which did not contain the API. The lacking amount of active is not compensated for, it is just omitted.
This allows a further evaluation of the NIR model with regard to its specificity. The method has to differentiate these film-coated tablets from the ones containing API. The predictions both for uncoated tablet cores which are present at the beginning of a regular coating process and for these blanks have to be zero.

For a first evaluation, a principal component analysis was carried out in order to determine if the chosen wavelength ranges are selected in a way which allows differentiating film-coated tablets containing active from the blanks. The score plot of this analysis is depicted in Figure 62.
The calibration spectra can be clearly assigned to the progress of the spraying process: the start samples (cyan) are on the very left side of the graph, followed by samples collected at ≈ 25 % amount of coating suspension sprayed (pink), then the calibration samples corresponding to ≈ 75 % API (blue) and the later samples (green). The blanks (red), on which the full amount of film-coat has been applied but which contain no API, are not discriminated. Very similar pictures are obtained when plotting the scores of any other combination of principal components. This means that the amount of film-coat is affecting the NIR prediction and not the content of API itself.
Therefore, the defined calibration model has to be modified by selecting more specific wavelength ranges for quantification of the API.

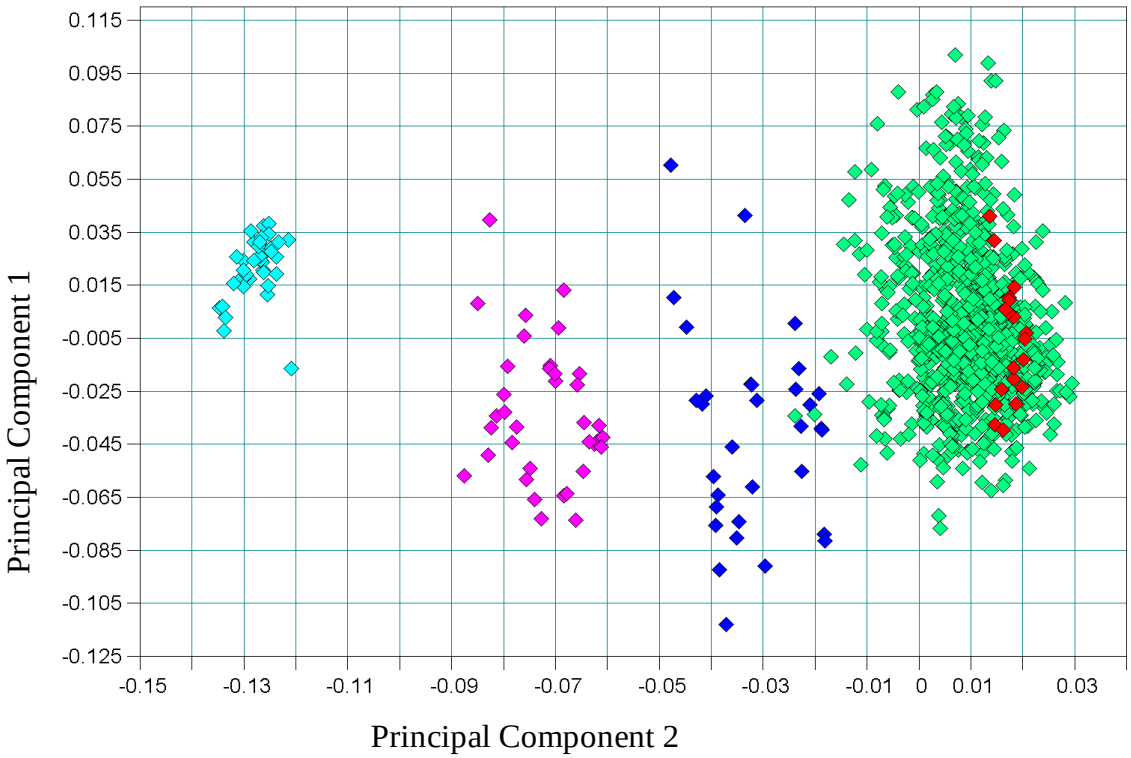

Figure 62 Score plot resulting from PCA of NIR model B-3, cyan: start samples, pink: ≈ 25 %, blue ≈ 50% , green: 75 – 117% API, red: blanks

5.4.6 Final NIR calibration model B-4

The existing NIR calibration model B-3 was further refined in order to increase the specificity of the predictions. The wavelength regions of the spectra included in the calculations have to be more selective to the API.

Then the NIR model could not only be applied as an endpoint detection tool but also in order to detect any process failures e.g. sedimentation of the API in the granulation liquid due to a potential stirrer-break-down. This is an important advantage of analysing directly the assay and not another parameter which can only indirectly be correlated to the amount of API as for instance the weight gain of tablets.

Table 22 summarises four refined calibration models (B-4a to B-4d) and the most important resulting parameters of the respective leave-one-out cross validation. The four models B-4a, B-4b, B-4c and B-4d are based on different wavenumber regions which have been taken into account for development of the calibration. Different combinations of

several wavenumber regions have been compared; Table 22 summarises the most important ones.

For data pre-processing, 1st derivation was chosen as appropriate technique for the presented calibration models since this procedure is known to equalise baseline drifts. Shifts in baseline can be due to different sample handling during the measurements, since the measuring set-up could not completely exclude straylight affecting the spectra. Furthermore, 1st derivation in combination with a smoothing procedure presented by Savitzky and Golay emphasises differences in spectra which are due to chemical changes, and reduce the influence of physical factors on the spectra.

The wavenumber regions are based on the NIR spectra of the pure API which was depicted in Figure 58. The goal was to constrain the wavenumber ranges in order to enhance the importance of API in the calibration spectra.

Further parameters as number of batches included in the calibration model, calibration spectra and thus the calibration range are same for all presented methods. The slight differences in number of calibration samples included are due to the automatic recognition of outliers of the applied software. The proposed outlier spectra were removed from the calibration set.

The coefficient of determination (R^2), the mean square error of cross validation (RMSECV) as well as the values for bias and offset are similar for all of the computed models. They differ in the calculated rank which is required for the PLS regression. The rank gives the number of principal components which are necessary to build the model with the calculated goodness of prediction. Model B-4c is based on five principal components to describe the variability present in the calibration spectra and on only one wavenumber region which is taken into account. In comparison, Model B-4b relies on two wavenumber regions requiring rank 6, while for Model B-4a, which is based on three ranges, even eight principal components have to be considered. Method B-4d is developed based on one big wavenumber range, which is a possible explanation for the higher resulting rank. As previously described, a low rank is considered as important prerequisite for a robust calibration model. However, a rank of three or below is probably not achievable in this particular project, since the absorption peaks of the API are not as distinct as the water absorption bands.

Therefore, Model B-4d with the most convincing performance parameters, i.e. R^2 and RMSECV, was assumed to deliver best predictions for the API content and chosen for an external validation procedure.

Table 22 Comparison of selected calibration models

Parameter	**B-4a**	**B-4b**	**B-4c**	**B-4d**
No. of batches incl. in calibration	11			
Scale of calibration batches	Pilot scale			
Calibration range	0 – 117.9 %			
Data pre-processing	1st derivation (smoothing: 5 pts)			
No. of calibration samples	511 incl. 7 blanks	497 incl. 7 blanks	497 incl. 7 blanks	494 incl. 7 blanks
Selected wavenumber ranges [cm^{-1}]	6591 – 6364 6000 – 5681 5102 – 4921	6591 – 6364 6000 – 5681	6000 – 5681	6553 – 5523
R^2 [%]	97.37	97.21	96.97	97.76
RMSECV [%]	4.44	4.27	4.44	3.81
Rank	8	6	5	7
Bias	-0.0109	0.00218	-0.0102	-0.001
Offset	2.272	2.415	2.684	1.966

5.5 VALIDATION APPROACH FOR THE NIR CALIBRATION MODEL

In the following chapters, the approach for the validation of an NIR method and the results for the developed model are presented. Although being conceptually different from conventional analytical methods, the following parameters can be taken into account:

- Specificity
- Linearity
- Range
- Accuracy
- Precision
    - Repeatability
    - Intermediate precision
    - Reproducibility
- Detection Limit
- Quantitation Limit
- Robustness

These major criteria for validation of an analytical method are discussed in the chapter 5.5.1 – 5.5.5 for the calibration model B-4d.

5.5.1 Specificity of NIR model B-4d

Specificity of an analytical method is defined as the ability to assess unequivocally the analyte in the presence of components which may be expected to be present e.g. impurities or a matrix [95].

As the determination of the API content is realised in presence of a predominant matrix, the API content of blank tablets is used as specificity test. The signals of the matrix, which is composed of the film-coating suspension and the tablet core, dominate the NIR reflectance spectra. Nevertheless, the NIR method has to discriminate film-coated tablets without API from the ones containing API. Physical parameters e.g. different moisture levels during the coating process are considered in the calibration method and will not affect the predictive ability significantly.

Thus, the method was challenged by measuring blank tablets and this test was used to evaluate the specificity of the NIR method.

The described procedure of a PCA is appropriate for a first estimation on the specificity of the calibration model. As has been previously described, each calibration spectrum can be plotted in a multidimensional space, in which the principal components represent the axes. Similar spectral features are located in clusters in the scatter plot.

The two-dimensional depiction of the scatter plot of model B-4d is presented in Figure 63. The discrimination of spectra belonging to the same set of sample as well as a clear differentiation of the blank tablets is most obvious when plotting the scores on the fourth and the first principal component. Tablet samples removed from the coater at the beginning of the manufacturing process (start sample, cyan) can be found on the very right of the PC 1 axis, tablets of sample set 1 (pink ≈ 25 % LA API) and sample set 2 (blue ≈ 50 % LA API) are located in the middle of the plotted range.

Thus, the course of film-coating applied on the tablets is visible in the score plot in form of a shift from right to left. The blank tablets (red) have similar scores for PC1, but clearly different ones for PC 5 than regular completely processed tablets (green) which is due to the lacking API.

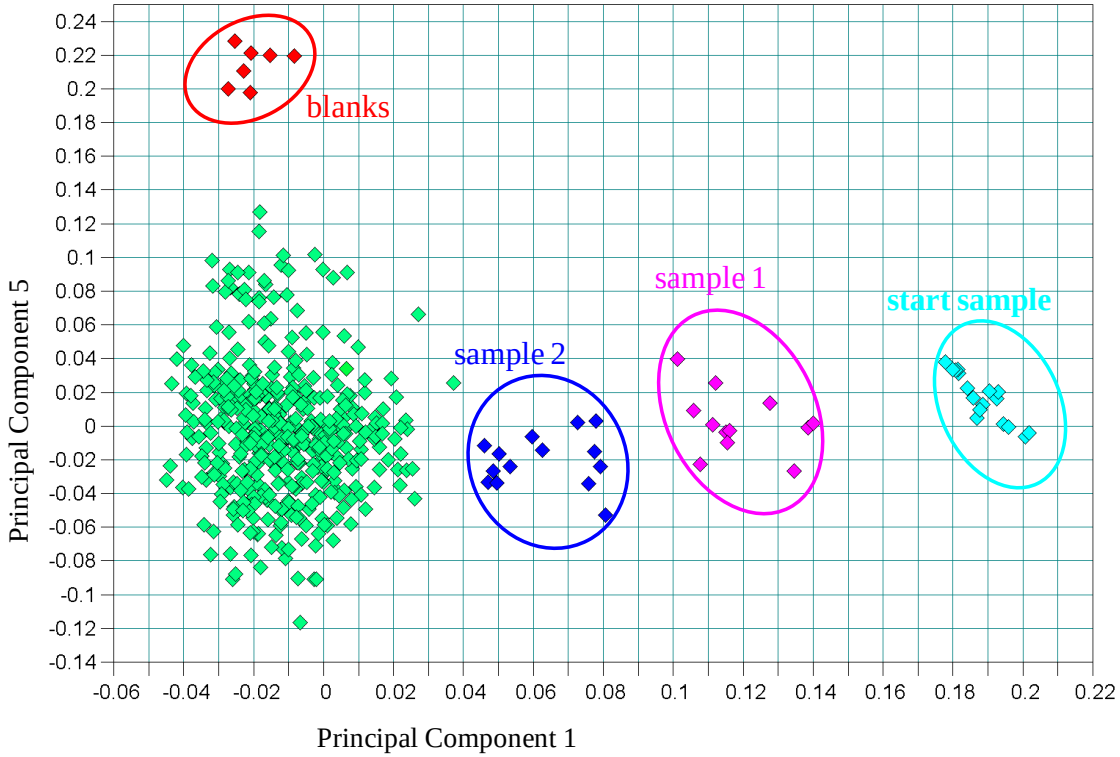

Figure 63 Score plot resulting from PCA, parameters based on model B-4d
cyan: start samples, pink: ≈ 25 % API, blue ≈ 50% API,
green: 75 – 117% API, red: blanks

A comparison of the API spectrum, pre-processed by 1st derivation, and the loading plot for the first principal component as part of the PLS regression model is shown in Figure 64. The exact positions of absorption peaks were calculated by the software and correlating wavenumbers of peaks are labelled.

It is obvious that the loading for PC 1 (blue) resembles the API spectrum (red), even when the exact positions differ slightly. This might be due to the fact that the presence of a matrix, i.e. the whole film-coated tablet, and therefore changed bonding forces lead to minor shifts in the spectrum.

In total, PC 1 accounts for 74.9 % of the modelled variability, PC 2 for 17.8 % and the succeeding ones capture even less.

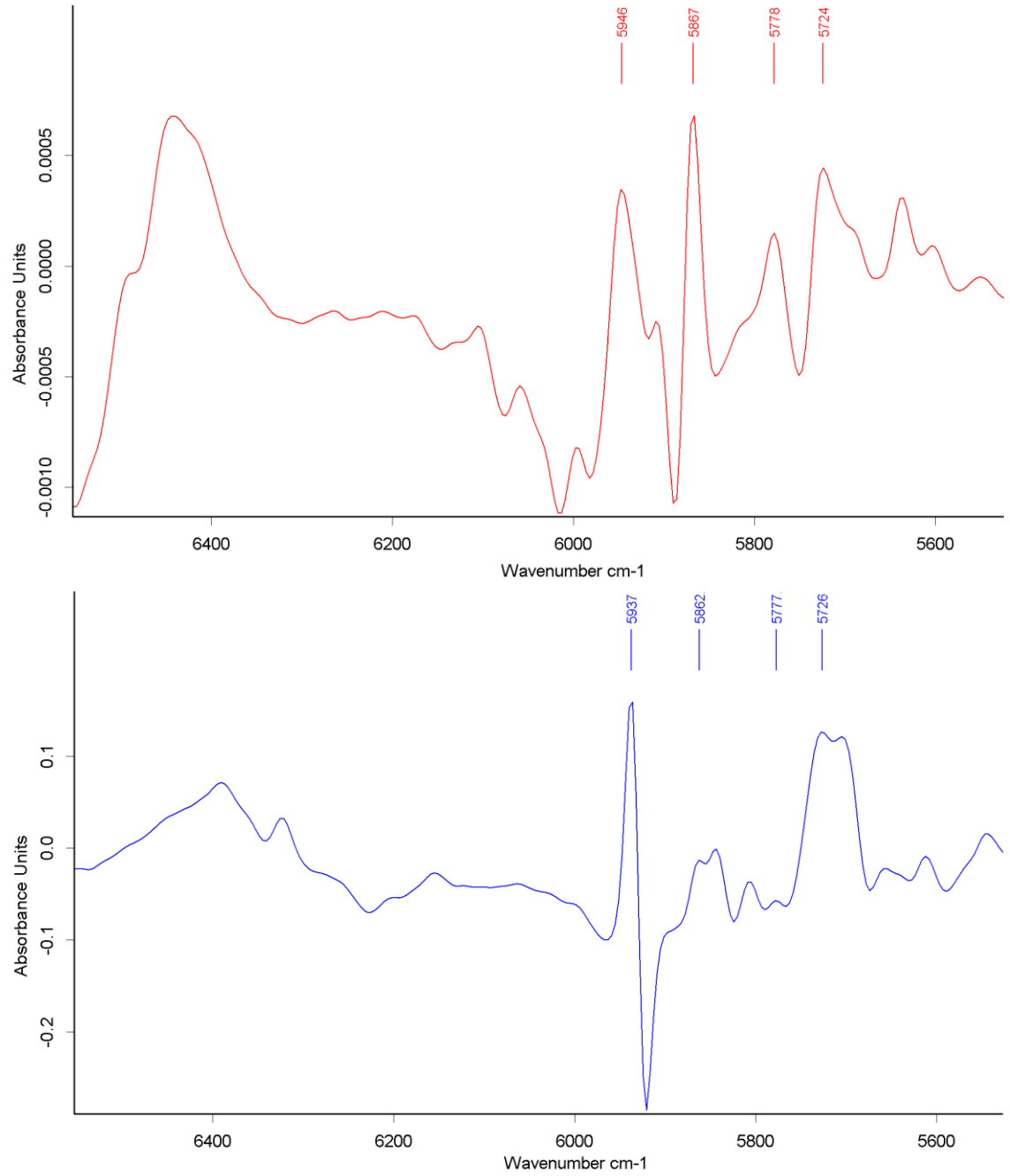

Figure 64 API spectrum 1st derivation (red) compared to PC 1 of PLS model (blue) based on calibration B-4d

The actual specificity of the calibration model is assessed by measuring several blank tablets which do not contain any API and predicting the API content respectively. Necessarily, the NIR spectra of these blanks are not incorporated into the calibration model but are particularly measured for validation purposes (see Table 23).

Table 23 NIR predictions for blank tablets

Tablet sample no.	**NIR prediction of % LA API**
1	4.9
2	5.2
3	6.9
4	7.1
5	6.5
6	5.4
7	-0.1
8	2.3
9	3.6
10	5.1

For all ten measured blank film-coated tablets, values between -0.1 and 7.1 % LA API content are obtained. The PLS model recognised all spectra as outliers when calculating the Mahalanobis distance. The Mahalanobis distance was 0.14 and thus 5 times above the threshold value indicating non-conformance of the tested samples. Hence, the model confirmed its specificity for the API. For a more detailed evaluation of the valid range of the NIR calibration model, the quantitation limit would have to be detected. This was not realised in the framework of this thesis, since only the feasibility of NIRS quantitation was to be proved and the manufacturing process itself has to be optimised. Then the measured samples could be assessed as more homogeneous and the variation and deviation in NIR predictions could be decreased. Beside of the quantitation limit, the detection limit is out of scope either and was not determined.

5.5.2 Linearity and range of NIR calibration model B-4d

As NIR data are typically multi-dimensional and thus opposed to conventional one-dimensional analytical data, the equivalent test on linearity of a NIR method is the mapping of a calibration surface. The validation test for NIR involves the demonstration of correlated NIR responses to samples distributed throughout the defined range [47]. For conventional analytical methods, linearity is usually evaluated by visual inspection of a plot of signals as a function of analyte concentration or content and by applying

appropriate statistical methods e.g. by calculating a regression line based on a least squares approach [95].

The equation of the linear regression line calculated by means of least squares is:

$$y = 0.977\,x + 1.9668 \qquad \text{Eq. 18}$$

The slope of the regression line of the cross validation of method B-4d is ≈ 0.98 and hence close to 1. However, the coefficient of correlation requires linearity as a prerequisite and can therefore not be its proof [64]. Yet, the scatter plot of single values of the cross validation, presented in Figure 65, does not reveal non-linearity of the predictions.

FGF

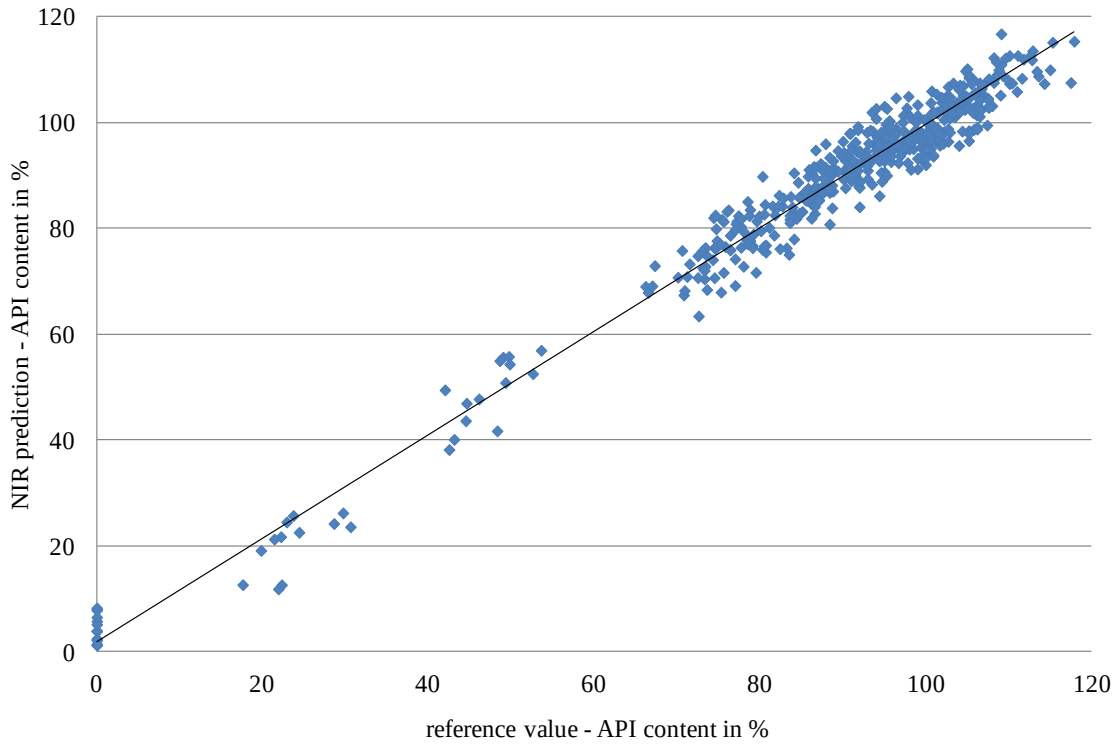

Figure 65 Cross validation of calibration model B-4d

The evaluation of the valid range includes assessment of limit of detection and limit of quantification. Both of these test points are out of scope because the developed NIR calibration model is intended to determine the end-point of the active coating process. So the lower limit of validity of the model is not to be explored.

5.5.3 Accuracy of NIR calibration model B-4d

"The accuracy of an analytical procedure expresses the closeness of agreement between the value which is accepted either as a conventional true value or an accepted reference value and the value found" according to the ICH guideline Q2 [95]. This guideline proposes to test at least three replicates on three different levels of % LA. The present case exceeds these numbers of samples considerably because the whole course of the manufacturing process was to be assessed.

For NIR methods, accuracy is usually demonstrated by correlation of NIR results with analytical reference data but is often constrained by the non-feasibility of performing recovery experiments, particularly for analysis of intact solid dosage forms [47].

The accuracy of the NIR model is determined as external validation by measuring validation samples which are not part of the calibration method. The predicted NIR values are then compared to the "true" values, which are in case of an indirect method like NIRS the results of the reference method, i.e. HPLC for API quantitation. This test was carried out by measuring samples which have been collected during manufacture of a feasibility batch in full scale (batch P). The scale change is not affecting the NIR method because the actual sample measurement takes place in an at-line set-up and determines the API content of single static tablets.

At first, the mean predictions for eight sample sets consisting of ten film-coated tablets each were determined and compared to the mean assay value which was found by performing the reference analysis HPLC/UV. The plot given in Figure 66 shows the mean NIR predictions per sample compared to the mean labelled amount of API (% LA) determined by the reference method. Obviously, the mean NIR predictions are close to the HPLC values and the deviations between the methods decrease with proceeding manufacturing process and are smallest for the coating endpoint. Thus, it is possible to monitor the coating process by near infrared spectroscopy.

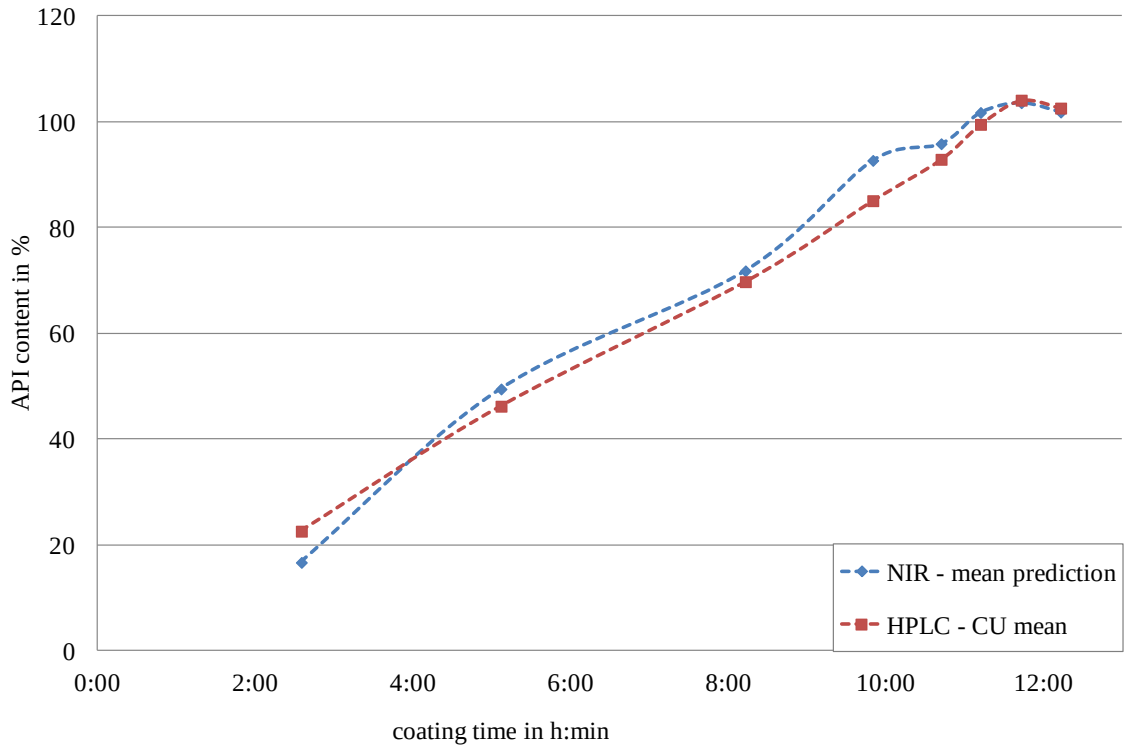

Figure 66 Comparison of mean NIR predictions to mean reference values for samples collected during active coating process of batch P

Accuracy in the absence of precision has little meaning, so the individual predictions for each single tablet out of the set of ten film-coated tablets are compared to the reference values during precision assessments.

5.5.4 Precision of NIR calibration model B-4d

The ICH Q2 Guideline on validation of analytical procedures defines precision as follows: "The precision of an analytical procedure expresses the closeness of agreement (degree of scatter) between a series of measurements obtained from multiple sampling of the same homogeneous sample under the prescribed conditions. Precision may be considered at three levels: repeatability, intermediate precision and reproducibility" [95]. If it is not possible to measure homogeneous, authentic samples, the test on precision may be performed by measuring artificially prepared samples.

The variation in NIR and HPLC determinations of the respective sample set is depicted in Figure 67, where mean values as well as minimum and maximum results of the respective sample set are indicated. As discussed before, the mean values of NIRS and HPLC are

quite close, but the variance of both the results of the reference method and the NIR method are high. The scatter of NIR predictions for individual tablets of the same sample set is even higher than the corresponding results of the reference analysis. The difference between minimum and maximum value of a sample set decreases during the active coating process. There are two possible reasons for this observation: On the one hand, the tablets are not equally layered by the coating suspension at the beginning of processing. On the other hand, the analytical method which was used as reference was only intended for analysing final film-coated tablets with an applied amount of API close to 100 %. Therefore, the accuracy of the HPLC method was only investigated from 70 to 130 % LA. Nevertheless, the accuracy of the reference method tested as recovery of API in spiked samples was slightly worse for samples containing 70 % than for 100 or 130 % LA of API. Thus, it is possible, that the accuracy of the reference method can only be assigned for values from 70 % LA onwards and thus only for samples collected closer to the end point.
In 1982, W. Horwitz [96] published similar findings: there is an exponential relationship between the relative standard deviation in reproducibility tests and the concentration of the analyte. Thus smaller numbers of % LA can per se be correlated to lower precision.

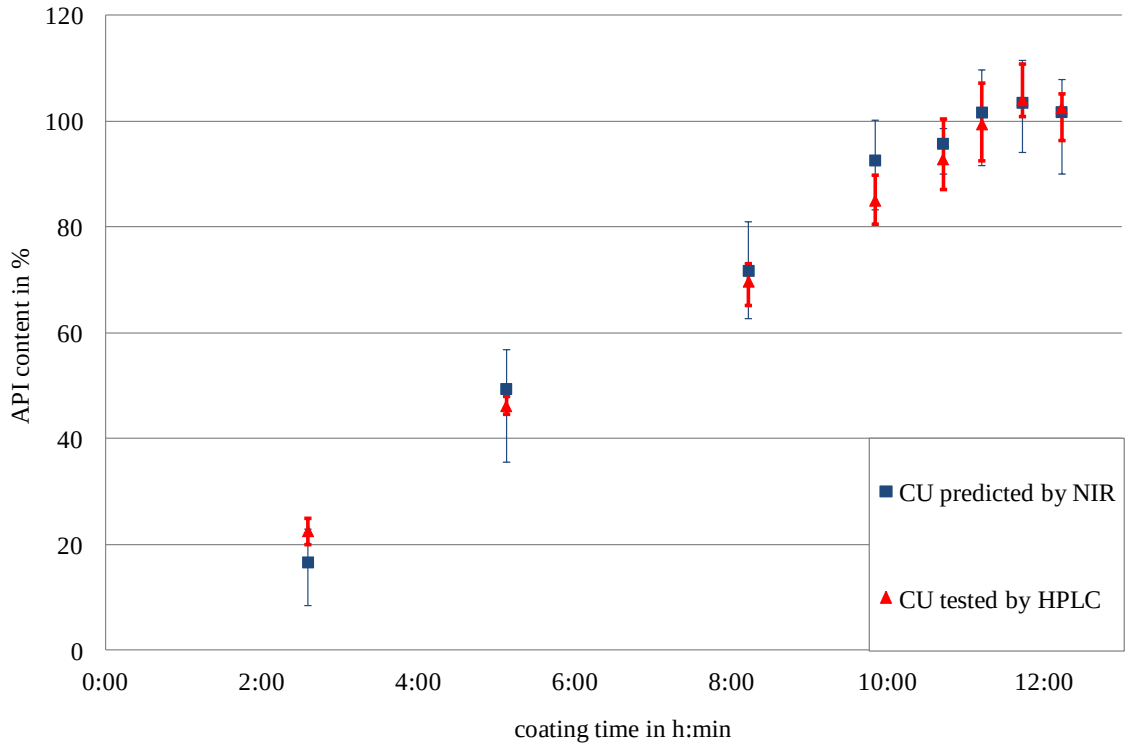

Figure 67 Comparison of NIR predictions for mean CU to reference values for samples collected during active coating process of batch P

The draft guideline on the use of NIRS by the pharmaceutical industry published in January 2012 [97] allows having a higher error for the NIR method than the reference method. In such a case, specification limits can be tighter for the spectroscopic technique than for the reference analysis.

Repeatability is assessed as repeated measurements of the same sample under the same conditions. The standard deviation at each single wavenumber (see Figure 68) was calculated out of three spectra recorded of the same sample and pre-processed as specified in the calibration model B-4d by 1st derivation and 5 smoothing points, yielding in the olive spectrum. The maximum deviation is approximately 0.00002 Absorption Units (AU), which is smaller than 1/10th compared to the maximum standard deviation of the calibration spectra (blue) with 0.0028 AU.

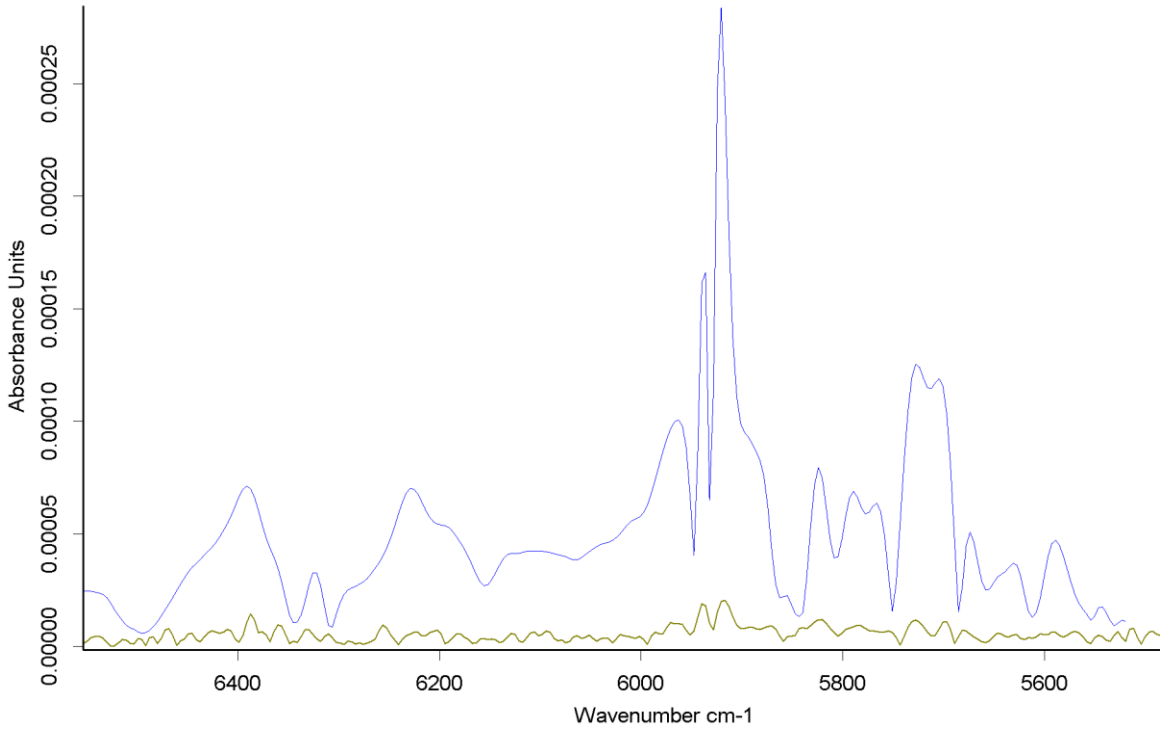

Figure 68 Standard deviation at each wavenumber calculated of a triple measurement

In summary, the NIR predictions for samples collected during processing of batch P are close enough to the reference values to claim feasibility for the application of near infrared spectroscopy as endpoint determinative tool. The mean NIR values are comparable to the reference values, but the variations in NIR predictions are higher than the ones of the

reference determination. The API content of the very last sample was found to be smaller than the preceding one, tested by NIRS and HPLC, and indicated the insufficient content uniformity of the manufactured film-coated tablets.

5.5.5 Robustness of NIR calibration model B-4d

The evaluation of the robustness of the model evaluates the predictive ability of the model in presence of variations from chemical or physical properties of the material. NIRS is sensitive to physical properties of the sample like hardness, particle size and embossments in case of tablets [65].

The presence of physical and chemical variation in the sample set was partly realised when assessing the specificity of the model, when the influence of different moisture contents during the coating process was removed (advancement from model B-1 to B-2). Another parameter, which was already discussed, is the sample presentation. As the distance between probe and sample and the position of the embossing is set, no influence is therefore expected.

Another potential influence is examined in the next trial, which excludes the effect of different masses of film-coat on the NIR predictions for the API content.

5.6 TRIAL ON THE UNIFORMITY OF THE APPLIED MASS OF FILM-COAT

This trial is performed to assess the uniformity of the applied mass of film-coat on the tablets of one batch. This allows evaluating both the manufacturing process, which should lead to uniformly film-coated tablets, and the NIR method, which should determine the API content as % labelled amount without any interference of the applied mass of film-coat. The following questions are to be answered by means of this trial:

- Is the film-coat uptake equal for all tablet weights?
- Is there a correlation between tablet core mass and NIR prediction?
- Does the expected correlation exist between API content and applied mass of film-coat?

5.6.1 Experimental procedure

Hundred tablet cores were individually weighed and marked with a number (1 – 100). These marked tablets were mixed with unmarked tablet cores and processed as one full scale batch of altogether 75 kg. Film-coating in this scale was realised in a drum coater GC 1250 (Glatt, Binzen, Germany). After completion of the film-coating process, the tagged tablets were separated and their exact final mass was redetermined. The applied mass of film-coat was calculated by subtracting the mass of the mean water uptake of another ten tablets from the mass difference of film-coated tablets and tablet cores.
Subsequently, the film-coated tablets were measured by NIR spectroscopy and their API content was evaluated. The NIR predictions were compared to the individual results of the reference analysis for each single tablet.

5.6.2 Results

86 of the 100 tagged film-coated tablets could be recovered and separated from the bulk product after film-coating, thus these 86 tablets are captured in the evaluation and the remaining fourteen tablets are neglected.
The API contents expressed as % LA, determined by NIRS and HPLC / UV for individual tablets, are given in Figure 69. The predicted API contents are close for the majority of the tablet samples, but some of them differ up to 13 % LA, corresponding to 0.325 mg API in

the final drug product. The mean value of the NIR predictions is 108.2 % LA and thus slightly higher than the mean reference value, which is 105.5 % LA.

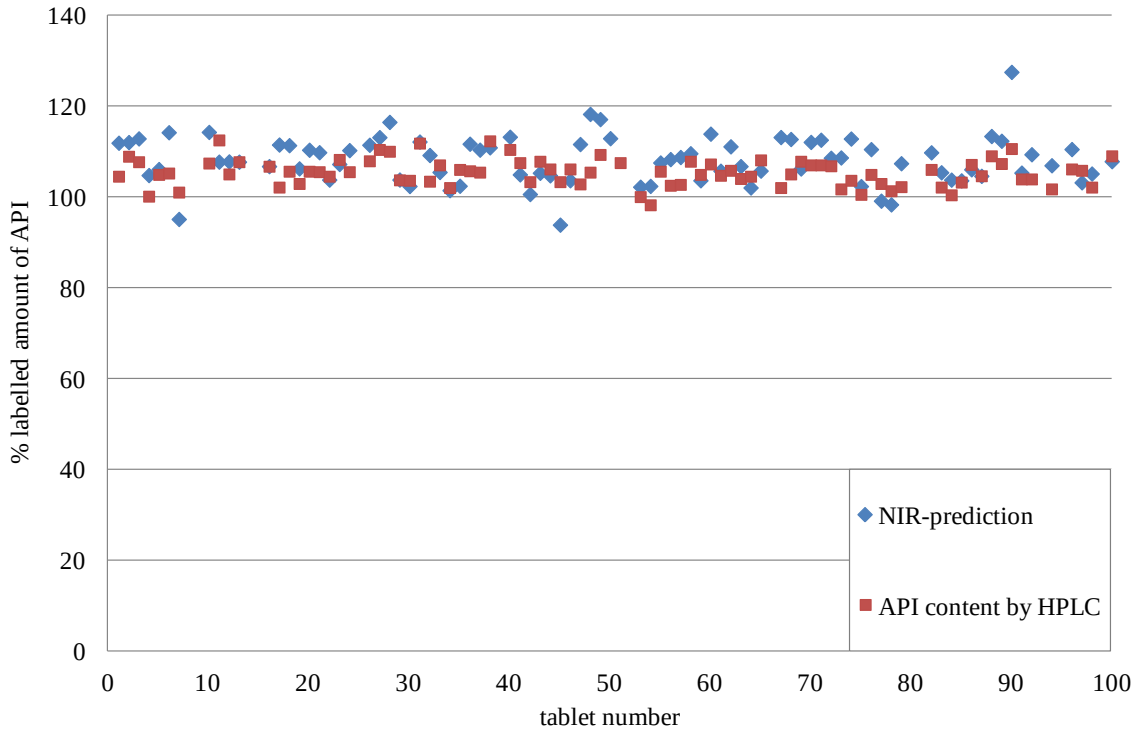

Figure 69 API content determined by NIRS (method: B-4d) and HPLC for marked tablets

At first, the uniformity of uptake of film-coat is to be evaluated. Figure 70 depicts the scatter plot of mass of the film-coated tablets after the film-coating process vs. the mass of the respective tablet cores. Although there is obviously high deviation from the target mass in some cases, the computed trend line (dashed line) has a slope close to 1 for the intercept of 60, which corresponds to the target mass of film-coat. Besides of the deviation up to 20 mg of the target mass, corresponding to 1.7 % of the total mass, there is no trend with regards to the mass of film-coat revealed by this plot. Therefore, the uptake of film-coat is independent of the mass of the tablet cores.

The relative standard deviation with regard to the mass is not affected by the coating process: it decreases slightly from 0.67 % for the cores to 0.64 % for the film-coated tablets.

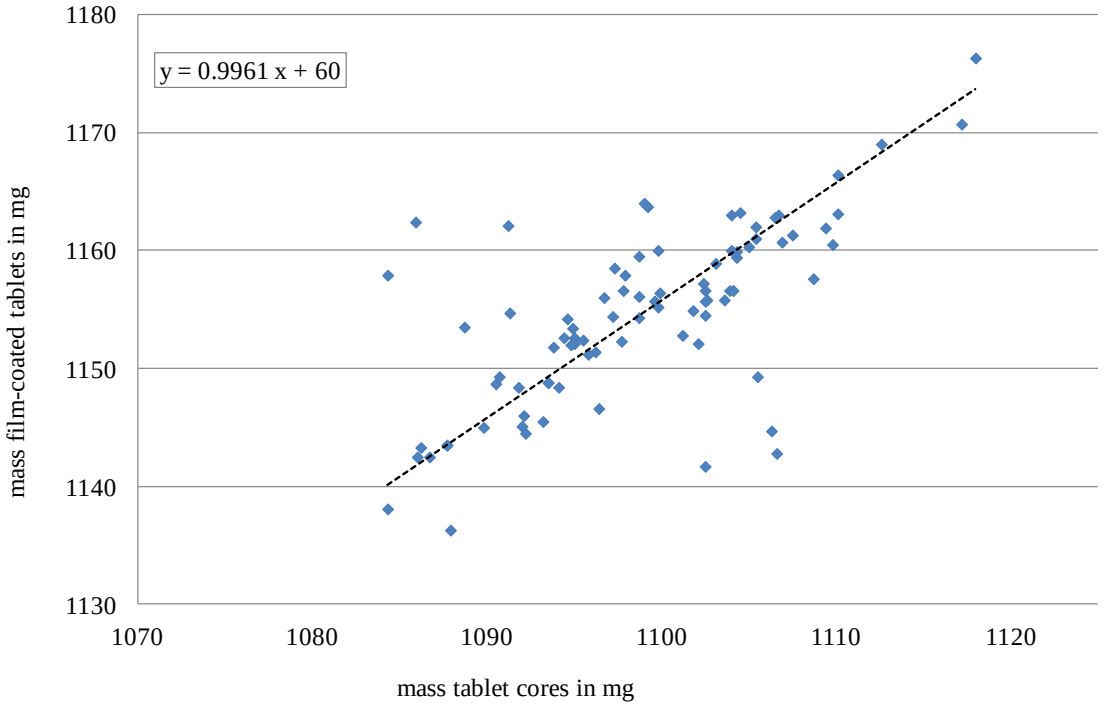

Figure 70 Correlation of mass before and after active coating

The next evaluation examines potential interferences for the NIR predictions by different masses of applied film-coat. The respective plot is presented in Figure 71, where neither any dependence of NIR predictions (blue) from the mass of film-coat on the tablet cores is observed, nor is such an interference evident for the reference values determined by HPLC (red). Hence, the results of both analysing techniques can be claimed as independent from tablet weight.

For the NIR calibration method, this was considered as requirement for the specificity of the model, which has been investigated previously. Moreover, the NIRS method measures only a small part of the film-coated surface, the actual thickness of the film-coat is thus not assumed as interfering parameter.

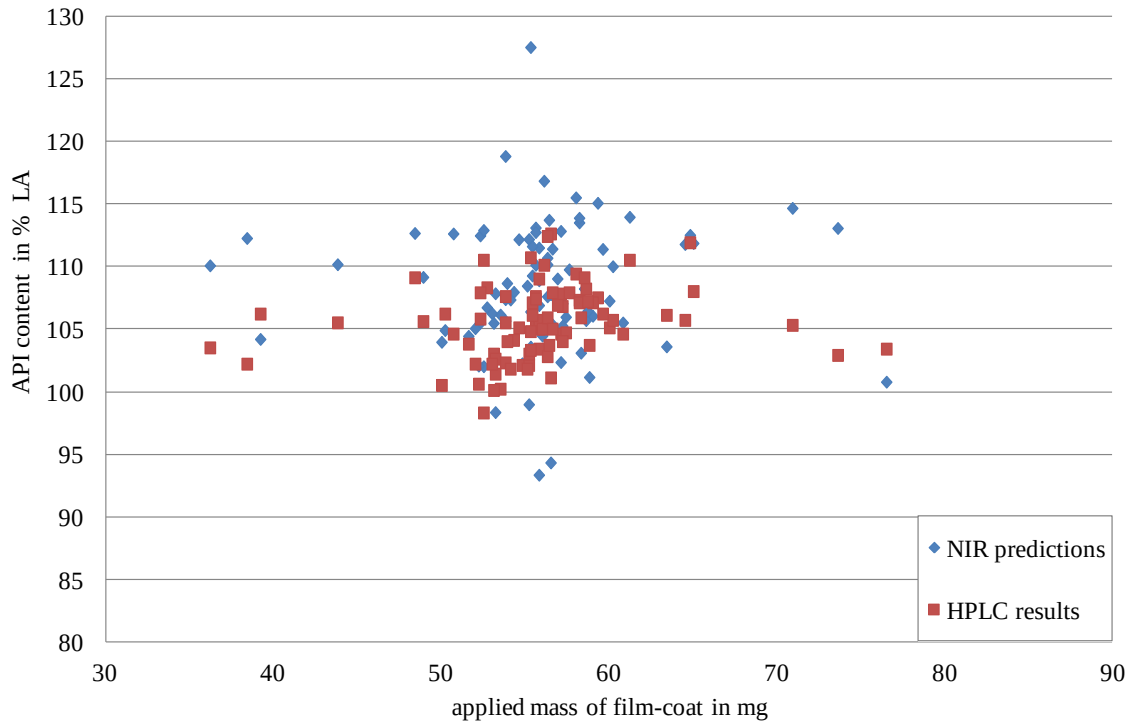

Figure 71 NIR predictions (method: B-4d) vs. applied mass of film-coat of marked tablets

Since the NIR measurements of tablet cores by means of the reflection probe are based on the reflection of an illuminated sample area with a diameter of no more than 3 mm, the API has to be distributed homogeneously in the film-coat applied on the surface. If this cannot be assured as in the present case, another measuring set-up has to be established. Using this set-up, the illuminated area of an NIR method should cover an area bigger or at least equal to a unit dose of the final drug product. Usually, conventional release analysis by HPLC also investigates at least one whole unit dose.

This might be realised by applying a rotating sample cup as measuring device, as discussed as follows.

5.7 IMPROVING THE MEASURING SET-UP BY MEANS OF A ROTATING SAMPLE CUP

The use of the rotating sample cup is assumed to improve the accuracy and precision of the NIR calibration model, because the sample surface, which is illuminated with radiation and reflects the light back exceeds the illuminated light for the probe considerably. The problem for the small measured sample size is only valid for static samples; in moving samples like a fluidised bed in a fluid bed granulator, the probe is constantly surrounded by new product throughout one single measuring cycle.

5.7.1 Measuring set-up

The rotating sample cup is comparable to a beaker with a diameter of 9.7 cm, which can be attached on the rotating holder of the spectrometer. By rotating the sample cup which is filled with sample material, the illuminated area is multiplied and potential unequal distribution of the ingredient of interest is likely to be averaged, see Figure 72. Thus, the issue of potential unequal distribution of the API on the surface of the big tablets might be overcome.

The measuring principle is diffuse reflection and hence the same than for the fibre optic probe.

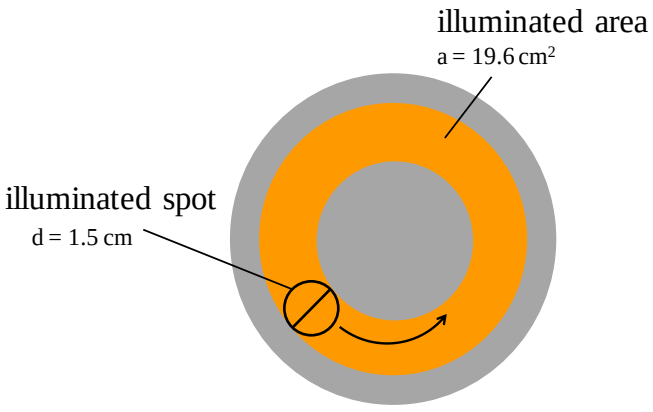

Figure 72 Comparison of illuminated areas of the rotating sample cup and the static integrating sphere (based on [98])

Furthermore, the sample cup rotates more than six times during one measurement cycle and thus allows measuring a large sample area.

The standard deviations of three spectra of the same sample measured with different settings are compared in Figure 73.

Best reproducibility of the spectra was found to be obtained when using a high resolution (8 cm^{-1}) and a high number of scans (128), which are averaged into the resulting spectrum. The corresponding spectrum based on the standard deviation calculated at each wavenumber (green spectrum) has lower values than the one for the coarser resolution 16 cm^{-1} (brown spectrum). Although the measurement time using these settings was longer compared to the measurement of a single tablet, the complete measurement is with ≈ 70 s still faster than the succeeding measurement of ten tablets of a sample set using the reflection probe set-up.

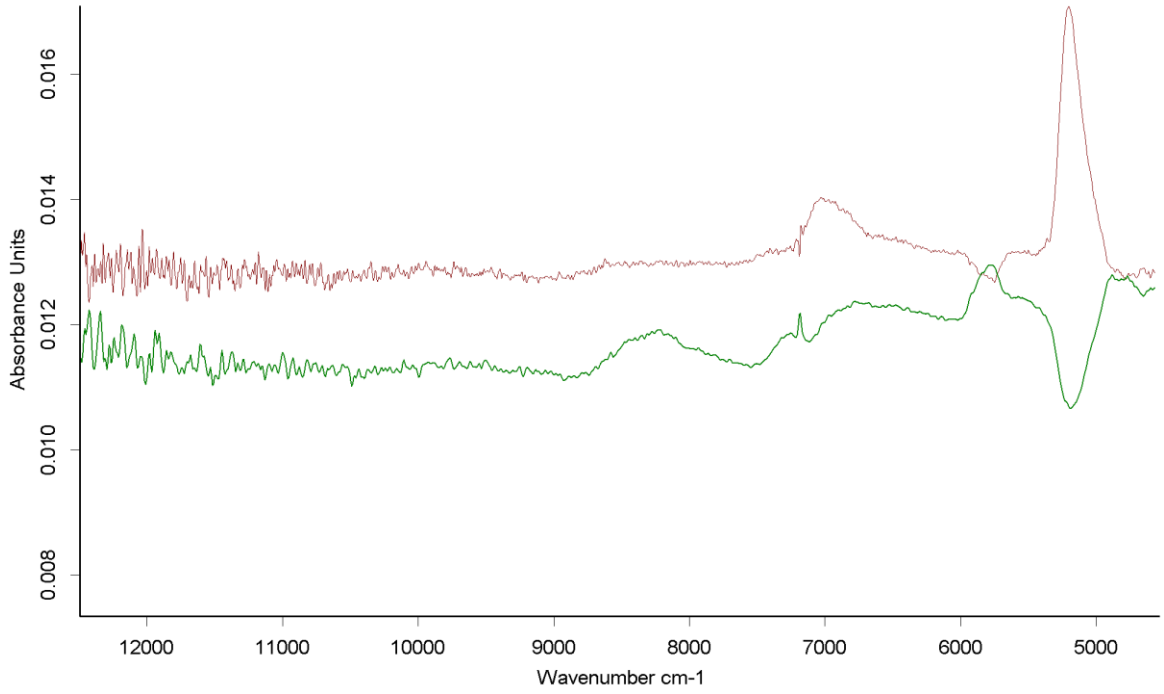

Figure 73 Comparison of standard deviation of spectra recorded with resolution 16 cm^{-1} and 64 scans (brown) to spectra of 8 cm^{-1} and 128 scans (green)

An overview of the adjustments for measurements with the rotating sample cup is presented in Table 24.

Table 24 Adjustments for NIR-measurements using the rotating sample cup

Parameter	**Value**
Measuring mode	Diffuse reflection
Wavenumber range	12500 – 4000 cm^{-1}
Resolution	8 cm^{-1}
No. of scans per spectrum	128
Preamplifier gain	Ref
Detector	PbS (Lead Sulfide)

The resulting NIR spectra are similar, but not identical to the ones obtained with the measuring set-up applying the fibre optic probe (see Figure 74). The spectral features of the NIR spectra recorded with the rotating sample cup (green) and with the fibre optic probe (blue) are similar, but they differ in the intensity of the absorption peaks. Moreover, the spectra recorded with the rotating sample cup display more noise especially in the regions above 11000 cm^{-1}. In this wavenumber region, the spectra are mainly affected by physical attributes and not by the chemical composition of the sample. The arrangement of tablets in the sample cup inevitably leads to vacancies in the measured surface. Even if these vacant spaces are covered with tablets in a higher layer, the amount of straylight in this region is higher, than with the probe which is in direct contact to the sample. Nevertheless, this is not considered as critical to the evaluation because the API, which is to be quantified, does not absorb NIR radiation in this region. Furthermore, the developed calibration models focus on the region from 7000 – 5500 cm^{-1} and appropriate smoothing algorithms can minimise influences of straylight.

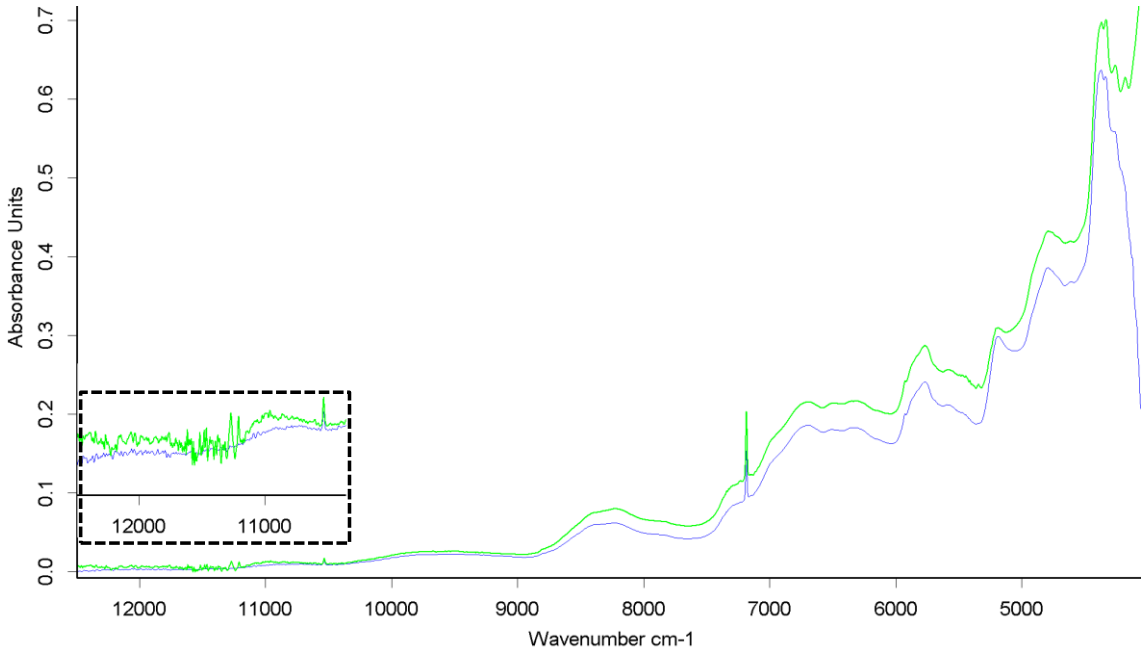

Figure 74 Comparison of offset-corrected raw spectra measured with rotating sample cup (green) and a single tablet measured by fibre optic probe (blue)

Pre-processing the wavelength range which is captured in the calibration model decreases the differences between spectra of the two measuring modes, but still they cannot be evaluated by the same calibration model. In Figure 75, the 1st derivation of the rotating sample cup spectrum (green) can be compared to the spectrum recorded by means of the probe (blue). Obviously, a completely new calibration model has to be established.

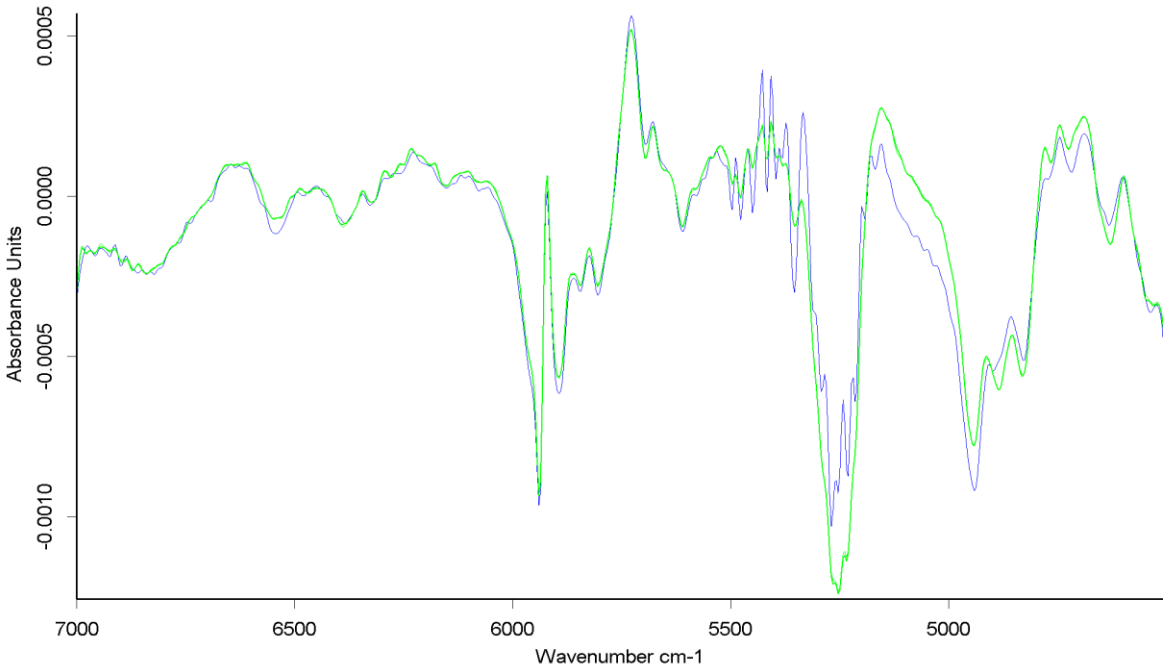

Figure 75 Comparison of spectra pre-processed by 1st derivation measured with rotating sample cup (green) and a single tablet measured by fibre optic probe (blue)

5.7.2 Development of NIR calibration model for the rotating sample cup

When developing the new calibration model, the first point to consider is again selecting meaningful wavelength ranges. Thus, the calibration spectra are searched for features which are probably impacted by the amount of API present in the sample. For this reason, Figure 76 shows pre-processed spectra of pure API (red), final film-coated tablets from different batches (green and brown) and blank film-coated tablets (blue), which are manufactured without applying API. The exact wavenumbers of two distinct absorption peak maxima are located at 6442 cm^{-1} and 5867 cm^{-1} and magnifications of these regions reveal evident differences between film-coated tablets with or without API.

The performance parameters of the leave-one-out cross validation procedure are obtained when selecting one wavenumber region which encompasses both of the illustrated absorption peaks of the API.

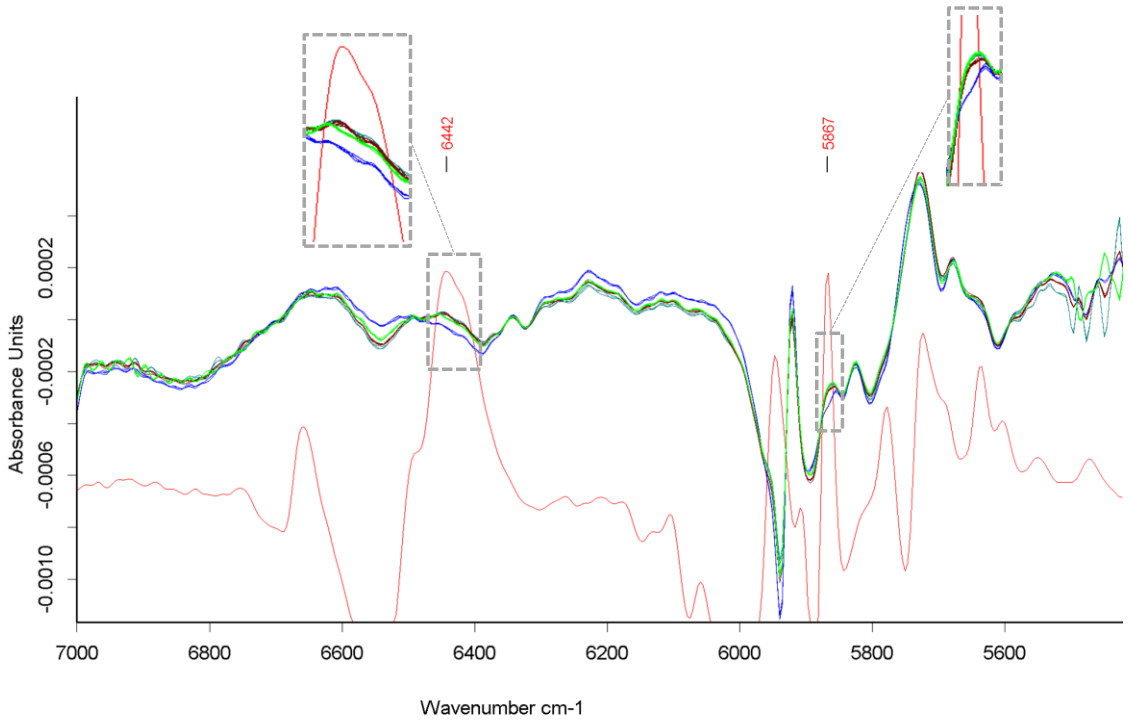

Figure 76 Rotating spectra of blanks (blue), final FCT (green and brown) and API (red), pre-processed by 1st derivations, 5 sm. pts. respectively

The calibration model applying the rotating sample cup was developed some time after the feasibility tests had taken place. Therefore, the number of available calibration samples is smaller compared to the calibration method based on measurements of single tablets. The smaller number of calibration spectra is additionally due to the fact that each calibration sample consists of approximately 20 tablets, which are unified to one calibration sample and hence one calibration spectrum. The reference value for this sample was defined as the mean HPLC value, determined out of ten tablets which were collected at the same time point when manufacturing the batch. Therefore, the maximum reference value is with 111 % LA smaller than the one for the calibration model for single tablets.

The described approach can lead to an improvement in two ways: potential variations or outlying results of the reference method are averaged as well as the prolonged measurement time and the increased measured sample surface of the NIR measurements can lead to more precise results.

Important parameters of the calibration model for the measuring device using the rotating sample cup are summarised in Table 25.

The most promising calibration was obtained when pre-processing the calibration spectra by Multiplicative Scatter Correction. The use of derivative pre-processing techniques was

not successful, contrary to the initial calibration model. This can be due to the fact that the increased signal to noise ratio of the spectra obtained by rotating sample cup-measurements required higher smoothing, which on the other hand decreases the contained degree of information in the spectral features.

The performance parameters obtained by cross validation have been slightly improved compared to the model B-4d, which is the final one for measurements using the probe.

The coefficient of determination has risen from 97.76 to 98.41 % and the Root Mean Square Error of Cross Validation dropped slightly from 3.81 onto 3.32. The only potential deficiency is the increased rank for the PLS model of 8 compared to formerly 7.

Table 25 Parameters of calibration model for rotating sample cup and results of cross validation

Parameter	**Value**
No. of batches included in calibration	10
No. of calibration samples	48
Scale (and no.) of calibration batches	Pilot scale (8), lab scale (1), full scale (1)
Calibration range	0 – 111.1 %
Data pre-processing	Multiplicative scatter correction
Selected wavenumber range	6182 – 5496 cm^{-1}
R^2 [%]	98.41
RMSECV [%]	3.32
Rank	8
Bias	-0.18
Offset	3.58

A first estimation of the performance of the calibration model can be derived from a score plot of the model. The score plot of the PLS model for the first and second principal component is depicted in Figure 77. The samples sets which have been collected at the same time points are clearly arranged in spatial clusters. The samples are located according to the course of the coating process which runs in inverse direction to PC 1: starting tablet cores (cyan) are located on the very right side, while the samples corresponding to an API content from 80 – 111 % LA (green) are on the very left side. The blank film-coated tablets

(red) and the regularly processed film-coated tablets (green) differ in their scores on the second principal component.

The scores of corresponding spectra are located very close together, compared to the larger clouds which are obtained from the PCA of the calibration method for single tablets. This indicates successful averaging of samples with varying properties between the tablets of the sample sets.

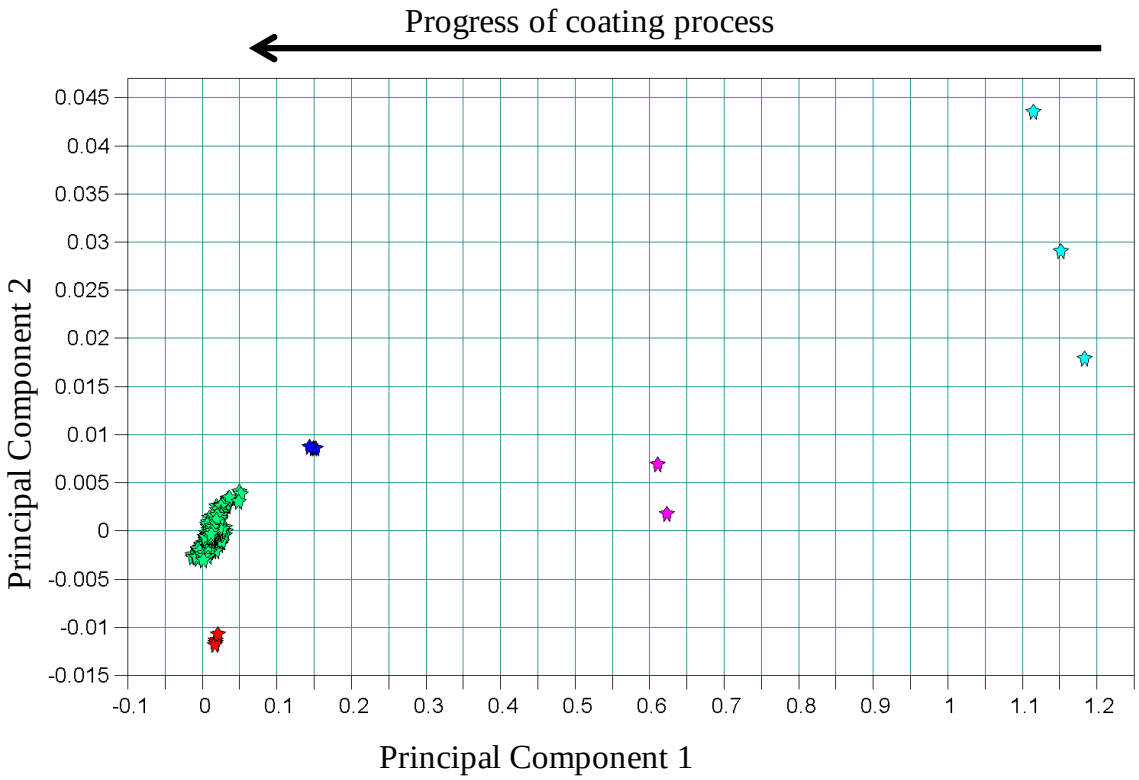

Figure 77 Score plot of PLS model for rotating sample cup tablet cores (cyan). sample 1 ≈ 25 % (pink), sample 2 ≈ 50 % (blue), 80-111 % LA (green), blanks (red)

This new measuring set-up and the associated calibration model have to be tested for its ability to predict the end-point of the active coating process of further batches before a final assessment is possible. Unfortunately, further tests are not possible due to project restrictions and timelines. Nevertheless, based on the current knowledge, the application of NIR spectroscopy is considered feasible. Additionally, the measurements realised by means of the rotating sample cup seem to lead to a more robust calibration model and prediction results. The influence of measuring larger surface areas is considered to be more pronounced in this early development phase, where the surface of the film-coated tablet is not yet uniformly layered by film-coat and API. Here, averaging clearly leads to

converging predicted NIR values and results of the reference test. In case of ideally homogeneous surfaces, this effect should be negligible and scattering results arise directly from measurement inaccuracies or different sample handling or positioning and not from the sample itself.

5.8 CONCLUSION PROJECT B AND ADDITIONAL VALUE OF APPLICATION OF PROCESS ANALYTICAL TECHNIQUES

Process Analytical Technology is understood as a toolbox and thus a system for designing, analysing and controlling manufacturing processes [10].

PAT tools like near infrared spectroscopy but also Design of Experiments supported effectively the experiments conducted for assessing the feasibility of active coating of tablets in pilot and full scale. Process parameters were screened and their effects on the content uniformity of the API on single dosage units were assessed by means of statistical planning and evaluation of experiments. The performed DoE is considered as starting point for further process optimisation activities and may be basis for a quantitative process model when more data and enhanced process knowledge is available. Process modelling and statistic simulation can be of immense value for the pharmaceutical industry, since every trial is closely related to high costs due to the API demand. The potential saving of development costs was estimated by Chen [99] to account for 30 – 70 % when modelling process development and scale-up of an active coating process by decreasing the total number of experimental runs.

The development of the NIR method implied the development of an appropriate sample presentation and measuring mode for at-line measurements. The film-coated tablets were measured separately using the reflection probe or as a complete sample set by means of a rotating sample cup. By measuring single film-coated tablets, the reference value can easily be correlated to the NIR spectrum of the respective sample. Yet, collecting NIR spectra of several tablets takes some time and although results are obtained much faster than with the standard method HPLC, the NIR method does not really work in real-time. When measurements with the rotating sample cup are performed, the NIR spectrum is an average of a large illuminated surface area.

The NIR calibration model was developed based on feasibility batches manufactured in pilot scale and one batch manufactured in full scale. The difference in batch scale had no effect on the NIR method, since the measurements were realised at-line. Finally, the NIR technique should be applicable to in-line measurements in the drum coater. In-line NIR applications have been reported in literature for monitoring of the conversion of cured acrylate coatings [100], for monitoring film-coat curing of sustained release coatings [101] and was intensively studied to determine coating thickness. Coating thickness of tablets in

fluid bed process can be monitored by NIRS [102], [103] as well as coating processes in pan-coaters or coating of granules [104] and pellets [105]. It was even possible to develop univariate models for coating thickness measurements [106]. This is due to the fact that spectral changes caused by variations in film-coat thickness are more easily accessible since the amount of applied film-coat is usually substantially higher than the applied amount of the low-dosed API which was quantified in the present work. However, it was possible to develop a calibration model with the required specificity for the API.
A prerequisite for further refinements of the calibration mode is to optimise the active coating process. More efforts need to be spent on the process development of the active coating process in order to achieve sufficient uniformity of the API and thus to be conform to the required uniformity of unit doses. After optimisation of the film-coating process, the accuracy and the precision of a NIR method for prediction of the API content are supposed to increase.

The validation approach described in chapter 5.5 is considered as an example because it is only based on feasibility trials and the final product does not yet meet the requirements of the pharmacopoeias with regard to the uniformity of dosage forms. Therefore, the calibration model includes a higher degree of variation which is induced by inhomogeneities within the tablet surface and which is evident in the high value for RMSECV [91]. In general, validation procedures start with the fixing acceptance criteria based on the performance parameters of the reference method. In this case, the reference method had not been fully validated for the particular formulation and it was hence omitted to derive any acceptance criteria for the PAT method. Nevertheless, the obtained results were sufficient to claim feasibility of applying near-infrared spectroscopy for monitoring the manufacturing process and determining the endpoint of active coating of tablets. The endpoint is detected by quantifying the API applied on the film-coat and is based on spectral differences due to the varying API content. Moreover, at-line measurements are able to detect process failures during manufacture and enable corrective actions. This could e.g. be realised by connecting a constant API content over a certain time period to an alarm and thus detect potential breakdown of the stirrer-breakdown in the coating suspension.
The benefit of applying NIRS as a PAT tool compared to conventional HPLC analysis is mainly related to saving of time, reducing logistics and turn-over times, since the bulk product can directly be processed further. This supports the intended reduction of the reported delay between completion of the unit operation, sampling, analysis, reporting, and

in-process or final product release [6] and hence decrease cycle times in production and is a first step in direction of real-time release. PAT can contribute to significantly reduce costs for quality control functions not only by replacing them completely by PAT sensors or process models, but also by enabling a more efficient operation of quality control activities [16].

6. REGULATORY REQUIREMENTS FOR SUBMISSION OF PAT DATA

Although a lot of efforts are spent by pharmaceutical companies to explore the potential of PAT applications during development and manufacturing of drug products, there is a lot of uncertainty with regards to regulatory affairs. On the one hand, there are the main authorities, the FDA in the United States and the EMA in Europe, which strongly encourage the use of new technologies and development principles focusing on process understanding and risk assessment. On the other hand, companies fear triggering more questions when they disclose their own applications and running into the risk of delayed approvals.

This chapter summarises the most important official documents, which are currently available.

In general, there are three different objectives for PAT applications:

- Effective support of QbD principles during development and scale-up of a new chemical entity (NCE)
- Increase of efficiency and potential reduction of regulatory efforts during continuous improvements of approved drug products
- PAT for trouble-shooting during manufacture for approved drug products

6.1 GENERAL DOCUMENTS CONCERNING THE IMPLEMENTATION OF PAT

The initial document and maybe the best known is the PAT Guidance of the FDA [10]. But unlike other guidelines, this one is not instructive or limiting, but has to be understood as a real "framework" and is open for interpretation [6]. Besides of definitions, it describes principles and tools and is "highlighting opportunities". Another important content is the different communication strategies required concerning PAT: a stronger direct interaction between regulators and scientists and engineers is anticipated rather than indirect communication via a department of regulatory affairs.

The ASTM Technical Committee E55 published an international standard called "Standard Practice for Pharmaceutical Process Design Utilizing Process Analytical Technology"[107], which is a collection of definitions related to principles and methodologies of PAT process design.

In 2006, the EMEA, (today EMA) published a reflection paper named "Chemical, pharmaceutical and biological information to be included in dossiers when Process Analytical Technology (PAT) is employed"[108]. Apart from general information and definitions, this early paper defines the status of raw data related to PAT: Some raw data is supposed to be necessary to support conclusions and enable independent assessments of the conclusions. Moreover, the data can be subject to an inspection as well as validation and calibration data, which have to be made available to the assessor on request.

A more illustrative way was chosen by the European Federation of Pharmaceutical Industries and Associations (EFPIA) when releasing their Mock P.2 Document. This was intended to provide assistance for use of models and algorithms, of in-line and at-line tools and for using prediction models to establish the design space and their description in the P.2 Pharmaceutical Development submission document by providing an exemplary submission document of a fictive drug product [109].

The FDA is reported as very supportive of companies participating in PAT projects by creating opportunities to develop less restrictive regulatory approaches to manage changes for well-understood processes [14].
FDA and EMA even started a pilot program for parallel assessment of Quality by Design applications, in order to provide advice to the applicants and ensure consistent implementation between EU and US of ICH Q8, Q9, Q10 guidelines [110].
This voluntary pilot program will end in 2014 with presentations through conferences or publications as appropriate and is meant to enhance the acceptance of PAT and QbD efforts throughout the pharmaceutical industry.
Until now, most approved PAT applications only imply the substitution of a conventional IPC method by in-line or at-line measurement tools, but no real implementation of PAT principles throughout the whole manufacturing process according to Dr. Jobst Limberg, 2011, who is assessor at the BfArM.
Finally, one goal and an enormous advantage of the PAT initiative is the possibility of real time release testing meaning that time-consuming end-product release testings can be moved upstream in the manufacturing process and can be substituted by in-line measurement tools as described in the Guideline on Real Time Release testing of the EMA [111].

6.2 SPECIFICATIONS FOR NIR DATA

Especially for data which are generated by means of an NIR spectrometer, there is now more and more information on the requirements and expectations of regulatory agencies available.

Meanwhile, the pharmacopoeias included quite detailed monographs about near infrared spectroscopy: the respective chapter <1119> in the USP [48] was included in 2003, the corresponding one <2.2.40> in the European Pharmacopoeia [45] became valid even earlier, but was revised in 2008 and is currently again under revision. This indicates the growing importance of the technique among pharmaceutical companies and also the increased need for clear instructions. The named monographs list requirements for control of instrument performance, namely parameters for the qualification of instruments, as well as validation parameters for the calibration model. Although the chapters are not officially harmonised, the tests and parameters described are often similar; they contain descriptions of instrument performance tests as

- Wavelength uncertainty or verification of wavelength scale which assesses the accuracy of peak localisation of a standard assuring its consistency to those determined by an external reference NIR system, accepted tolerance: ± 8 cm^{-1}
- Photometric linearity between concentration and response with a slope of 1 ± 0.05 and intercept 0.0 ± 0.05
- Spectroscopic noise determined at high and low light flux and
- Response stability verified using suitable standards.

The EMA is working on a guideline on the use of near infrared spectroscopy by the pharmaceutical industry and the data requirements for new submissions and variations [97], of which the draft was published in January 2012. This guideline uses some of the proposals made by the Pharmaceutical Analytical Sciences Group (PASG) in their Guidelines for the Development and Validation of Near Infrared (NIR) Spectroscopic Methods. This paper discusses in detail equipment possibilities, and technical guidelines for qualitative and quantitative methods.

The NIR calibration models presented in this thesis are focusing on quantitative determinations; therefore the most important points with regard to quantitation are briefly mentioned.

It is recommended to use, where possible, a mixture of calibration samples collected from production batches and synthetically produced laboratory samples to incorporate a wider

range of the analyte of interest in the calibration. This approach also allows including the normal variability during production, e.g. differences in the sample matrix due to different lots of excipients. If laboratory samples are included, they are to be prepared using the same manufacturing processes than for process samples. The number of calibration samples should be much greater than the number of principal components of the respective NIR model. The calibration is then developed and firstly assessed by an internal cross validation approach to identify the most appropriate calibration parameters. Then the actual validation us realised on independent samples as external validation. If a reference method is used, its performance should also be discussed and compared to the predictive ability of the NIR calibration model.

The method is to be validated by performing the tests which have already been explained and discussed: specificity, linearity, range, accuracy, precision, robustness and limits of detection and quantitation. A critical review on published NIR methods in pharmaceutical applications was recently presented by C. De Bleye et al. [112]. The authors blame that despite of all available guidelines, NIR methods are often only assessed by R^2 and RMSEP, ignoring further relevant validation parameters.

The lifecycle of a NIR calibration model is of great importance and therefore described in a whole chapter in the guideline. The management of the NIRS procedure lifecycle has to be indicated and changes concerning the performance of an approved NIRS method bring about the necessity for re-calibration and / or re-validation of the method according to valid change management protocols. Changes within the scope of the method can be subject to GMP inspections; this may also include maintenance of the spectral library and equipment. Changes outside the scope of the approved method have to be subject to a variation application.

All recorded spectra have to pass a statistical spectral quality test which identifies samples of which the spectral characteristics do not fall into the calibrated range of variation before being used for predictions.

Out of specification (OOS) results have to be followed by an investigation of the batch and, if confirmed, the release has to be rejected. If OOS results are not obtained using a reference method, the NIR model may need to be updated and re-validated. A batch should not be released if the result of NIRS is OOS and the one of the reference method in specification.

The data should be generated on equipment, which is suitable for the intended use demonstrated by Design Qualification, Installation Qualification, Operational Qualification and Performance Qualification. Appropriate test parameters are described in the PASG Guideline [47].

The method validation of a NIR calibration model has to be included into the dossier, but not the model itself. The level of detail is comparable to the presentation of a HPLC model. Nevertheless, the NIR calibration data can be subject to audits.

Most of the parameters for method validation are similar to the ones described in the ICH Q2 (R1) "Validation of Analytical Procedures: Text and Methodology" [95]. However, an important difference to conventional methods e.g. HPLC for assay determination is the clearly distinct statistics based on in-line measurements with continuous measurements compared to measuring a very limited number of samples with conventional testing. This has to be taken into account when specifications are set and justified.

Only few examples of approved NIRS procedures are described in literature. A first review of installed PAT applications was given by G. Dünnebier and H. Tups [113] reaching from identification of excipients during dispensing over end point prediction during fluid bed drying to in-line monitoring of blending and of compression processes. Another, more recent paper describes the application of the PAT principles and analytical validation of an in-line NIR method for water content measurements during fluid bed drying in commercial scale [31].

However, these examples are limited because their focus is on substitution of other in-process controls or analytical methods and are validated with regards to the reference method. Though, consequent implementation of PAT principles would lead to a stand-alone approach of these techniques: data generated during manufacture of batches are validated based on their results in clinical trials. This could be realised, for instance, by carrying out principal component analysis and cluster analysis of good and bad batches, but is still a long way off.

7. REFERENCES

[1] J. Woodcock, The Concept of Pharmaceutical Quality, Am. Pharm. Rev. 7 (2004) 10–15.

[2] Department of Health and Human Services, U.S. Food and Drug Administration, Strategic Priorities 2011-2015: Responding to the Public Health Challenges of the 21st Century, 2011.

[3] IBM Global Services, The metamorphosis of manufacturing - From art to science. An IBM Institute for Business Value executive brief, 2005, http://www-935.ibm.com/services/us/imc/pdf/ge510-4034-metamorphosis-of-manufacturing.pdf, accessed 10 June 2012.

[4] D. Dean, F. Bruttin, Productivity and the Economics of Regulatory Compliance in Pharmaceutical Production, 2001, http://www.fda.gov/ohrms/dockets/ac/02/briefing/3841B1_07_PriceWaterhouseCoopers.pdf , accessed 22 June 2011.

[5] Department of Health and Human Services, U.S Food and Drug Administration, Pharmaceutical cGMPs for the 21st Century — A Risk-Based Approach, Final Report, 2004. http://www.fda.gov/downloads/Drugs/DevelopmentApprovalProcess/Manufacturing/QuestionsandAnswersonCurrentGoodManufacturingPracticescGMPforDrugs/UCM176374.pdf, accessed 03 July 2012

[6] R.P. Cogdill, S.C. Gad, Case for Process Analytical Technology: Regulatory and Industrial Perspectives, in: Pharmaceutical Sciences Encyclopedia, John Wiley & Sons, Inc., 2010.

[7] L.X. Yu, Pharmaceutical Quality by Design: Product and Process Development, Understanding, and Control, Pharm. Res. 25 (2008) 781–791.

[8] International Conference on Harmonisation of Technical Requirements for Registration of Pharmaceuticals for Human Use, Guidance for Industry, Q8(R2) Pharmaceutical Development, 2009.

[9] M.L. Balboni, Process Analytical Technology, Concepts and Principles, Pharm. Technol. 27 (2003) 54.

[10] U.S. Department of Health and Human Services, Food and Drug Administration, Guidance for Industry PAT - A Framework for Innovative Pharmaceutical Development, Manufacturing and Quality Assurance, 2004.

[11] K.A. Bakeev (Ed.), Process Analytical Technology: Spectroscopic Tools and Implementation Strategies for the Chemical and Pharmaceutical Industries, 2nd ed., Wiley, Chichester, West Sussex, 2010.

[12] P. Suresh, P. Basu, Improving Pharmaceutical Product Development and Manufacturing: Impact on Cost of Drug Development and Cost of Goods Sold of Pharmaceuticals, J. Pharm. Innov. 3 (2008) 175–187.

[13] E. Räsänen, N. Sandler, Near infrared spectroscopy in the development of solid dosage forms, J. Pharm. Pharmacol. 59 (2007) 147–159.

[14] J.F. deSpautz, K.S. Kovacs, Managing the risks of PAT, Pharm. Technol. Eur. 21 (2009) 32–35.

[15] F.J. Muzzio, T. Shinbrot, B.J. Glasser, Powder technology in the pharmaceutical industry: The need to catch up fast, Powder Technol. 124 (2002) 1–7.

[16] R.P. Cogdill, T.P. Knight, C.A. Anderson, J.K. Drennen III, The Financial Returns on Investments in Process Analytical Technology and Lean Manufacturing: Benchmarks and Case Study, J. Pharm. Innov. 2 (2007) 38–50.

[17] D.C. Hinz, Process analytical technologies in the pharmaceutical industry: the FDA's PAT initiative, Anal. Bioanal. Chem. 384 (2006) 1036–1042.

[18] N.K. Ebube, S.S. Thosar, R.A. Roberts, M.S. Kemper, R. Rubinovitz, D.L. Martin, G.E. Reier, T.A. Wheatley, A.J. Shukla, Application of Near-Infrared Spectroscopy for Nondestructive Analysis of Avicel Powders and Tablets, Pharm. Dev. Technol. 4 (1999) 19–26.

[19] J. Rantanen, H. Wikström, R. Turner, L.S. Taylor, Use of In-line Near-Infrared Spectroscopy in Combination with Chemometrics for Improved Understanding of Pharmaceutical Processes, Anal. Chem. 77 (2005) 556–563.

[20] Y. Sulub, M. Konigsberger, J. Cheney, Blend uniformity end-point determination using near-infrared spectroscopy and multivariate calibration, J. Pharm. Biomed. Anal. 55 (2011) 429–434.

[21] K.M. Morisseau, C.T. Rhodes, Near-Infrared Spectroscopy as a Nondestructive Alternative to Conventional Tablet Hardness Testing, Pharm. Res. 14 (1997) 108–111.

[22] S.H. Tabasi, V. Moolchandani, R. Fahmy, S.W. Hoag, Sustained release dosage forms dissolution behavior prediction: A study of matrix tablets using NIR spectroscopy, Int. J. Pharm. 382 (2009) 1–6.

[23] R. Wirth, M. Dienz, NIR-Technologie - Ein neuer Ansatz für thermische Prozesse bei der Verpackung von Pharmaprodukten, Teil 1, Pharm. Ind. 69 (2007) 234–238.

[24] T. De Beer, A. Burggraeve, M. Fonteyne, L. Saerens, J.P. Remon, C. Vervaet, Near infrared and Raman spectroscopy for the in-process monitoring of pharmaceutical production processes, Int. J. Pharm. 417 (2011) 32–47.

[25] A.J. Fitzgerald, B.E. Cole, P.F. Taday, Nondestructive Analysis of Tablet Coating Thicknesses Using Terahertz Pulsed Imaging, J. Pharm. Sci. 94 (2005) 177–183.

[26] J.A. Zeitler, Y. Shen, C. Baker, P.F. Taday, M. Pepper, T. Rades, Analysis of Coating Structures and Interfaces in Solid Oral Dosage Forms by Three Dimensional Terahertz Pulsed Imaging, J. Pharm. Sci. 96 (2007) 330–340.

[27] J.A. Zeitler, P.F. Taday, D.A. Newnham, M. Pepper, K.C. Gordon, T. Rades, Terahertz pulsed spectroscopy and imaging in the pharmaceutical setting – a review, J. Pharm. Pharmacol. 59 (2007) 209–223.

[28] R.P. Cogdill, R.N. Forcht, Y. Shen, P.F. Taday, J.R. Creekmore,C.A. Anderson, J.K. Drennen III, Comparison of Terahertz Pulse Imaging and Near-Infrared Spectroscopy for Rapid, Non-Destructive Analysis of Tablet Coating Thickness and Uniformity, J. Pharm. Innov. 2 (2007) 29–36.

[29] L. Maurer, H. Leuenberger, Terahertz pulsed imaging and near infrared imaging to monitor the coating process of pharmaceutical tablets, Int. J. Pharm. 370 (2009) 8–16.

[30] R.K. May, M.J. Evans, S. Zhong, I. Warr, L.F. Gladden, Y. Shen, J.A. Zeitler, Terahertz In-Line Sensor for Direct Coating Thickness Measurement of Individual Tablets during Film Coating in Real-Time, J. Pharm. Sci. 100 (2011) 1535–1544.

[31] A. Peinado, J. Hammond, A. Scott, Development, validation and transfer of a Near Infrared method to determine in-line the end point of a fluidised drying process for commercial production batches of an approved oral solid dose pharmaceutical product, J. Pharm. Biomed. Anal. 54 (2011) 13–20.

[32] C. Buschmüller, W. Wiedey, C. Döscher, J. Dressler, J. Breitkreutz, In-line monitoring of granule moisture in fluidized-bed dryers using microwave resonance technology, Eur. J. Pharm. Biopharm. 69 (2008) 380–387.

[33] R. Kappes, C. Grimm, J. Scholz, Moisture Analysis Methods - From Laboratory to Process: Feuchtemesstechnik vom Labor bis in den Prozess, Pharm. Ind. 72 (2010) 1231–1238.

[34] J. Huang, C. Goolcharran, J. Utz, P. Hernandez-Abad, K. Ghosh, A. Nagi, A PAT Approach to Enhance Process Understanding of Fluid Bed Granulation Using In-line Particle Size Characterization and Multivariate Analysis, J. Pharm. Innov. 5 (2010) 58–68.

[35] S. Schmidt-Lehr, H.-U. Moritz, K.C. Jürgens, Online Control of Particle Size during Fluidised Bed Granulation, Pharm. Ind. 69 (2007) 478–484.

[36] A. Ruf, J. Worlitschek, M. Mazzotti, Modeling and Experimental Analysis of PSD Measurements through FBRM, Part. Part. Syst. Charact. 17 (2000) 167–179.

[37] X. Hu, J.C. Cunningham, D. Winstead, Study growth kinetics in fluidized bed granulation with at-line FBRM, Int. J. Pharm. 347 (2008) 54–61.

[38] D.L. Wetzel, Near-Infrared Reflectance Analysis, Anal. Chem. 55 (1983) 1165 A.

[39] W. Herschel, Experiments on the Refrangibility of the Invisible Rays of the Sun, Philosophical Transactions of the Royal Society of London 90 (1800) 284–292.

[40] K.H. Norris, J.R. Hart, 4. Direct spectrophotometric determination of moisture content of grain and seeds, J. Near Infrared Spectrosc. 4 (1996) 23–30.

[41] A.V.V. Nampoothiri, S.L. Dexheimer, Ultrafast carrier dynamics in amorphous semiconductors determined by time-resolved THz and NIR spectroscopy, Quantum Electronics and Laser Science Conference, Conference Paper 1 (2005) 452–454.

[42] R.M. Balabin, R.Z. Safieva, Motor oil classification by base stock and viscosity based on near infrared (NIR) spectroscopy data, Fuel 87 (2008) 2745–2752.

[43] S.F. Malin, T.L. Ruchti, T.B. Blank, S.N. Thennadil, S.L. Monfre, Noninvasive prediction of glucose by near-infrared diffuse reflectance spectroscopy, Clin. Chem. 45 (1999) 1651–1658.

[44] T. Davies, The history of near infrared spectroscopic analysis: Past, present and future – "From sleeping technique to the morning star of spectroscopy", Analusis 26 (1998) M17.

[45] European Department for the Quality of Medicines, Council of Europe (Eds.), European Pharmacopoeia 7.6, 7th edition, Strasbourg, France.

[46] C. Pasquini, Near Infrared Spectroscopy: Fundamentals, Practical Aspects and Analytical Applications, J. Braz. Chem. Soc. 14 (2003) 198–219.

[47] Pharmaceutical Analytical Sciences Group NIR Sub Group, Guidelines for the Development and Validation of Near Infrared (NIR) Spectroscopic Methods, 2001, http://www.pasg.org.uk/NIR/NIR_Guidelines_Oct_01.pdf, accessed 9 June 2012.

[48] United States Pharmacopeial Convention (Ed.), USP34-NF29: United States Pharmacopeia-National Formulary.

[49] H. Siesler, Y. Ozaki, S. Kawata, H. Heise (Eds.), Near-Infrared Spectroscopy: Principles, Instruments, Applications, Wiley-VCH, Weinheim, 2006.

[50] O. Berntsson, L.-G. Danielsson, B. Lagerholm, S. Folestad, Quantitative in-line monitoring of powder blending by near infrared reflection spectroscopy, Powder Tech. 123 (2002) 185–193.

[51] MPA Multi Purpose Analyzer, Bruker Optics GmbH, http://www.brukeroptics.com/mpa.html?&L=1, accessed 8 June 2012.

[52] W. Kessler, Multivariate Datenanalyse für die Pharma-, Bio- und Prozessanalytik. Ein Lehrbuch, Wiley-VCH, Weinheim, 2006.

[53] P.R. Griffiths, J.M. Olinger, Continuum Theories of Diffuse Reflection, in: J.M. Chalmers, P.R.Griffiths (Eds.), Handbook of Vibrational Spectroscopy, John Wiley & Sons Ltd., Chichester, 2002.

[54] R.K. Roy, Design of Experiments Using the Taguchi Approach: 16 Steps to Product and Process Improvement, John Wiley & Sons, Inc., New York, 2001.

[55] D.C. Montgomery, Design and Analysis of Experiments, 5th ed., John Wiley & Sons, Inc, Hoboken, NJ, 2000.

[56] M.J. Anderson, P.J. Whitcomb, Design of Experiments, in: Kirk-Othmer Encyclopedia of Chemical Technology, John Wiley & Sons, Inc, 2000.

[57] M. Anderson, Design of Experiments, Ind. Phys. 3 (1997) 24.

[58] D. Xiang, J. Berry, S. Buntz, P. Gargiulo, J. Cheney, Y. Joshi, B. Wabuyele, H. Wu, M. Hamed, A.S. Hussain, M.A. Khan, Robust Calibration Design in the Pharmaceutical Quantitative Measurements with Near-Infrared (NIR) Spectroscopy: Avoiding the Chemometric Pitfalls, J. Pharm. Sci. 98 (2009) 1155–1166.

[59] H. Martens, T. Næs, Multivariate Calibration, John Wiley & Sons Ltd., 1991.

[60] C.P. Meza, M.A. Santos, R.J. Romañach, Quantitation of Drug Content in a Low Dosage Formulation by Transmission Near Infrared Spectroscopy, AAPS PharmSciTech. 7 (2006) E1.

[61] Å. Rinnan, F.d.v. Berg, S.B. Engelsen, Review of the most common pre-processing techniques for near-infrared spectra, Trends Anal. Chem. 28 (2009) 1201–1222.

[62] A. Candolfi, R. de Maesschalck, D. Jouan-Rimbaud, P.A. Hailey, D.L. Massart, The influence of data pre-processing in the pattern recognition of excipients near-infrared spectra, J. Pharm. Biomed. Anal. 21 (1999) 115–132.

[63] R.J. Barnes, M.S. Dhanoa, S.J. Lister, Standard Normal Variate Transformation and De-trending of Near-Infrared Diffuse Reflectance Spectra, Appl. Spectrosc. 43 (1989) 772–777.

[64] J. Ermer, J.H. McB Miller (Eds.), Method Validation in Pharmaceutical Analysis, Wiley-VCH Verlag GmbH & Co. KGaA, 2005.

[65] D. Xiang, M. Konigsberger, B. Wabuyele, K. Hornung, J. Cheney, Development of robust quantitative methods by near-infrared spectroscopy for rapid pharmaceutical determination of content uniformity in complex tablet matrix, Analyst 134 (2009) 1405–1415.

[66] M.C. Sarraguça, S.O. Soares, J.A. Lopes, A near-infrared spectroscopy method to determine aminoglycosides in pharmaceutical formulations, Vib. Spectrosc. 56 (2011) 184–192.

[67] R.A. Forbes, M.L. Persinger, D.R. Smith, Development and validation of analytical methodology for near-infrared conformance testing of pharmaceutical intermediates, J. Pharm. Biomed. Anal. 15 (1996) 315–327.

[68] R.P. Cogdill, T. Herkert, C.A. Anderson, J.K. Drennen III, Synthetic Calibration for Efficient Method Development: Analysis of Tablet API Concentration by Near-Infrared Spectroscopy, J. Pharm. Innov. 2 (2007) 93–105.

[69] D. Petrak, Simultaneous measurement of particle size and particle velocity by the spatial filtering technique, Part. Part. Syst. Charact. 19 (2002) 391–400.

[70] D. Petrak, S. Dietrich, G. Eckardt, M. Köhler, In-line particle sizing for real-time process control by fibre-optical spatial filtering technique (SFT), Adv. Powder Technol. 22 (2011) 203–208.

[71] H. Ehlers, A. Liu, H. Räikkönen, J. Hatara, O. Antikainen, S. Airaksinen, J. Heinämäki, H. Lou, J. Yliruusi, Granule size control and targeting in pulsed spray fluid bed granulation, Int. J. Pharm. 377 (2009) 9–15.

[72] S. Virtanen, O. Antikainen, H. Räikkönen, J. Yliruusi, Granule Size Distribution of Tablets, J. Pharm. Sci. 99 (2010) 2061–2069.

[73] A. Burggraeve, T. Van Den Kerkhof, M. Hellings, J.P. Remon, C. Vervaet, T. De Beer, Batch statistical process control of a fluid bed granulation process using in-line spatial filter velocimetry and product temperature measurements, Eur. J. Pharm. Sci. 42 (2011) 584–592.

[74] P.H. Stahl, Feuchtigkeit und Trocknen in der pharmazeutischen Technologie, Dr. Dietrich Steinkopff Verlag, Darmstadt, Germany, 1980.

[75] G. Rücker, M. Neugebauer, G.G. Willems (Eds.), Instrumentelle pharmazeutische Analytik, Lehrbuch zu spektroskopischen, chromatographischen, elektro-chemischen und thermischen Analysemthoden, 3rd ed., Wissenschaftliche Verlagsgesellschaft mbH Stuttgart, Stuttgart, 2001.

[76] Pharmaceutical and Medical Devices Agency, Japan (Ed.), Japanese Pharmacopoeia, 16th ed., 2011.

[77] H.G. Brittain, Particle-size distribution, Part I: Representations of Particle Shape, Size, and Distribution, Pharm. Technol. 25 (2001) 38–45.

[78] K.H. Bauer, K.H. Frömming, C. Führer, Lehrbuch der Pharmazeutischen Technologie, Mit einer Einführung in die Biopharmazie, 8th ed., Wissenschaftliche Verlagsgesellschaft mbH, Stuttgart, 2006.

[79] D.M. Parikh (Ed.), Handbook of pharmaceutical granulation technology, 2nd ed., Taylor & Francis, 2005.

[80] S.M. Iveson, J.D. Litster, K. Hapgood, B.J. Ennis, Nucleation, growth and breakage phenomena in agitated wet granulation processes: a review, Powder Technol. 117 (2001) 3–39.

[81] T. Lipsanen, T. Närvänen, H. Räikkönen, O. Antikainen, J. Yliruusi, Particle Size, Moisture, and Fluidization Variations Described by Indirect In-line Physical Measurements of Fluid Bed Granulation, AAPS PharmSciTech. 9 (2008) 1070–1077.

[82] J. Litster, B. Ennis, L. Liu, The science and engineering of granulation processes, Kluwer, Dordrecht, 2004.

[83] T. Närvänen, T. Lipsanen, O. Antikainen, H. Räikkönen, J. Yliruusi, Controlling granule size by granulation liquid feed pulsing, Int. J. Pharm. 357 (2008) 132–138.

[84] S.H. Schaafsma, N.W.F. Kossen, M.T. Mos, L. Blauw, A.C. Hoffmann, Effects and control of humidity and particle mixing in fluid-bed granulation, AIChE J. 45 (1999) 1202–1210.

[85] S.H. Schaafsma, T. Marx, A.C. Hoffmann, Investigation of the particle flow pattern and segregation in tapered fluidized bed granulators, Chem. Eng. Sci. 61 (2006) 4467–4475.

[86] P. Khanna, T. Pugsley, H. Tanfara, H. Dumont, Radioactive particle tracking in a lab-scale conical fluidized bed dryer containing pharmaceutical granule, Can. J. Chem. Eng. 86 (2008) 563–570.

[87] Glatt GmbH Binzen, Fluid bed systems: GPCG and WST / G, 2005, http://www.glatt.com/cm/en/equipment/drying/batch-fluid-bed/production-size.html, accessed 8 June 2012.

[88] M. Blanco, J. Coello, H. Iturriaga, S. Maspoch, C. de la Pezuela, Quantitation of the active compound and major excipients in a pharmaceutical formulation by near infrared diffuse reflectance spectroscopy with fibre optical probe, Anal. Chim. Acta 333 (1996) 147–156.

[89] G.X. Zhou, Z. Ge, J. Dorwart, B. Izzo, J. Kukura, G. Bicker, J. Wyvratt, Determination and Differentiation of Surface and Bound Water in Drug Substances by Near Infrared Spectroscopy, J. Pharm. Sci. 92 (2003) 1058–1065.

[90] R.L. Green, G. Thurau, N.C. Pixley, A. Mateos, R.A. Reed, J.P. Higgins, In-Line Monitoring of Moisture Content in Fluid Bed Dryers Using Near-IR Spectroscopy with Consideration of Sampling Effects on Method Accuracy, Anal. Chem. 77 (2005) 4515–4522.

[91] M. Andersson, M. Josefson, F.W. Langkilde, K.-G. Wahlund, Monitoring of a film coating process for tablets using near infrared reflectance spectrometry, J. Pharm. Biomed. Anal. 20 (1999) 27–37.

[92] E.W. Ciurczak, J. Ketolainen, R. Laitinen, J. Aaltonen, H.H. Lindén, Taking PAT to the next level, Eur. J. Pharm. Sci. 42 (2011) 1–2.

[93] M. Blanco, J. Coello, A. Eustaquio, H. Iturriaga, S. Maspoch, Analytical control of pharmaceutical production steps by near infrared reflectance spectroscopy, Anal. Chim. Acta 392 (1999) 237–246.

[94] P. Corti, G. Ceramelli, E. Dreassi, S. Mattii, Near infrared transmittance analysis for the assay of solid pharmaceutical dosage forms, Analyst 124 (1999) 755–758.

[95] International Conference on Harmonisation of technical requirements for registration of pharmaceuticals for human use, ICH Q2 (R1) Validation of Analytical Procedures: Text and Methodology, 1994.

[96] W. Horwitz, Evaluation of Analytical Methods Used for Regulation of Foods and Drugs, Anal. Chem. 54 (1982) 67 A–76 A.

[97] European Medicines Agency, Guideline on the use of Near Infrared Spectroscopy (NIRS) by the pharmaceutical industry and the data requirements for new submissions and variations - Draft, 2012.

[98] H. Li, Bruker Optics, Bruker, Bruker Solutions for feed and forage testing http://www.foragetesting.org/files/2008/16a._Bruker_solution_for_Feed_and_forage_testing[1].Hui_Li.pdf, accessed 10 June 2012.

[99] W. Chen, S.-Y. Chang, S. Kiang, A. Marchut, O. Lyngberg, J. Wang, V. Rao, D. Desai, H. Stamato, W. Early, Modeling of Pan Coating Processes: Prediction of Tablet Content Uniformity and Determination of Critical Process Parameters, J. Pharm. Sci. 99 (2010) 3213–3225.

[100] G. Mirschel, K. Heymann, T. Scherzer, Simultaneous In-Line Monitoring of the Conversion and the Coating Thickness in UV-Cured Acrylate Coatings by Near-Infrared Reflection Spectroscopy, Anal. Chem. 82 (2010) 8088–8094.

[101] S.H. Tabasi, R. Fahmy, D. Bensley, C. O'Brien, S.W. Hoag, Quality by Design, Part III: Study of Curing Process of Sustained Release Coated Products Using NIR spectroscopy, J. Pharm. Sci. 97 (2008) 4067–4086.

[102] M.-J. Lee, C.-R. Park, A.-Y. Kim, B.-S. Kwon, K.-H. Bang, Y.-S. Cho, M.-Y. Jeong, G.-J. Choi, Dynamic Calibration for the In-Line NIR Monitoring of Film Thickness of Pharmaceutical Tablets Processed in a Fluid-Bed Coater, J. Pharm. Sci. 99 (2010) 325–335.

[103] J.J. Moes, M.M. Ruijken, E. Gout, H.W. Frijlink, M.I. Ugwoke, Application of process analytical technology in tablet process development using NIR spectroscopy: Blend uniformity, content uniformity and coating thickness measurements, Int. J. Pharm. 357 (2008) 108–118.

[104] Y. Kato, D. Sasakura, T. Miura, A. Nagatomo, K. Terada, Evaluation of Risk and Benefit in the Application of Near-Infrared Spectroscopy to Monitor the Granule Coating Process, Pharm. Dev. Technol. 13 (2008) 205–211.

[105] M. Andersson, S. Folestad, J. Gottfries, M.O. Johansson, M. Josefson, K.-G. Wahlund, Quantitative Analysis of Film Coating in a Fluidized Bed Process by In-Line NIR Spectrometry and Multivariate Batch Calibration, Anal. Chem. 72 (2000) 2099–2108.

[106] J.D. Pérez-Ramos, W.P. Findlay, G. Peck, K.R. Morris, Quantitative Analysis of Film Coating in a Pan Coater Based on In-Line Sensor Measurements, AAPS PharmSciTech. 6 (2005) E127–E136.

[107] ASTM, E 2474-06 Standard Practice for Pharmaceutical Process Design Utilizing Process Analytical Technology, 2006.

[108] EMA, Reflection Paper: Chemical, pharmaceutical and biological information to be included in dossiers when Process Analytical Technology (PAT) is employed, 2006, http://www.ema.europa.eu/docs/en_GB/document_library/Other/2009/10/WC500004890.pdf, accessed 12 July 2011.

[109] C. Potter, S. Folestad, R. Beerbohm, G. Muirhead, S. Roenninger, A. Coupe, A. Swanson, F. Erni, G. Fischer, A guide to EFPIA's mock P.2 document, Pharm. Technol. Eur. 18 (2006) 39–44.

[110] European Medicines Agency, Food and Drug Administration, EMA-FDA pilot program for parallel assessment of Quality by Design applications, 2011 http://www.fda.gov/downloads/InternationalPrograms/FDABeyondOurBordersForeignOffices/EuropeanUnion/UCM259808.pdf, accessed 12 June 2012.

[111] European Medicines Agency, Guideline on Real Time Release Testing (formerly Guideline on Parametric Release), Draft, 2009.

[112] C. de Bleye, P.-F. Chavez, J. Mantanus, R. Marini, P. Hubert, E. Rozet, E. Ziemons, Critical review of near-infrared spectroscopic methods validations in pharmaceutical applications, Article in Press, Corrected Proof, J. Pharm. Biomed. Anal (2012).

[113] G. Dünnebier, H. Tups, US Food and Drug Administration (FDA) Process Analytical Technology (PAT) Initiative A user's view on technical possibilities and present industrial changeover: FDA PAT Initiative - Eine Anwendersicht zu technischen Möglichkeiten und aktueller industrieller Umsetzung, Chem. Ing. Tech. 79 (2007) 2019–2028.

8. ANNEX

LIST OF FIGURES

LIST OF TABLES